SYNTHESIS OF RHODAMINE CHEMOSENSORS WITH HIGH SELECTIVITIY AND SENSITIVITY FOR MULTIPLE METAL IONS DETECTION

NUR AMIRA SOLEHAH BINTI PUNGUT

FACULTY OF SCIENCE
UNIVERSITI MALAYA
KUALA LUMPUR

2021

SYNTHESIS OF RHODAMINE CHEMOSENSORS WITH HIGH SELECTIVITIY AND SENSITIVITY FOR MULTIPLE METAL IONS DETECTION

NUR AMIRA SOLEHAH BINTI PUNGUT

THESIS SUBMITTED IN FULFILMENT OF THE REQUIREMENTS FOR THE DEGREE OF DOCTOR OF PHILOSOPHY

DEPARTMENT OF CHEMISTRY
FACULTY OF SCIENCE
UNIVERSITI MALAYA
KUALA LUMPUR

2021

UNIVERSITI MALAYA

ORIGINAL LITERARY WORK DECLARATION

Name of Candidate: **NUR AMIRA SOLEHAH BINTI PUNGUT**

Matric No: **SVA180024**

Name of Degree: **DOCTOR OF PHILOSOPHY**

Title of Thesis ("this work"):

SYNTHESIS OF RHODAMINE CHEMOSENSORS WITH HIGH SELECTIVITIY AND SENSITIVITY FOR MULTIPLE METAL IONS DETECTION

Field of Study:

INORGANIC CHEMISTRY

I do solemnly and sincerely declare that:

(1) I am the sole author/writer of this Work;
(2) This Work is original;
(3) Any use of any work in which copyright exists was done by way of fair dealing and for permitted purposes and anu excerpt or extract from, or reference' to or reproduction of any copyright work has been disclosed expressly and sufficiently and the title of the Work and its authorship have been acknowledged in this Work;
(4) I do not have any actual knowledge nor do I ought reasonably to know that the making of this work constitutes an infringement of any copyright work;
(5) I hereby assign all and every rights in the copyright to this Work to the University of Malaya ('UM"), who henceforth shall be owner of the copyright in this Work and that any reproduction or the used in any form or by any means whatsoever is prohibited without the written consent of UM having been first had and obtained;
(6) I am fully aware that if in the course of making this Work I have infringed any copyright whether intentionally or otherwise, I may be subject to legal action or any other action as may be determined by UM.

Candidate's Signature Date: 30/9/2021

Subscribed and solemnly declared before,

Witness's Signature

Name: Date: 30/9/2021

Designation:

SYNTHESIS OF RHODAMINE CHEMOSENSORS WITH HIGH SELECTIVITIY AND SENSITIVITY FOR MULTIPLE METAL IONS DETECTION

ABSTRACT

Four rhodamine B based chemosensors have been synthesized through condensation reaction between rhodamine B hydrazide with 2-hydroxy-3-methoxybenzaldehyde (**RBOV**), fluorene-2-carboxaldehyde (**RFC**), trans-4-(Diethylamino)cinnamaldehyde (**RT4**) and 3,4,5-trimethoxybenzaldehyde (**R3**). The compounds were characterized by FTIR, ^{1}H NMR, ^{13}C NMR, mass spectroscopy, and single crystal x-ray diffraction. These chemosensors exhibit different and unique properties as **RBOV** can detect Cu^{2+}, Ni^{2+} and Co^{2+} ions, **RFC** is able to detect Al^{3+} and Cu^{2+} ions, **RT4** detects Cu^{2+} and Fe^{3+} ions and **R3** is able to detect Fe^{3+} ions only. The detection of these metal ions was further investigated using UV-vis and fluorescence spectroscopy. For all sensors, a 1:1 binding stoichiometry of the chemosensors-metal ions were determined through Job's plot analysis while the detection limit (in μM) of the chemosensors were determined from the UV-vis and fluorescence titration experiments. Furthermore, the binding of the chemosensors with the metal ions were also illustrated by the partial FTIR and ^{1}H NMR spectrum. In determining the potential application of the sensors both biologically and environmentally, reversibility, test strips and MTT assays have been successfully prepared and studied.

Keywords: Rhodamine B, Chemosensors, Fluorescence, Test Strips, MTT.

SINTESIS KEMOSENSOR RHODAMINA DENGAN SELEKTIVITI DAN SENSITIVITI YANG TINGGI BAGI PENGESANAN PELBAGAI ION LOGAM

ABSTRAK

Empat kemosensor berasaskan rhodamina B telah disintesis melalui tindak balas kondensasi antara hidrazida rhodamine B dengan 2-hidroksi-3-metoksibenzaldehid (**RBOV**), fluorene-2-karboxaldehid (**RFC**), trans-4-(Dietlamino)sinnamaldehid (**RT4**) dan 3,4,5-trimetoksibenzaldehid (**R3**). Sebatian tersebut dicirikan oleh FTIR, ^{1}H NMR, ^{13}C NMR, spektroskopi jisim, dan pembelauan sinar-x kristal tunggal. Kemosensor ini menunjukkan sifat yang berbeza dan unik kerana **RBOV** dapat mengesan ion Cu^{2+}, Ni^{2+} dan Co^{2+}, **RFC** dapat mengesan ion Al^{3+} dan Cu^{2+}, **RT4** mengesan ion Cu^{2+} dan Fe^{3+} dan **R3** hanya dapat mengesan ion Fe^{3+} sahaja. Pengesanan ion logam ini disiasat dengan menggunakan spektroskopi UV-vis dan pendarfluor. Untuk semua sensor, stoikiometri pengikat 1:1 chemosensor-logam ditentukan melalui analisis Job's plot sementara had pengesanan (dalam μM) kemosensor ditentukan dari eksperimen titrasi UV-vis dan pendarfluor. Selanjutnya, pengikatan chemosensor dengan ion logam juga digambarkan oleh spektrum FTIR separa dan ^{1}H NMR. Dalam menentukan potensi penggunaan sensor dari segi biologi dan persekitaran, ujian kebolehbalikan, jalur ujian, dan ujian MTT telah berjaya dilakukan.

Kata kunci: Rhodamina B, kemosensor, pendarfluor, jalur ujian, MTT.

ACKNOWLEDGEMENTS

First, all praises to the Almighty for getting me through the ups and downs throughout my research and completing my thesis.

I would like to express sincere gratitude to my supervisor, Assoc. Prof. Dr. Tan Kong Wai, for his unfaltering guidance, aid, and encouragement throughout this project. Without his continuous support and adroitness, it would be difficult for me to complete this project.

I am indebted to the Higher Ministry of Education and Universiti Malaysia Sabah (UMS), for the scholarship provided, which have helped me tremendously. In addition to that, I would also like to show my gratitude to Universiti Malaya for their research grant (FRGS/1/2019/STG01/UM/02/11).

Furthermore, I am thankful for the undying love and support from my parents, siblings, and friends throughout this journey. Finally, I am grateful for all the help given by my colleagues, Savina Savir, Cheah Poh Wei, Chan Wei Chuen, and Lee Shiaw Xian.

TABLE OF CONTENTS

LIST OF FIGURES AND SCHEMES

LIST OF TABLES

LIST OF SYMBOLS AND ABBREVIATIONS

Å	:	Angstrom
K_a	:	Association constant
λ	:	Lambda
μ	:	Micro
v	:	Wavenumber
ATR	:	Attenuated total reflection
CCDC	:	Cambridge Crystallographic Data Centre
EPA	:	Environmental Protection Agency
EDTA	:	Ethylenediaminetetraacetic acid
HT-29	:	Human colorectal adenocarcinoma cell
CCD-18Co	:	Normal colon fibroblast cell
TN	:	Tris-sodium chloride
Tris-HCl	:	Tris-Hydrochloride
UV-vis	:	Ultraviolet visible
WHO	:	World Health Organization

LIST OF APPENDICES

CHAPTER 1: INTRODUCTION

1.1 Problem Statement

Rhodamine chemosensors ability in providing ‘’naked eye’’ detection and “switch-on” fluorescence mechanism has been of great importance in detection of trace metal ions environmentally and biologically. Although the detection of analyte by this method is easier than the usual conventional methods, factors affecting the solubility of sensors, quenching of fluorescence, and different colour changes of solution would need to be studied. Because of this, different experiments need to be done in order to figure out the optimum condition in which the sensor would exhibit the desired result upon recognition towards target analyte.

1.2 Objectives

1. To synthesize and characterize new rhodamine chemosensors which are able to detect presence of single and/or multiple metal ions simultaneously through colorimetric and/or fluorometric sensing.
2. To determine the optimum condition(s) in which the rhodamine chemosensors exhibit a great selectivity and sensitivity toward metal ions detected.
3. To determine the reusability and cytotoxicity of rhodamine chemosensors for practical applications.

1.3 Scope of Studies

Over the years, due to the high sensitivity, selectivity and simplicity of chemosensors, the design and development of such probes have been of great interest. The development of these artificial probes is important for detection of metal ions which plays an important role in the environmental and biological system. Since there is an increasing use of heavy metal ions in the industry, environmental pollution and health hazards are inevitable

(Lenart-Boroń, 2014; Mohammed, 2011). Therefore, it is critical to study and understand the benefits and risks these metal ions possess, so that a selective probe for detection of certain metal ions could be designed and developed.

These days, unimolecular sensors for recognition of multiple analytes have garnered more attention as it is more cost and time efficient than single analyte detection (Kim et al., 2016; Singh & Das, 2018; Sun et al., 2017). However, achieving this feat is challenging as the recognition of metal ions by sensors requires suitable coordination environment as it produces different response in different environment. Because of this, the use of different solvent medium towards recognition of sensors for multianalytes are rarely discussed (Fang et al., 2015; Ghorai et al., 2016; Tang et al., 2017). Furthermore, the use of different solvent medium may also affect the mode of detection by sensors, either via fluorometric and/or colorimetric sensing (Behera & Bag, 2016; Wang et al., 2018).

Although solvent medium may alter the mode of detection of sensors, the design and composition of the probe itself plays a larger role in this matter. This is because, in designing excellent fluorescent probes, the organic functional groups are strategically selected in order to enhance its fluorescence properties. Besides that, colorimetric properties are also favourable as it enables naked eye detection upon binding with metal ions. Although it is not as sensitive as fluorescent sensing, the rapid colorimetric response may provide preliminary qualitative and quantitative information without any means of spectroscopic instruments (Milindanuth & Pisitsak, 2018). Because of this, fluorophores such as rhodamines and fluoresceins, with high emission wavelength are usually preferred in developing chemosensors, so that the absorbance and emission wavelength are within visible spectrum.

This research focuses on developing rhodamine B Schiff-base chemosensors by reacting rhodamine B hydrazide with 2-hydroxy-3-methoxybenzaldehyde (RBOV), fluorene-2-carboxaldehyde (RFC), trans-4-(Diethylamino)cinnamaldehyde (RT4), and 3,4,5-trimethoxybenzaldehyde) (R3), through a one-step reaction. Characterization of these sensors were done by using FT-IR, NMR, Mass (ESI) spectroscopy and x-ray crystallography.

In this work, 3 metal ions were detected simultaneously by RBOV (Cu^{2+}, Co^{2+} and Ni^{2+}) and RFC (Al^{3+}, Cu^{2+} and Fe^{2+}) sensors, while RT4 sensor detects Cu^{2+} and Fe^{3+} and R3 sensor detects single metal ion (Fe^{3+}), in their respective solvent medium. Since RBOV, RFC and RT4 sensors detect multiple ions simultaneously, several methods were used in order to discern the recognition of sensor with metal ions detected. This includes addition of oxidizing agent into the solution containing RBOV-M^{n+} complex and altering the pH of the solvent medium for RFC sensor. In the case of RT4 sensor, the difference in colorimetric and fluorometric properties were used in discerning the detection between the two metal ions.

Since each of the sensors developed consists of different fluorophores, the binding mode of each sensor towards metal ions were also studied. In determining the binding stoichiometry of sensor-metal complex, Job's plot analysis was done. The results obtained from this analysis were further supported by the FT-IR and ^{1}HNMR spectra of sensor-metal complexes. The practicality of the sensors was also tested by conducting the reversibility assay, developing on-site assay kit and MTT assay to determine its cytotoxicity towards living cells.

CHAPTER 2: LITERATURE REVIEW

2.1 Biological and Environmental Importance of Metal Ions

Metal ions have been known to occur naturally in the environment, where metals such as aluminium and calcium can be found in the earth's crust, and biologically such as iron and copper ions, which are directly involved in sustaining living organisms. These metal ions are essential for the continuity of life as it plays a crucial role in our biological system such as regulation of DNA transcription, proper functioning of the muscles, transport of oxygen, energy production and also neurological functions (Lansdown, 1995). For example, calcium being the most abundant metal ion in the human body is known for its importance in building strong bones and teeth. However, it also plays an important role in transport of ion (Lutwak, 1974). Magnesium on the other hand, is essential as it acts as cofactor in many enzyme-catalyzed reactions, specifically in adenosine triphosphate (ATP) metabolism, which results in production of energy for the cells in our body (Ryan, 1991).

In recent years, rapid modernization and industrialization have contributed to the increase in concentration of metal ions in the environment (Heike, 2005). The accumulation of excessive amount of metal ions in the environment is caused by the extensive use and discharge of heavy metal ions in pharmaceuticals (Gopalakrishnan et al., 2015), textile (Körbahti et al., 2011), automotive (Miller et al., 2000) and burning of coal (McConnell & Edwards, 2008). The waste discharge from these industries will not only have adverse effects to the environment but also to the human health (Fergusson, 1990).

For example, the significant increase in the use of metal ions has resulted in an increase of metal pollutant into the soil and aquatic environment (Knopf & König, 2010). When accumulation of metal ions such as copper, nickel and lead occur, this will indirectly cause a change in the properties of the soil, which includes organic matter, clay content and pH (Speir et al., 1999). Furthermore, the increase in metal pollutant will have an adverse effect on the soil microbial community which is important for the synthesis of enzymes. This will lead to a change in the respiration rate and enzymatic activity of the soil, which may indirectly indicates soil pollution (Mora et al., 2005).

Trace amount of metal ions such as copper, zinc, nickel, iron and cobalt are essential for the proper growth and metabolism of plants. However, the discharge of heavy metal ions by industrial activities will lead to increase in concentration of these metal ions into the soil and cause poisoning of the plants (Rascio & Navari-Izzo, 2011). In addition to that, the production of reactive oxygen species (ROS) is promoted because of heavy metal poisoning which directly interferes with electron transport activities of plants and damages aquatic organisms (Woo et al., 2009; Zitka et al., 2013).

Since the uptake of heavy metals occurs in the soil, followed by the plants and subsequently the aquatic organisms, the probability of exposure to the heavy metal pollutants from this food chain is inevitable. As heavy metal ions enter the aquatic environment where fish are present, these metals may enter the fish through gills, skin and water consumption. Once it enters the fish, these heavy metal ions are transported throughout the organs and tissues of fish by blood. Since most of the metal ions are found in the tissues, the consumption of fish containing high concentration of heavy metal ions may cause health problems (Soliman, 2006).

To put it simply, the consumption of food crops and aquatic life contaminated with heavy metal ions is one of the principal ways of human exposure to these metal pollutants. As the intake of food contaminated with heavy metal ions accumulates, long-term intoxications may occur as they are unable to be metabolized by the body (Cuadrado et al., 2000; Sobha et al., 2007). For example, exposure to excess copper, cadmium and cobalt may lead to DNA damage induction and DNA repair inhibition (Hengstler et al., 2003). Excess levels of lead which can enter via food through canned food and alcoholic drinks, may cause damages to the liver, kidney, and the central nervous system (Assi et al., 2016). While exposure to high concentration of sulfidic and oxidic nickel has been known to cause lung and nasal cancer (Shen & Zhang, 1994). Overtime, continual ingestion of heavy metals will have detrimental effects on the human health.

2.1.1 Aluminium

Being the third most abundant element and the most abundant metal in the Earth's crust, it is not surprising that aluminium is easily exposed to the general population on the day-to-day basis. Biologically, aluminium does not play any essential role in sustaining life. Even so, in the environmental aspect of things, the aluminium industry is burgeoning with the majority of the current growth in pharmaceuticals (Reinke et al., 2003), automotive (Miller et al., 2000), textile industry (Ciardelli & Ranieri, 2001) food additive (Saiyed & Yokel, 2005) and water purification (Krewski et al., 2007).

Environmentaly, soil acidification caused from acid rain and human activities does not only hinder crop production, but it may also mobilize aluminium into nearby water (Godbold et al., 1988). When this occur, pH of water is altered and this will lead to intoxication of the aquatic life. Due to its widespread application in industrialization and occurrence in the environment, human exposure to aluminium will be inevitable. Accumulation and long uptake of aluminium in high concentration has been shown to

cause lung, breast and bladder cancer (Armstrong et al., 1994; Darbre, 2005). Besides, since aluminium is known to be highly neurotoxic, excess levels of aluminium may also damage the nervous system and cause Alzheimer's disease, Parkinson's disease and dementia (Verstraeten et al., 2008).

2.1.2 Copper

Other than being the third most abundant essential trace element in the human body after iron and zinc, copper is important in many aspects such as biochemical and physiological processes. Biochemically, copper plays an important role in proper functioning of several enzymes such as copper-zinc superoxide, which is the key in conversion of superoxide radicals (Tainer et al., 1983).

In the biological system, copper is usually bound to proteins. When it is present in excess, these proteins may release copper and generation of highly reactive hydroxyl radicals would take place (Gaetke & Chow, 2003). Consequently, these radicals would cause further damage towards various cellular components. In addition to that, high concentration of copper has been known to cause various neurodegenerative disorders such as Alzheimer's disease, Parkinson's disease and amyotrophic lateral sclerosis disease (Gaggelli et al., 2006). On the other hand, the deficiency in copper is known to cause cardiovascular disease (Klevay, 2000).

Environmentally, copper has been widely used in the construction industry, combustion of coal, oil and gasoline, industrial machinery and agricultural use (Georgopoulos et al., 2001). Although copper is one of the essential elements needed for plant growth, the increase in industrial and agricultural activities have caused an increase of copper in nearby ecosystems. The accumulation of copper in soil which leads to copper cytotoxicity will induce stress and may also damages the protein synthesis. As a result, growth retardation of plants will occur (Lewis et al., 2001). On the other hand, excess amount of copper has been proven to affect the growth rate of rainbow trout (Marr et al., 1996).

2.1.3 Cobalt

In general, cobalt is mainly used in the production of steel, abrasion-resistant glasses, ceramics, paints, and batteries. Although cobalt is not as abundant as compared to copper and aluminium, it is still one of the essential elements found in Vitamin B_{12} and cobalamins. In addition to that, cobalt also plays a vital role in the metabolism of iron and the synthesis of hemoglobin (Taylor & Marks, 1978).

Although cobalt is not needed in large amount, deprivation of it has shown to cause a decline in weight, anemia, and loss of appetite in sheep (Becker et al., 1949). Besides that, even though cobalt is non-carcinogenic, high and continuous exposure may lead to diseases such as cardiomyopathy, contact dermatitis and interstitial lung disease, of workers in hard metal industries (Donald G. Barceloux & Donald Barceloux, 1999; Kennedy et al., 1981). In addition to that, studies conducted on barley, oilseed rape and tomato has shown that cobalt toxicity in soil can inhibit biomass and shoot growth (Li et al. 2009). As oppose to copper, excess amount of cobalt have been found to lower the transpiration rate and water potential in plants (Nagajyoti et al., 2010).

2.1.4 Iron

After aluminium, iron is the most abundant metal in the Earth's crust. Steel is an alloy made up of iron with different percentage of carbon. As production of steel requires extraction of iron from mined iron ores, high energy is usually required in the process. Consequently, this also means that emission of toxic gases such as nitrogen, carbon monoxide, and carbon dioxide is inevitable (Vallero, 2014). Besides air pollution, the improper handling of iron ore tailings from manufacturing of iron has also shown substantial negative impact on the environment. This is evident from a study done which proves that contamination by iron ore tailings has caused an increase in pH of the soil which subsequently affects the plant growth (Wong & Tam, 1977).

In the physiological aspect of things, iron plays an indispensable role in the development and sustainment of living organisms as. Other than being the essential element for blood production, iron is also required in electron transport chain, iron–sulfur proteins and enzymes such as ribonucleotide reductase, making it important for the neuronal and immune functions of the body (Arredondo & Núñez, 2005). Because of this, iron deficiency does not only affect the immune system but is also well known as the main cause of anemia (Clark, 2008). This is evident from a study conducted whereby deficiency in iron affects the immune response by reducing protein kinase C activity which is responsible in proliferation of T lymphocyte (Kuvibidila et al., 1999). On the other hand, excess of iron will cause various detrimental diseases such as, osteoporosis (Weinberg, 2008), Parkinson's disease (Berg et al., 2001), and Alzheimer's disease (Bishop et al., 2002).

2.1.5 Nickel

Nickel is the fifth most abundant element on Earth. Attributing to its availability and great resistance against corrosion and high temperature, nickel possess a lot of industrial and commercial uses. Nickel metal and its alloys are used widely in the industrial machinery, construction and transportation (Reck et al., 2008). Some of the nickel salts greatest commercial importance are nickel chloride and nitrate for electroplating, sulphate as medicinal agent, and carbonate in metallurgical (D. G. Barceloux & D. Barceloux, 1999).

Biologically, nickel is an essential micronutrient for higher plant. However, when it is present above the permissible limit, it may interfere with the functions of many cellular components, thereby causing toxic symptoms which include chlorosis, necrosis, stunting, inhibition of root growth and decrease in leaf area (Shaw et al., 2004). On the other hand, nickel toxicity in aquatic ecosystem was not observed due to the decrease in concentration of nickel with increasing levels of the food chain (Maass et al., 1991).

The exposure of the general population to nickel is mainly through dietary intake, either as a contaminant in drinking water or leaching of nickel during food processing (Cempel & Nikel, 2006). Study has shown that the accumulation of nickel in the body may cause a disturbance of several cellular metabolic processes, due to its ability to replace other metal ions such as magnesium and calcium in enzymes, and strong binding affinity towards proteins and nucleic acids (Coogan et al., 1989). In addition to that, nickel exposure through use of jewellery has been found to cause an immune response resulting in contact dermatitis (Peltonen, 1979). Occupational nickel exposure has also been reported, mainly affecting the respiratory system causing asthma in acute cases, and lung and nasal cancer in chronic cases (Andersen et al., 1996; Novey et al., 1983).

2.2 Detection of Metal Ions

As the biological and environmental importance of metal ions have been discussed earlier, it is apparent that detection of metal ions by a new method is needed. Over the years, the detection of trace amount of metal ions has been done through several analytical techniques and instrumentation. The conventional analytical techniques include, the atomic absorption spectroscopy (AAS), inductively coupled plasma atomic emission spectroscopy (ICP-AES), inductively coupled plasma mass spectrometry (ICP-MS), anodic stripping voltammetry and liquid chromatography mass spectrometry (LCMS). However, these methods have several limitations and efficiency in detection of metal ions in the field. This is due to its tedious sample preparation, expensive instrumental cost, require experienced operators, time consuming, and is not portable.

The modern form of atomic absorption spectroscopy (AAS) was developed back in 1950s by Alan Walsh and his colleagues. The application of AAS is based on the absorption of individual elements at their characteristic wavelengths which are then measured against standards. The schematic of the AAS process is shown in **Figure 2.1.**

First, the liquid or solid sample is atomized by either flames or electrothermal atomizer. The atoms are then irradiated by the cathode which then traverses the flame and passes through the slit of monochromator and finally measured by the readout system. The chopper in the figure shown is used to block any incident beam thus eliminating the interference of light emitted from the flame (Robinson, 1960).

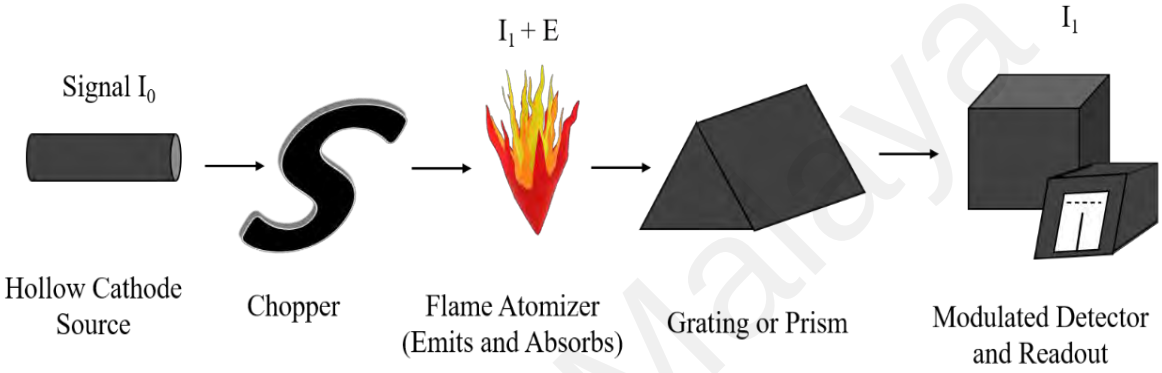

Figure 2.1 Schematic of equipment involved in AAS (Robinson, 1960).

Mass spectrometry is known for its ability in accuracy and sensitivity in mass analysis of samples containing organic compounds. On the other hand, liquid chromatography is a technique used to separate individual components of a mixture. Ever since LCMS is invented, this tandem technique has been favored due to its ability in analyzing wide range of complex biochemical, organic and inorganic compounds. There are numerous interfaces for LCMS, but the most commonly used interfaces are electrospray ionization (ESI), atmospheric pressure chemical ionization (APCI), and atmospheric pressure photoionization (APPI). **Figure 2.2** shows the simplified schematic for LCMS. To put it simply, the liquid sample is first injected into the LC column. After individual components are separated in the column, it will then be transferred into the MS ion source which will then provide the structural identity of these components.

With the two given examples of conventional detection techniques (**Figure 2.1** and **Figure 2.2**), a new method which provides rapid, efficient, and inexpensive detection of

metal ions is required. Although these conventional method serves its purpose, the time required in preparation of the sample, being processed by the instruments, and finally acquiring the results is rather time consuming. For example, even after sample injection into the LCMS instrument, the flow rate of components in the LC column by different interfaces used ranged from 0.02 to 2.00 ml/min, which also dependent on the quantity of the components in the sample tested (Niessen & Tinke, 1995). Furthermore, sample preparation in using AAS involves sample digestion with concentrated acid. Because of this, optical detection method which provide a more rapid, efficient, low cost and high sensitivity via chemosensors has been introduced and continually developed and by many researchers around the world.

2.3 Chemosensors

Generally, chemosensors are capable of monitoring analyte concentrations in real-time and real-space at the molecular levels. In recent years, the development of chemosensors have been experiencing a rapid growth due to their applicability in wide range of fields including medical diagnostic, environmental monitoring, and toxicology analysis (Prodi et al., 2000). Usually, chemosensor or molecular sensor which is composed of organic or inorganic complex, produces a detectable change or a signal upon binding with an analyte (Wang & Anslyn, 2011).

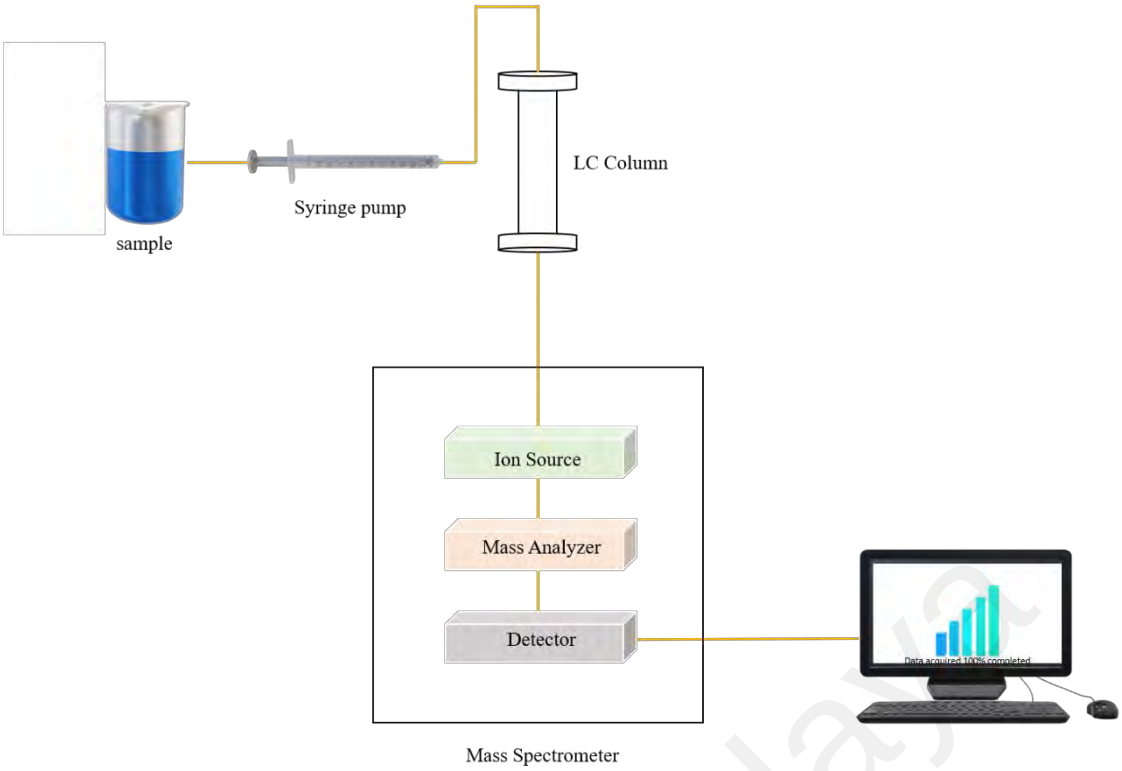

Figure 2.2 Simplified schematic for LCMS.

There are two different processes needed in order to detect the presence of the target analyte. These processes are known as molecular recognition and signal transduction. In an attempt to execute this, the chemosensors must be built by three key components. These components are made up of receptors, which binds to specific analytes, an active unit, which properties changes upon complexation of receptor with analyte, and the spacer that facilitates the interaction between the two components (**Figure 2.3**). The change in properties of the active unit may include changes in redox potential, colorimetric and fluorometric spectra (Bargossi et al., 2000). As seen in **Figure 2.3**, the active unit seem to experience a change in colour where it lights up upon the complexation of the receptor and analyte.

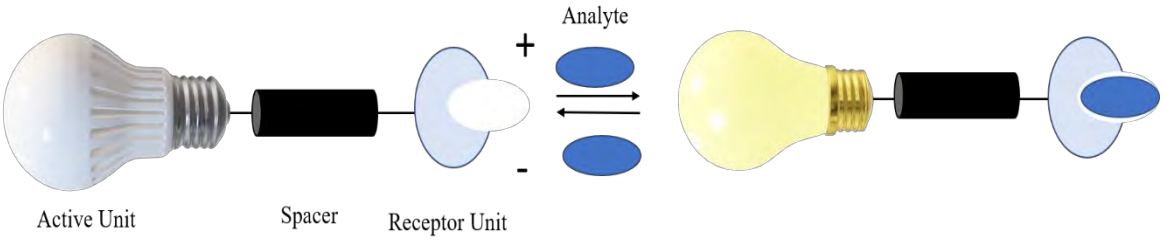

Figure 2.3 Components of chemosensors with target analyte (Bargossi et al., 2000).

In analytical chemistry, a sensor is known as the chemical indicator that produces an output in the presence of analyte. In this case, the sensor is equivalent as the receptor unit shown in **Figure 2.3**. Before the detection of metal ions was done by chemosensors, chemosensors such as boronic-acid-based chemosensor, imine/aminol based chemosensor and chemosensors based on reactions between aldehydes and alcohols, or other nucleophiles via covalent interactions have existed.

In developing and designing these chemosensors, it is important to ensure its reversibility in binding so that application of the chemosensor is not limited like a reagent in a stoichiometric reaction. Out of all three mentioned chemosensors, boronic-acid-based chemosensor is one of the most used in the build-up of a chemosensor due to its strong interactions with diols (Yoon & Czarnik, 1992), amino alcohols (Aharoni et al., 2008), cyanide (Badugu et al., 2005) and fluoride (DiCesare & Lakowicz, 2002). However, boronic acid is usually used in complexation with diols as shown in **Scheme 2.1** where it was first described in the early 1990s.

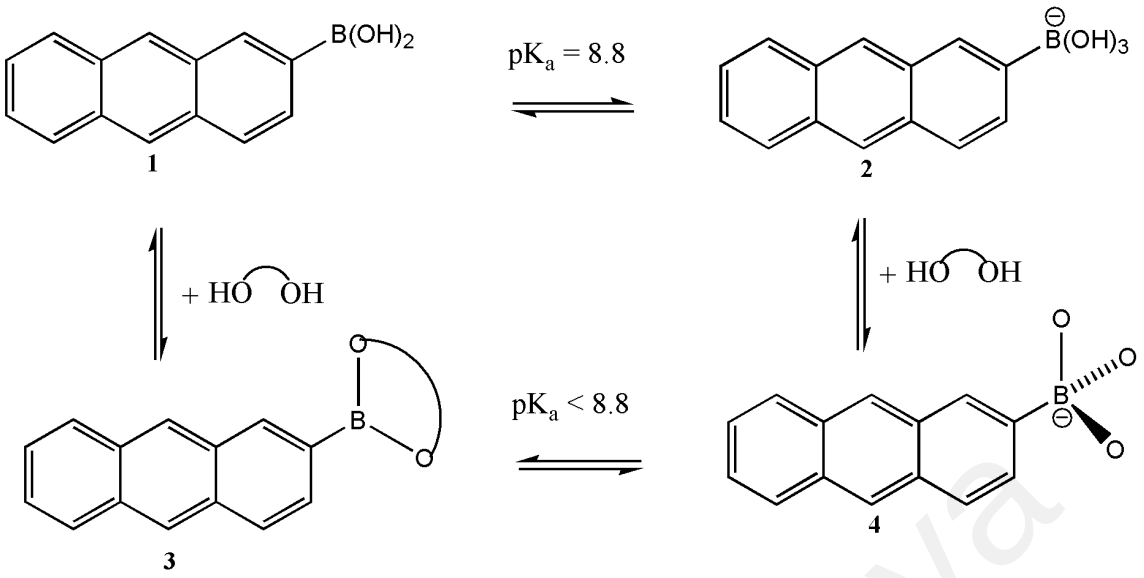

Scheme 2.1 Schematic representation of complexation of anthrylboronic acid (1) in the presence of a generic polyol (Yoon & Czarnik, 1992).

Next is the imine/aminol based chemosensor, which are exploited due to its strong interactions, reversibility, and solubility in protic solvents. One example from the numerous optical sensors developed is the (trifluoreacetyl)azobenzene dye (**5**) in which its chromogenic properties changes upon complexation with amine (**Scheme 2.2**) . The change in colour from red-orange to yellow is attributed to the change in absorption spectra from $\lambda = 475$ nm to 425 nm.

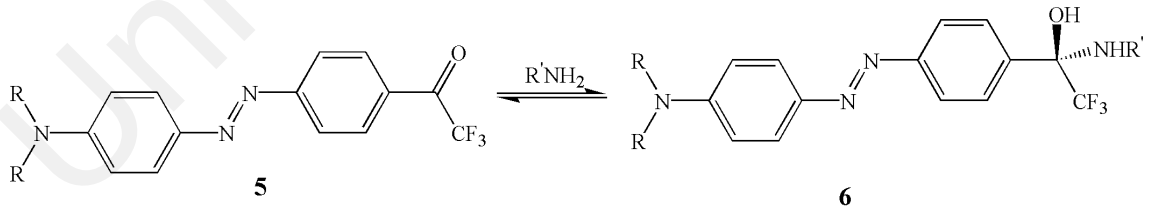

5

(trifluoroacetyl)azobenzene

6

Scheme 2.2 Schematic of reversible reaction of (trifluoroacetyl)azobenzene with primary amine (Mertz & Zimmerman, 2003).

The aldehyde based chemosensor, 4-*N,N*-Dioctylamino-4-formyl-2-nitroazobenzene (7) has been developed for the optical detection of bisulfite anion (Mohr, 2005). In this reaction, a colorimetric change from pink to orange was observed upon complexation (**Scheme 2.3**) of 7 with bisulfite anion. Furthermore, the sensor developed has shown great selectivity as no colorimetric changes was observed when tested with other anions such as sulfate, chloride, and phosphate.

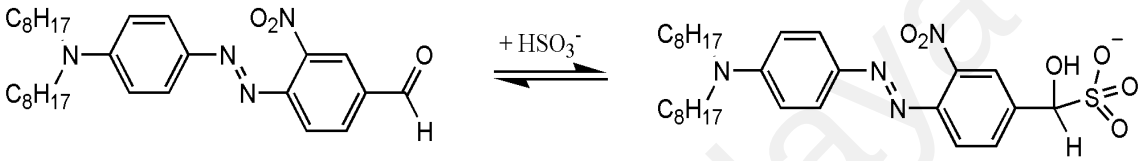

7 **8**

Scheme 2.3 Schematic reaction of 4-*N,N*-Dioctylamino-4-formyl-2-nitroazobenzene (7) with bisulfite anion (Mohr, 2005).

From the few types of chemosensors discussed above, it could be seen that each functional group plays and important role in developing a chemosensor for desired target analyte and outcome. For the detection of metal ions by chemosensors, there are two kinds of chemosensors that has been the favored and continued to gain interests among researches; the colorimetric and fluorometric chemosensors. On account of its high sensitivity, ‘’on-off’’ switch ability, and ability of offering sub-nanometer spatial resolution, fluorescence-based chemosensors is becoming of increasing importance for detection of trace analytes as compared to other types of chemosensors (de Silva et al., 1997). On the other hand, besides being able to provide rapid data without any use of conventional techniques discussed earlier (Quinlan et al., 2007), colorimetric chemosensors are also desired due to its flexibility and wide range of dyes to choose from, as it does not require a fluorophore in its design.

2.3.1 Fluorogenic and Chromogenic Chemosensors

As discussed earlier, the design of ligands for selective detection of analytes, such as metal ions are important as it occurs in abundance naturally, in our biological system and environmentally, due to rapid and widespread applications attributed by modernization. Because of this, developing a sensitive and selective prove for monitoring their concentration whether *in vitro* or *in vivo*, and environmental samples is critical for the continuation of life.

Before, it was mentioned that a sensor should be able to produce a measurable signal upon detection or binding to an analyte. The mechanism by which the interaction of the sensor and analyte yields measurable signal is known as signal transduction. In developing fluorescent chemosensor, the signal transduction would be observed by a change in the photophysical properties of the sensor, where this phenomena is also often called as 'switch-on' mechanism, as the sensor (non-fluorescent) becomes fluorescent upon binding with an analyte (Rurack, 2001). This type of chemosensor is usually favoured due to its excellent sensitivity in detecting low concentration of analyte. Consequently, by incorporating fluorophores moiety into the design of sensors, the detection applications of analyte could be done in real-time which provides high sensitivity with inexpensive instruments.

Therefore, in designing fluorescent sensors, it is crucial to carefully select the fluorophore (signalling moiety) and the receptor (recognition moiety) as the individual properties of each moiety may affect the overall system of the sensor developed. The fluorophore incorporated acts as the signal transducer, where it converts changes that occurs in an event into an optical response. On the other hand, the role of the receptor is to bind selectively to an analyte.

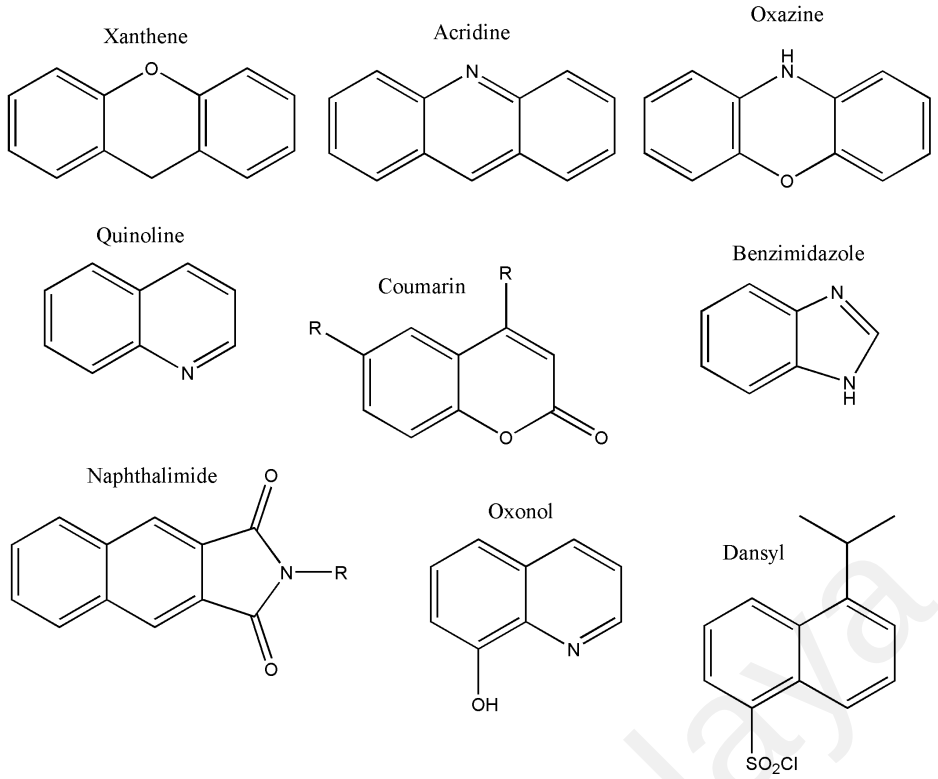

Figure 2.4 Variety of organic scaffolds as the signalling moiety in designing fluorescent chemosensors.

Herein, some of the fluorescent scaffolds that have been widely used as shown in **Figure 2.4**. As evident from the figure, the common feature in developing fluorophores is the heterocyclic rings. The extent of the conjugation in these rings, substituent groups and receptors will provide a multitude of paths that will tune the photophysical properties of the sensors developed. For example, a decrease and an increase in conjugation of the whole system of a sensor may result in the blue-shift or a red-shift in the wavelength (Rurack, 2001).

As mentioned earlier, the selection of fluorophores and receptors with substituted groups is important as it will alter the existing photophysical properties of individual components. When there is less conjugation of the sensor, blue-shift or hypochromic effect will be observed. This could be seen in the quinoline based chemosensor, **QC** in **Figure 2.5** upon recognition of Al^{3+}, where hypochromic effect is observed, and this results in blue fluorescence enhancement. On the other hand, when a highly conjugated sensor is synthesized, red-shift or bathochromic effect is observed. As evident in **Figure**

2.6, upon recognition of Cu^{2+} by **RS** (a xanthene derivative-based sensor), orange fluorescence was observed.

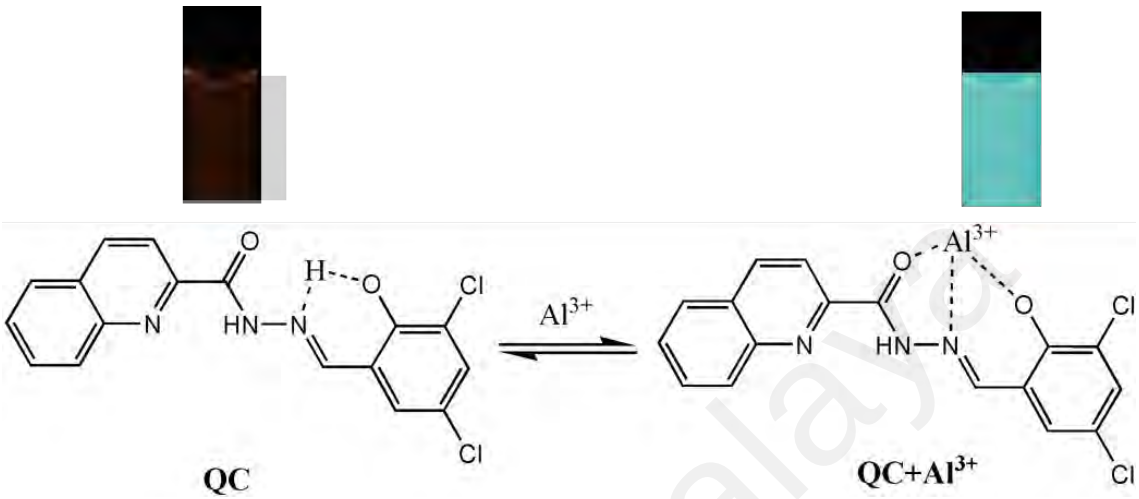

Figure 2.5 Proposed binding mechanism and fluorescence enhancement of QC upon recognition of Al^{3+} (Zhou et al., 2018).

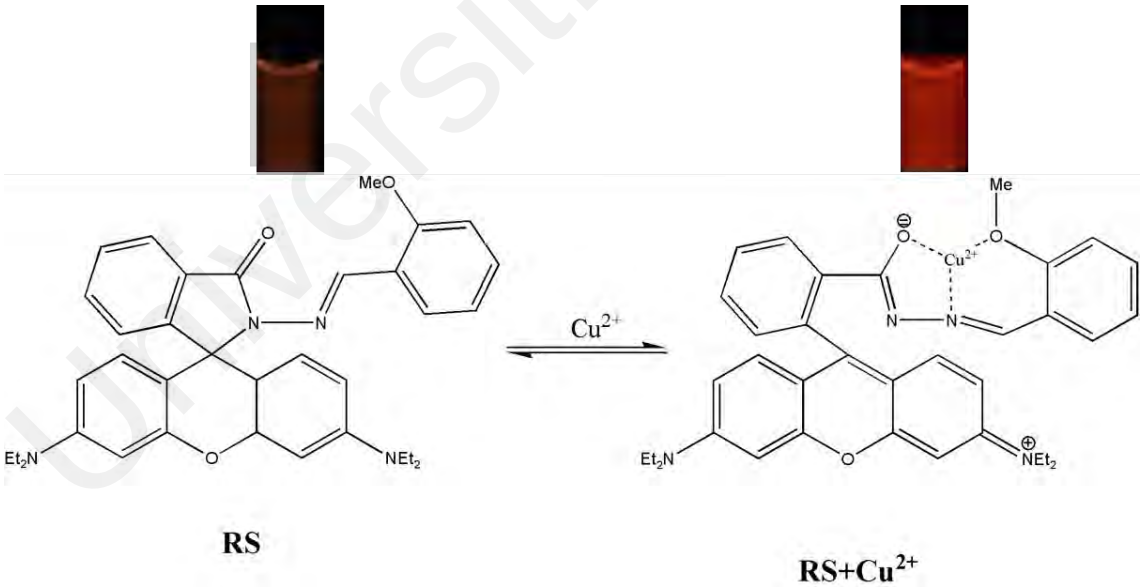

Figure 2.6 Proposed binding mechanism and fluorescence enhancement of RS upon recognition of Cu^{2+} (Dong et al., 2010).

Generally, chromogenic is a process that involves the production of colour or pigments which is useful in the means of identification. Therefore, chromogenic chemosensors would mean a change in colour upon detection of target analyte at molecular levels. Although the essence of chromogenic chemosensor is less attractive when compared to fluorescent/fluorogenic chemosensor, its ease of detection have been utilized in a few diagnostic assays which predominantly relies on change of colour, such as blood-glucose monitoring (Blake & McLean, 1989) and early pregnancy tests (Bangs, 1996). Furthermore, the basis of chromogenic sensors is also useful for in field contamination assessment, which is used in sensing explosive traces in soil (Erçağ et al., 2009).

The wide range of applications of chromogenic chemosensor is owed to its rapid colour change which could be seen via naked eyes. Because of this, the components and analysis techniques required are usually inexpensive, and easily operated without any need of experienced personnel. Other than that, the organic dyes to choose from in designing chromogenic chemosensors are not limited to fluorophores only. Making it more readily available and cost efficient as compared to fluorescent chemosensors. However, since chromogenic chemosensors are not very sensitive, therefore their limit of detection would not be as low as those of fluorogenic chemosensors.

The fundamental design in chromogenic chemosensors follows that of fluorogenic chemosensor (Martínez-Máñez & Sancenón, 2003). However, the signal pattern in fluorogenic and chromogenic chemosensors differs in such a way that, the former is usually clear signal whereby the sensor is "switch-on" from its off state. On the contrary, for chromogenic chemosensor, the signal pattern is either by a change in intensity of the colour (fixed wavelength) or by a change of one colour into another different colour (variable wavelength). In addition to that, the signal transduction (change in colour) for chromogenic chemosensors may be brought on by electron density, extent of conjugation, or dye formation (Bicker et al., 2011).

The signal transduction caused by the change in electron density and extent of conjugation is usually observed upon recognition of analyte or even change in pH. When the sensor is placed in an acidic medium, protonation of the molecule occurs. **Figure 2.7** shows an example of a protonated rhodamine based chemosensor (**RBOV**) in an acidic medium. As shown in the figure, rehybridization of **RBOV** have extended the conjugation of the molecule, causing a bathochromic shift in the visible region (400-700 nm), thus producing the purple colour of the solution. The bathochromic (red) shift in the visible region, attributed to the decrease in the highest occupied molecular orbital and lowest unoccupied molecular orbital (HOMO–LUMO) energy gap.

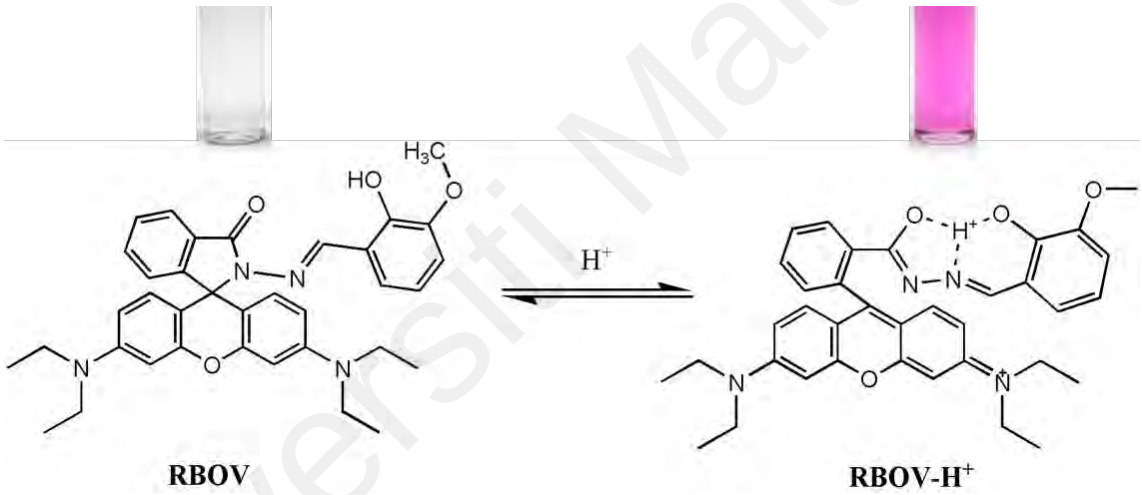

Figure 2.7 Bathochromic shift is observed due to the protonation of RBOV in acidic medium.

Figure 2.7 shows a great example for the first signal pattern of a chromogenic chemosensor. The second signal, which is by change of one colour into another different colour could be seen in **Figure 2.8**. The free coumarin-thiocarbonohydrazone (**CTC**) exhibit yellow colour in 40 % of acetonitrile (50 mM HEPES, pH 7.2) solution. In the presence of various metal ions, the colour changes from yellow to deep pink only upon

addition of Co^{2+}, showing a shift of the maximum absorption wavelength from 470 nm (yellow) to 510 nm (deep pink) (Maity & Govindaraju, 2011).

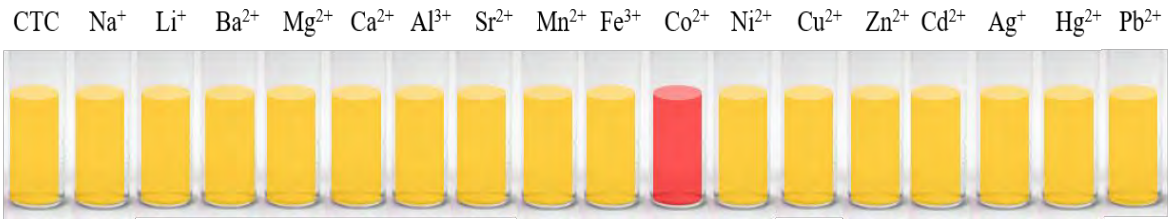

Figure 2.8 Colorimetric changes of CTC (10 µM) solution upon addition of various metal ions (50 µM) (Maity & Govindaraju, 2011).

Briefly, it is clear that fluorogenic and chromogenic sensors possess its own unique signal transduction that is beneficial in detection of metal ions, be it biologically or environmentally in sub-molar concentrations. Since each sensor system has its merits and limitations, a lot of researches have decided to incorporate the principle of these systems and developed sensors which exhibit both fluorometric and colorimetric properties. Where detection of single or multiple analytes could be done via different detection mode, either by fluorescence enhancement/quenching or by colorimetric changes. One instance, a sensor, **SPd3** was developed by reacting 1H-benzimidazole-2-ethanamine with a rhodamine B moiety, for the detection of Pd^{2+} via fluorogenic and chromogenic changes (Chen et al., 2016). While In multiple analytes detection, the rhodamine-based sensor, **RH,** detects Cu^{2+} and Al^{3+} through colorimetric sensing, and Fe^{3+} through fluorometric sensing (Gupta et al., 2016).

2.4 Xanthene Derivatives

As mentioned earlier, out of all the organic dyes that exists, those that are heterocyclic and highly conjugated would be the most feasible option in developing a probe. This is because, as the conjugation of a compound increases, the size of the fluorophore increases, thus enhancing the absorption and emission wavelength of the whole compound. Among various organic dyes developed, xanthene derivatives, especially rhodamines and fluoresceins (**Figure 2.9**) have been favoured due to their excellent photophysical properties such as high absorption coefficient, long emission wavelength, and impressive photostability (Zheng et al., 2013).

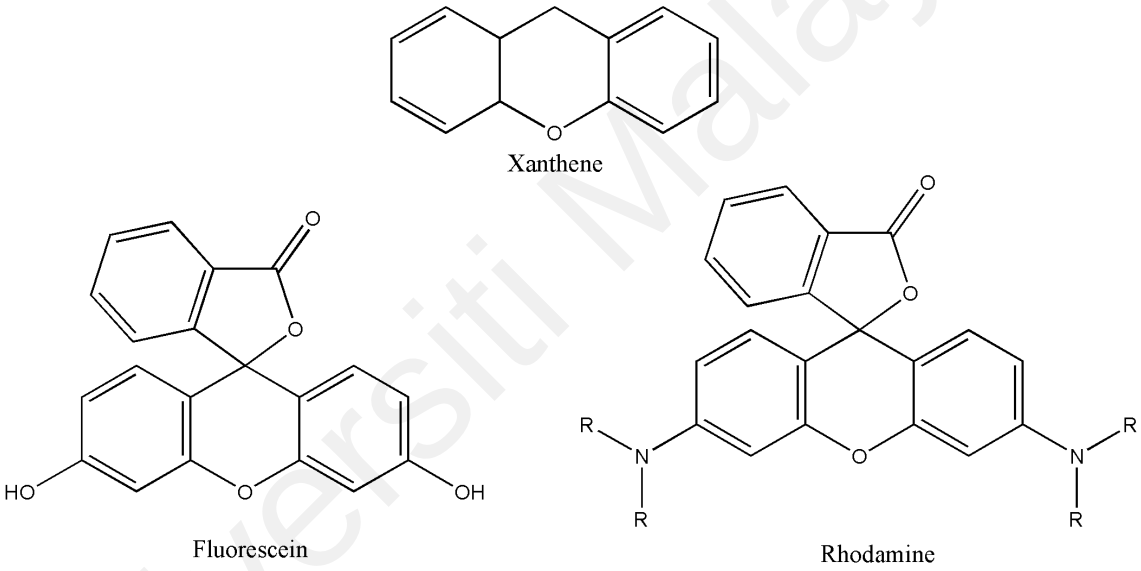

Figure 2.9 General structure of xanthene and its derivatives, fluorescein and rhodamine.

Fluorescein was originally prepared by Adolf von Bayer in 1871, by reacting phthalic anhydride and resorcinol in the presence of zinc chloride via the Friedel-crafts reaction (Baeyer, 1871). Owing to its excellent photophysical properties such as solubility, long excitation and emission wavelength at visible region, good photostability and excellent brightness at physiological pH (Chen et al., 2012), it's no wonder that fluorescein and its derivatives have been widely used in many applications. This includes but not limited to,

dye tracing, as colouring additives in food, drugs microscopy, DNA sequencing, and cellular microscopy (Duan et al., 2009; Giepmans et al., 2006). **Figure 2.9** shows fluorescein in its lactone form, in which it is non fluorescent. However, the ring opened form may induce colour change and fluorescence enhancement. **Figure 2.10** shows a a proposed mechanism for fluorescein derivative sensor, **1** with Cu^{2+}.

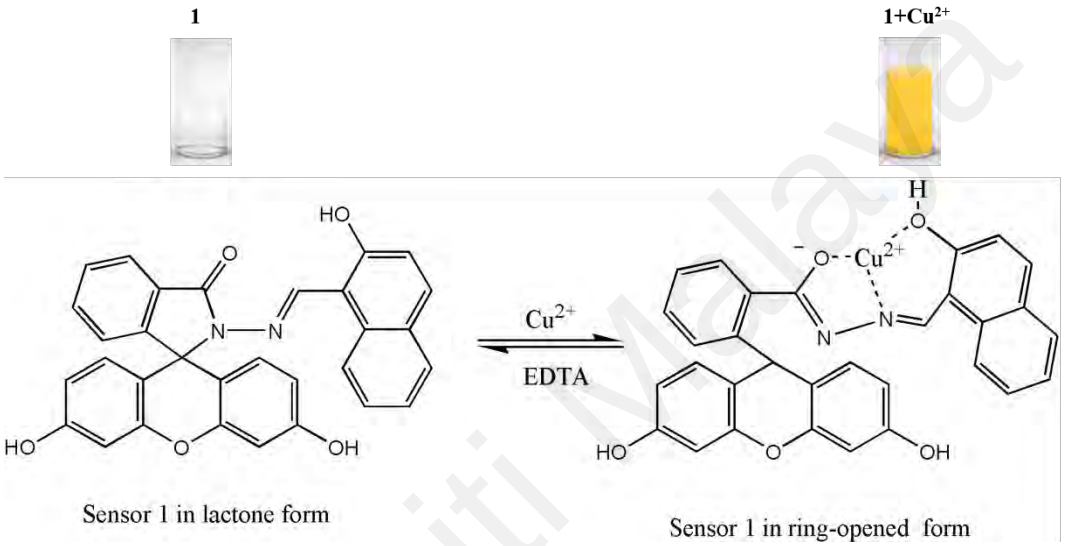

Figure 2.10 Proposed mechanism of fluorescence change of sensor 1 with Cu^{2+} (Abebe & Sinn, 2011).

The second infamous derivative of xanthene is rhodamine, which was first synthesized in 1905 (Noelting & Dziewoński, 1905). Even so, it was not until Czarnik and its group work back in 1997 that rhodamine B derivatives begin to garner attention of other chemists (Dujols et al., 1997). They reported a fluorescent chemodosimeter (rhodamine-B hydrazide) for detection of Cu^{2+}, where pink colour and fluorescence characteristic of rhodamine B appear instantaneously upon addition of $Cu(OAc)_2$, which is attributed to the open-ring form, a similar process to fluorescein shown in **Figure 2.10**. In the earlier days, rhodamine derivatives such as rhodamine 6G and rhodamine B has been used as laser dyes. These days, it is also used as fluorescent markers in flow cytometry, cell imaging, environmental sensors, and even as nerve gas sensors (Chen et al., 2012).

In hindsight, it is evident that spirocyclic derivatives of rhodamine and fluorescein are great choices in developing sensors. The unique ring-opening process which lead to a turn-on fluorescence and colour change provides rapid detection via naked-eyes and preliminary information on analyte present. Ever since the first rhodamine-based fluorescent chemosensor for Cu^{2+} was reported in 1997, numerous sensors utilizing the ring-opening process has been reported. Even so, there are more numbers of rhodamine based chemosensors published than that of fluorescein. This is because, several studies have shown the superiority of rhodamine over fluorescein.

In one instance, an experiment on fluorescein, rhodamine B and rhodamine 6G was conducted to evaluate the performance of these dyes that are used as tracers in water flow. From the experiment conducted, it was found that fluorescein is the least stable among the three. Furthermore, only rhodamine B and rhodamine 6G shows a linear response of fluorescence to the incident light at a concentration of 0.004 mg/L (Arcoumanis et al., 1990). The second study was on emission efficiency of green fluorescent dyes after internalization into cancer cells, which includes fluorescein, rhodamine green, Oregon green and BODIPY-FL, that was done by Kobayashi and his colleagues back in 2006. Although Av-FITC (fluorescein) shows the brightest fluorescence *in vitro*, after the chemical changes induced by the low pH of lysosome/endosome (*in vivo*), it was found that Av-RhodG (Rhodamine Green) demonstrated the brightest fluorescence (Hama et al., 2006). Another emission study for single-color fluorescence immunocytochemistry has also shown the superiority of rhodamine over fluorescein (Wessendorf & Brelje, 1992).

2.5 Schiff-base based chemosensors

The first Schiff base was reported and named after Hugo Schiff back in 1864 (Schiff, 1864). Basically, Schiff bases are compounds that contain the azomethine group (-C=NR) that are the products of condensation of ketones or aldehydes with primary amines in which the C=O group of ketone or aldehyde is replaced by the C=N-R group. In addition to that, the condensation reaction in forming Schiff base ligands with aldehydes are typically more reactive and formed readily than with ketone. This is because, there is less steric hindrance and more partial positive charge in aldehyde, than that of ketone.

In synthesizing Schiff base compound, aromatic aldehydes and amines especially with an effective conjugation system are highly preferred than aliphatic aldehydes and amines as they are known to be more stable (Atta et al., 2006). Essentially, the Schiff bases forms stable complexes with metal ions, where it chelates either by forming bi, tri or tetra-dentate ligands (Xavier & Srividhya, 2014). Therefore, it is important to design and develop Schiff base derivatives with nitrogen and oxygen rich atoms as receptors as it will establish better stability upon binding with metal ions and stronger fluorescence sensing properties.

Scheme 2.4 shows the synthesis of the first C_3-symmetric Schiff-base fluorescent chemosensor, tris(2-pyridinecarboxaldehyde)triaminoguanidinium chloride (**L**), that could detect Zn^{2+} in 100% aqueous media. **L** sensor has showed a sensitive fluorescence turn-on property with detection limit as low as 2.5 μM upon recognition of Zn^{2+}. By enhancing the coplanarity of the conjugated system, the fluorescence sensing of sensor **L**-Zn^{2+} was not affected in pH 7-10, which enable its intracellular monitoring in physiological pH (Zhou et al., 2012). This is not surprising as Schiff base ligands have been known to be used as pigments, dyes, and catalysts because of their high thermal and moisture stability. Furthermore, they have also been reported to show some degree of

biological properties which includes, antifungal, antibacterial, anticancer, antimalarial and antiviral activity (da Silva et al., 2011; Pryzbylski et al., 2009; Savir et al., 2020).

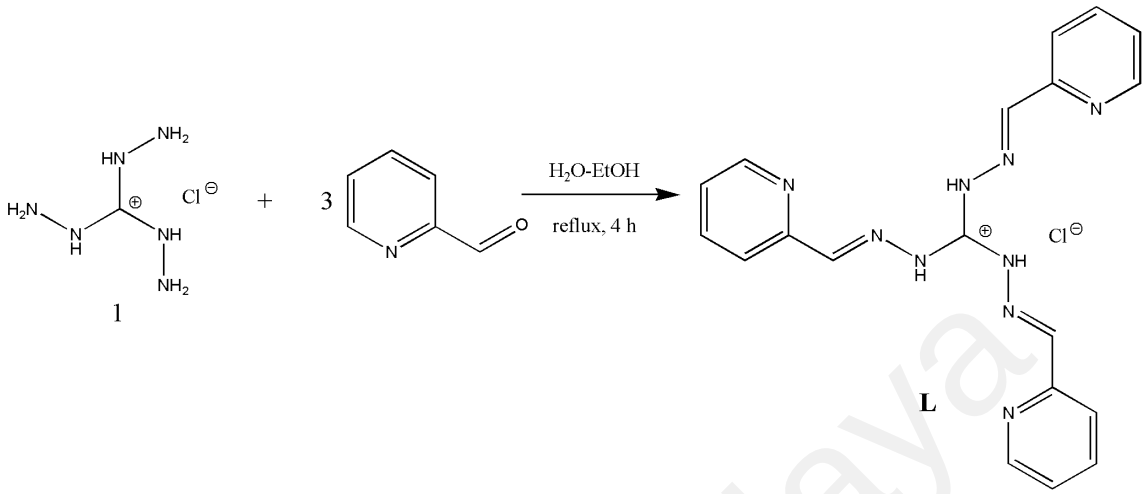

Scheme 2.4 Synthesis of fluorescent sensor L (Zhou et al., 2012).

2.6 Rhodamine B Schiff-base chemosensors

Since the report of Czarnik's rhodamine-B hydrazide, plenty of exciting papers on the utilization of the unique ring-opening process of the spirolactam ring have been published. The first rhodamine hydrazone synthesized by Tong (Xiang et al., 2006) from Czarnik's rhodamine has shown a high selectivity and sensitivity towards detection of Cu^{2+}. They reported that the sensor (**9**) exhibit selective fluorescent sensing and opening of the spirolactam ring upon detection of Cu^{2+} in 50% CH_3CN (v/v, 1:1, 10 mM tris-HCl buffer, pH 7.0) solution (**Scheme 2.5**).

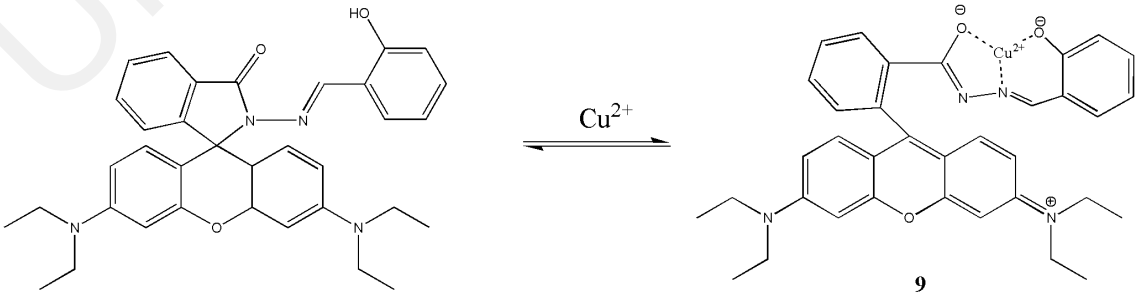

Scheme 2.5 Proposed binding mode of sensor 9 with Cu^{2+} (Xiang et al., 2006).

Earlier, it was briefly mentioned that the detection of metal ions by sensors are also affected by the pH and solvent medium. Czarnik's rhodamine B hydrazide sensor has shown a selective detection towards Cu^{2+} in 20 % CH_3CN (0.01 HEPES buffer, pH 7) solution. However, in 2007, Kim and his team has reported rhodamine B hydrazide as a selective chemodosimeter for Hg^{2+} (Kim. et al., 2008). In this work, they have reported that the sensor has a detection limit of 0.2 μM in an acetate-buffered aqueous with 10% methanol solution at pH 5. Similar "switch-on" signalling mechanism was observed upon detection of Hg^{2+} which induced the hydrolysis of the spirolactam ring as that of Czarnik's towards Cu^{2+}.

Besides that, the extent of conjugation and presence of nitrogen and oxygen atoms of the sensor has also been discussed earlier. Since the first rhodamine hydrazone was reported by Tong, few of its derivatives displaying unique sensing properties and applications has been reported. One example can be seen where a sensor, **RH** has been synthesized by Gupta and his team as shown in **Scheme 2.6**. It was reported that **RH** was able to act as multianalyte sensor, where it detects Cu^{2+} and Al^{3+} through colorimetric sensing, while Fe^{3+} through fluorometric sensing in 50 % of methanol solution. Herein, it was also reported that the colorimetric sensing of Cu^{2+} and Al^{3+} could be differentiated by altering the pH. It was observed that detection of Cu^{2+} by **RH** was not affected at pH 6-10. On the other hand, there was no distinct colour change in the detection of Al^{3+} by **RH** at pH 7-10.

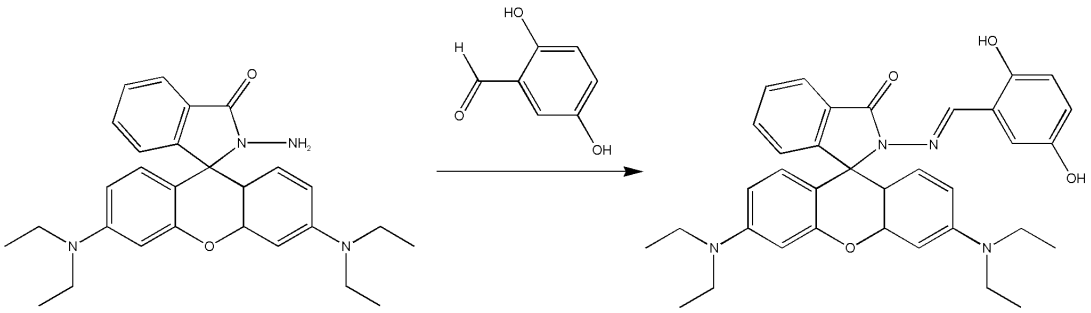

Rhodamine B Hydrazide **RH**

Scheme 2.6 Synthesis of sensor RH from rhodamine B hydrazide (Gupta et al., 2016).

Another rhodamine B based salicylaldehyde hydrazone sensor (**10**) was synthesized by reacting 4-*N,N*-diethylaminosalicylaldehyde with rhodamine B hydrazide (Li et al., 2014). This sensor shows a unique photochromic property upon complexation with Zn^{2+} in THF. This unique property could be observed in **Figure 2.11**, where solution containing **10**-Zn^{2+} complex changes from light-yellow (closed-ring) to purple (opened-ring) gradually upon irradiation at 365 nm. Once the UV source was removed, it changes back to light-yellow colour in a span of 10 minutes.

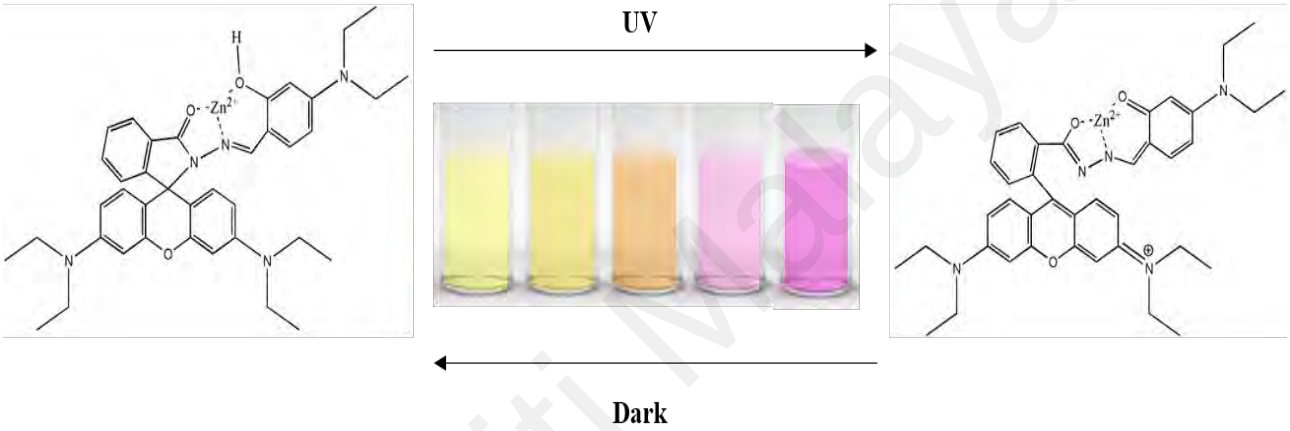

Figure 2.11 Colorimetric and proposed mechanism of sensor 10 upon UV irradiation of 10-Zn^{2+} in THF (Li et al., 2014).

These days, chemosensor for detection of multiple metal ions by altering the pH and solvent system has been reported more as it is more cost efficient than single analyte sensors. For instance, rhodamine B hydrazide was reacted with 2-formylphenyl boronic acid to produce sensor **11**, which is able to detect Cu^{2+} through colorimetric sensing in 50 % ethanol solution. By altering the solvent system, sensor **11** was able to detect Al^{3+} and Fe^{3+} through fluorometric sensing in pure ethanol. The detection of **11** towards Al^{3+} and Fe^{3+} was also easily differentiated as they exhibit different maximum emission wavelength of 580 nm and 572 nm respectively (Tang et al., 2017).

Aside from single analyte sensors, numerous multiple analyte sensors with different sensing mode without the need of altering the solvent medium has also been published. A bifunctional chemosensor (**RHDN**) for the recognition of Cu^{2+} and Zn^{2+} has been synthesized from the condensation reaction of 3,5-dinitrosalicylaldehyde with rhodamine B hydrazide. The free **RHDN** (10 μM) displays light-yellow colour in CH_3CN/HEPES buffer (1 mM, pH 7.2; 7:3 v/v) solution. However, upon addition of metal ions, only Cu^{2+} (10 equivalent) showed a colour change from light-yellow to pink. On the other hand, when placed under the UV light, an intense fluorescence from **RHDN**-Zn^{2+} was observed, exhibiting a selective "turn–on" fluorescence sensing for Zn^{2+} (Rai et al., 2015).

CHAPTER 3: METHODOLOGY

3.1 Materials and Solutions

The chemicals used for synthesis (rhodamine B, hydrazine hydrate, 2-hydroxy-3-methoxybenzaldehyde, fluorene-2-carboxaldehyde, trans-4-(Diethylamino)cinnamaldehyde, and 3,4,5-trimethoxybenzaldehyde) were purchased from Sigma Aldrich, Merck and Alfa Aesar. The solvents used (ethanol, DMF, DMSO, chloroform, acetonitrile) were purchased from Merck. Analytical grade of nitrate and chloride salts of the metal ions used for analysis were purchased from Merck and Alfa Aesar. Distilled deionized water were used for preparations of buffer and metal ions stock solutions.

3.2 Physical Measurements

FT-IR spectra were recorded on a Perkin-Elmer Spectrum RX-1 spectrometer using the ATR method. NMR were recorded in deuterated $CHCl_3$ on a JEOL ECX 400 MHz instrument. UV-vis analysis was conducted on a Shimadzu UV-2600 series spectrophotometer while Cary Eclipse fluorescence spectrophotometer was utilized for fluorescence measurements. Jeol AccuTOF Mass Spectrometer was used to perform the mass spectrometry. X-ray crystallography was done on the Rigaku Oxford Super Nova Dual diffractometer with Mo-Kα X-ray source (λ =0.71073 Å). The melting point was recorded using the Mel-Temp II apparatus.

3.3 Syntheses

3.3.1 Synthesis of Rhodamine B Hydrazide, RBH

Synthesis of rhodamine B hydrazide, RBH follows a straightforward path with some modifications from a previous described method (Dujols et al., 1997). 10 mL of ethanol was added to a round bottom flask containing rhodamine B (0.5 g, 1.0 mmol). Hydrazine hydrate (1.0 mL) was then added dropwise. After it was refluxed for 6 hours, it was then extracted with dilute hydrochloric acid (HCl) and sodium hydroxide (NaOH). Finally, the

precipitate is left to dry and was then recrystallise with DMF. The RBH obtained was then characterized by using FTIR, ^{1}H NMR and ^{13}C NMR. Yield = 0.388 g, 85% . FT-IR (cm^{-1}, s = strong; m = medium; w = weak): 3327 w, 2963 m, 2922 m, 1716 m, 1687 m, 1613 s, 1515 s, 1216 s, 1117 s. **^{1}H NMR** (400 MHz, $CHCl_3$-d, s = singlet; d= doublet; t = triplet; q = quadruplet; m = multiplet), δ (ppm): 1.15 (t, 12H, NCH_2CH_3); 3.32 (q, 8H,NCH_2CH_3); 3.60 (s, 2H, NH_2); 6.28 (dd, 2H, Xanthene-H); 6.41 (d, 2H, Xanthene-H); 6.45 (d, 2H, Xanthene-H); 7.09 (m, 1H); 7.43 (m, 2H); 7.92 (m, 1H) (Aromatic-H). **^{13}C NMR** (400 MHz, $CHCl_3$-d), δ (ppm): 12.70 (NCH_2CH_3); 44.45 (NCH_2CH_3); 6.01 (C-N); 98.03, 104.61, 108.10, 123.07, 123.91, 128.18, 130.11, 132.60, 148.96, 151.64, 153.94 (Aromatic-C); 166.24 (C=O). Melting point: 180-182 °C.

3.3.2 Synthesis of Rhodamine B 2-hydroxy-3-methoxybenzaldehyde, RBOV

RBOV was synthesized by reacting 2-hydroxy-3-methoxybenzaldehyde (also known as ortho-vanillin) with RBH in ethanol. To a 100 mL flask, rhodamine B hydrazide (0.20 g, 0.4 mmol) was dissolved in 25 mL ethanol, and ortho-vanillin (0.06 g, 0.4 mmol) was added into the mixture and refluxed for 6 hours. The reaction mixture was then concentrated and dried at room temperature. Red product obtained was then recrystallised with ethanol and placed in room temperature for slow evaporation. Yield = 0.194 g, 82%. FT-IR (cm^{-1}, s = strong; m = medium; w = weak): 3388 m, 2965 m, 2926 w, 1715 s, 1686 s, 1612 s, 1515 s, 1217 s, 1117 s. **^{1}H NMR** (400 MHz, DMSO-d_6, TMS, s = singlet; d= doublet; t = triplet; q = quadruplet; m = multiplet), δ (ppm): 1.01 (t, 12H, NCH_2CH_3); 3.24 (q, 8H, NCH_2CH_3); 3.67 (s, 3H, O-CH_3); 6.28 (d, 1H, Xanthene-H); 6.30 (d, 1H, Xanthene-H); 6.37 (q, 4H, Xanthene-H); 6.70 (t, 1H, Xanthene-H); 6.83 (dd, 1H, Aromatic-H); 6.89 (dd, 1H, Aromatic-H); 7.05 (d, 1H, Aromatic-H); 7.55 (m, 2H, Aromatic-H); 7.87 (dd, 1H, Aromatic-H); 9.07 (s, 1H, imine-H); 10.18 (s, 1H, C-OH). **^{13}C NMR** (400 MHz, DMSO-d_6, TMS), δ (ppm): 12.89 (NCH_2CH_3); 44.17 (NCH_2CH_3); 56.19 (O-CH_3); 66.05 (C-N); 97.74, 105.19, 108.64,

114.32, 119.54, 121.12, 123.59, 124.37, 128.21, 129.30, 134.55, 148.32, 149.04, 150.38, 151.53, 153.22 (Aromatic-C); 147.40 (C=N); 164.12 (C=O). HRESIMS m/z calculated for $C_{36}H_{39}N_4O_4$ $[M+H]^+$= 591.2978; found = 591.2971. Melting point: 176-178 °C.

3.3.3 Synthesis of Rhodamine B fluorene-2-carboxaldehyde, RFC

RFC was synthesized by reacting RBH with fluorene-2-carboxaldehyde in ethanol. To a 100 mL flask, rhodamine B hydrazide (0.20 g, 0.4 mmol) was dissolved in 15 mL ethanol, and fluorene-2-carboxaldehyde (0.08 g, 0.4 mmol) was added into the mixture and refluxed for 5 hours. The reaction mixture was then concentrated and dried at room temperature. Orange product obtained was then recrystallised with DMF and placed in room temperature for slow evaporation. Yield = 0.152 g, 60%. FT-IR (cm^{-1}, s = strong; m = medium; w = weak): 2969 m, 2929 w, 1676 s, 1614 s, 1514 s, 1303 s, 1217 s, 1118 s. **^{1}H NMR** (400 MHz, $CHCl_3$-d, s = singlet; d = doublet; t = triplet; q = quadruplet; m = multiplet), δ (ppm): 1.15 (t,12H, NCH_2CH_3); 2.90 (d, 1H); 3.32 (q, 8 H, NCH_2CH_3); 3.83 (s, 2 H); 6.24 (dd, 2 H); 6.46 (d, 2 H), 6.55 (d, 2 H)(Xanthene-H); 7.11 (dd, 1H), 7.29 (m, 1H), 7.48 (m, 4H), 7.65 (d, 1H), 7.72 (d, 1H), 7.81 (s, 1H), 8.01 (dd, 1H) (Aromatic-H); 8.56 (s, 1 H, imine-H). **^{13}C NMR** (400 MHz, $CHCl_3$-d, TMS), δ (ppm):12.71 (NCH_2CH_3); 36.83; 44.41 (NCH_2CH_3); 65.95 (C-N); 97.99, 106.05, 108.19, 119.61, 120.26, 123.70, 125.15, 127.16, 128.31, 129.10, 133.42, 134.03, 141.24, 143.36, 144.00, 149.05, 152.23, 153.09 (Aromatic-C); 147.21 (C=N); 165.16 (C=O). Melting point: 174-176 °C. CCDC: 2064878.

3.3.4 Synthesis of Rhodamine B trans-4-(Diethylamino)cinnamaldehyde, RT4

RT4 was synthesized by reacting trans-4-(Diethylamino)cinnamaldehyde (0.08 g, 0.4 mmol) with RBH (0.20 g, 0.4 mmol) in 20 mL of ethanol. After a 5 hours reflux, the reaction mixture was then concentrated and dried at room temperature. The yellow precipitate obtained was then recrystallised with DMF and placed in room temperature for slow evaporation. Yield = 0.180 g, 70%. FT-IR (cm^{-1}, s = strong; m = medium; w =

weak): 2969 m, 2930 w, 1678 s, 1597 s, 1515 s, 1305 s, 1219 s, 1117 s. **^{1}H NMR** (400 MHz, $CHCl_3$-d, s = singlet; d = doublet; t = triplet; q = quadruplet; m = multiplet), δ (ppm): 1.14 (t,18H, NCH_2CH_3); 2.59 (s, 2H); 2.90 (d, 1H); 3.32 (m, 12H, NCH_2CH_3); 6.25 (dd, 2H); 6.43 (d, 2H), 6.54 (d, 3H); 6.65 (m,1H)(Xanthene-H); 7.03 (m, 1H), 7.20 (d, 1H), 7.40 (m, 2H), 7.96 (m, 1H (Aromatic-H); 8.10 (d, 1 H, imine-H). **^{13}C NMR** (400 MHz, $CHCl_3$-d, TMS), δ (ppm): 12.74 (NCH_2CH_3); 44.44 (NCH_2CH_3); 65.60 (C-N); 98.05, 105.92, 108.23, 111.43, 122.17, 123.39, 123.48, 123.56, 127.97, 128.10, 128.62, 130.96, 133.19, 139.90, 148.99, 150.56, 152.71, 152.83 (Aromatic-C); 148.14 (C=N); 165.19 (C=O). Melting point: 200-202 °C. CCDC: 2064879.

3.3.5 Synthesis of Rhodamine B 3,4,5-trimethoxybenzaldehyde, R3

R3 was synthesized by reacting RBH (0.20 g, 0.4 mmol) with 3,4,5-trimethoxybenzaldehyde in ethanol. After 4 hours reflux, the reaction mixture was concentrated and dried at room temperature. White product obtained was then recrystallised with DMF and placed in room temperature for slow evaporation. Yield = 0.216 g, 85%. FT-IR (cm^{-1}, s = strong; m = medium; w = weak): 2967 m, 2931 w, 1686 s, 1606 s, 1506 s, 1314 s, 1232 s, 1117 s. **^{1}H NMR** (400 MHz, $CHCl_3$-d, s = singlet; d = doublet; t = triplet; q = quadruplet; m = multiplet), δ (ppm): 1.17 (t,12H, $NCH_2\mathbf{CH_3}$); 2.16 (s, 1H); 3.31 (q, 8H, $N\mathbf{CH_2}CH_3$); 3.81 (d, 9H, OCH_3); 6.23 (dd, 2H); 6.41 (d, 2H,); 6.49 (d, 2H); 6.79 (s, 2H) (Xanthene-H); 7.17 (dd, 1H), 7.50 (m, 2H) 7.97 (d, 1H) (Aromatic-H); 8.78 (d, 1H, imine-H). **^{13}C NMR** (400 MHz, $CHCl_3$-d, TMS), δ (ppm): 12.67 (NCH_2CH_3); 44.42 (NCH_2CH_3); 56.15; 60.96 (O-CH_3); 66.49 (C-N); 97.77, 104.42, 106.57, 107.97, 123.42, 124.14, 128.17, 128.53, 130.35, 131.33, 133.34, 139.48, 148.99, 150.91, 153.17, 153.70 (Aromatic-C); 147.03 (C=N); 163.68 (C=O). Melting point: 152-154 °C.

3.4 X-ray Crystallography

The x-ray single crystal data of RFC, RT4 and R3 were collected at room temperature by using Oxford Rigaku SuperNova Dual diffractometer equipped with a Mo-Kα X-ray source (λ =0.71073 Å) with Atlas detector to generate the unit cell parameter and intensity data. Cell refinement, data acquisition and reduction were carried out with CrysAlis Pro software (CrysAlis, 2009). The structures were solved by direct methods and refined by using SHELXL-97 (Sheldrick, 2008). Crystal visualization of these compounds were done by using Mercury CSD 2.0 (Macrae et al., 2008) while the crystallographic information was edited and formatted by using publCIF (Westrip, 2010).

3.5 Selectivity Studies

The spectral assay was investigated with different metal ions including, Ag^{+}, Al^{3+}, Ca^{2+}, Cd^{2+}, Co^{2+}, Cu^{2+}, Fe^{3+}, La^{3+}, Mn^{2+}, Na^{+}, Ni^{2+}, Pb^{2+}, Sn^{2+} and Zn^{2+}. The metal ion stock solutions (100 mM) were prepared in distilled water. While the sensor stock solutions (100 mM) were prepared in DMF (RBOV, RT4), chloroform (RFC) and acetonitrile (R3). Then, fixed concentration of chemosensors would be added into their respective solvent system containing known concentration of metal ions. All colorimetric changes as seen by the naked-eyes were further recorded using the UV-vis spectrometer while fluorometric changes were recorded by the fluorescence spectrometer.

3.6 Effects of pH

The effect of pH on the absorbance and fluorescence response of the sensor towards metal ions was evaluated to determine the suitable pH in which the sensor could be used efficiently. The pH was varied from 2-12 by adjusting the acidity and alkalinity of the solvent system by using dilute hydrochloric acid, HCl and sodium hydroxide, NaOH.

3.7 Titration Experiments

Sensitivity of the chemosensors were investigated by conducting UV-vis and fluorescence titration experiments. In this assay, the concentration of the sensors was fixed while the concentration of metal ions was gradually increased until it reaches the saturation point. This was done by pipetting known amount of metal ions to sensor solution until the absorption/emission intensity centered at their respective λ_{max} no longer increased, which implied that the interaction between chemosensors and metal ions reached an equilibrium. Repetition of the experiment was done in order to confirm the point of saturation. The data acquired from this assay were further used to calculate the association constant, K_a and limit of detection, LOD of these chemosensors.

3.7.1 Limit of Detection, LOD

From the titration experiments conducted, by plotting a graph of absorbance/fluorescence against concentration of metal ions, the LOD of the chemosensors were determined. The LOD of the sensors towards metal ions were calculated based on equation 3.1. S_d is the standard deviation of blank measurement and m is the slope between absorbance/fluorescence intensity and the concentration of metal ions.

$$DL = 3S_d/m \tag{3.1}$$

3.7.2 Association Constant, K_a

The association constant, K_a of the chemosensors were determined by using the Benesi-Hildebrand equations (Benesi & Hildebrand, 1949; Tayade et al., 2014) as follow

$$\frac{1}{A-A_0} = \frac{1}{K_a(A_{max}-A_0)[M^{n+}]} + \frac{1}{A_{max}-A_0} \quad (3.2)$$

$$\frac{1}{F-F_0} = \frac{1}{K_a(F_{max}-F_0)[M^{n+}]} + \frac{1}{F_{max}-F_0} \quad (3.3)$$

A/F and A_0/F_0 is the absorbance/fluorescence of chemosensor in the presence and absence of M^{n+} respectively; A_{max}/F_{max} is the saturated absorbance/fluorescence in the presence of excess amount of M^{n+}; while $[M^{n+}]$ is the concentration of metal ions added. From the equation, by plotting a graph of $1/(A-A_0)$ or $1/(F-F_0)$ versus $1/[M^{n+}]$, linear regression equation was obtained. Through the slope and intercept, K_a of the chemosensors were able to be determined.

3.8 Competitive Studies

The anti-interference property of the chemosensors toward metal ions were studied by conducting the competitive experiment. In this assay, equivalent concentration of chemosensor and metal ions were used. The chemosensor will be added into the system containing the target analyte and competing metal ions. The change in absorbance/fluorescence were then recorded and compared with the controlled (absence of other competing metal ions) system.

3.9 Plausible Binding Mechanism

The complexation of sensor-metal ions was further confirmed by FT-IR and ^{1}H NMR spectra.

3.9.1 Job's Plot

To further determine the recognition mode of chemosensors with metal ions detected, Job's plot was carried out by using UV-vis spectroscopy. In this study, the molar concentration of metal ions was varied from 0 to 1 while the total concentration of metal ions and chemosensor was fixed. By plotting a graph of absorbance versus the molar concentration of metal ions, the intercept of the linear regression lines was taken as the binding stoichiometry for the complexation of sensor with metal ions.

3.9.2 FT-IR Spectra of Sensor-Metal Complexes

The sensor-metal complexes of RBOV, RFC, RT4 and R3 with their respective metal ions were synthesized by reacting the sensor (0.10 g, 0.1 mmol) with the respective metal salts (0.2 mmol) in ethanol. The solution was then concentrated and left to evaporate in room temperature. The solid obtained was then collected and characterized by FTIR.

3.9.3 ^{1}H NMR Spectra of Sensor-Metal Complexes

The ^{1}H NMR spectra analysis of sensor and sensor-metal complexes were carried out by preparing three separate tubes in the order of, sensor, sensor-metal ions (2 equivalent), and sensor-metal ions (4 equivalent) in deuterated chloroform. The shifting and broadening of the peaks were compared and recorded.

3.10 Practical Application

In order to investigate the practicality of the sensors developed, reversibility, on-site assay kit and MTT assay were done.

3.10.1 Reversibility

The reversibility of the sensors was studied by utilizing EDTA (0.5 M) solution. In this assay, the absorbance/fluorescence intensity of sensor-metal complex before and after addition of EDTA, and re-addition of metal ions into the solvent system were measured and recorded. The process was repeated for several cycles until the intensity is 50% lesser than the initial value.

3.10.2 On-site Assay Kit

The in-situ practicality of sensors was also investigated by immersing filter paper into solution containing known concentration of sensors for 5 minutes and dried in air. Then, the coated filter papers were immersed in different concentration of metal ions and dried in air. All color changes of the filter papers were recorded.

3.10.3 MTT Assay

In order determining the cytotoxicity of RBOV, RFC, RT4 and R3 sensors, MTT assay was conducted on the human colorectal adenocarcinoma (HT-29) and normal (CCD-18Co) cell lines with cisplatin as the positive control. The cells were cultured in McCoy's 5A medium (HT-29), and T75 medium (CCD-18Co), supplemented with 10% fetal bovine serum and incubated at 37◦C in a humidified atmosphere containing 5% CO_2.

The MTT assay was performed as described by Mosmann with modifications (Heng et al., 2020). Briefly, the HT-29 (2×10^3 cells/well) and CCD-18Co (10×10^3 cells/well) cells were seeded into a 96-well microplate and incubated overnight prior the treatment with various concentrations of sensor. After 72 h of incubation, 20 µL of MTT solution (5 mg/mL) was added into each well and incubated for another 3 h. The medium was then removed, and the formazan crystals were dissolved in 200 µL of DMSO. The absorbance of each well was measured using Tecan M200 Infinite Pro Microplate Reader at 570 nm with 650 nm as reference wavelength. Cisplatin was used as positive control in this study. The data was expressed as mean ± standard deviation of triplicate experiments.

CHAPTER 4: RESULTS AND DISCUSSION

4.1 Synthesis of Rhodamine B Hydrazide and Rhodamine B Chemosensors

4.1.1 Synthesis of Rhodamine B Hydrazide, RBH

The reaction of rhodamine B with hydrazine hydrate in ethanol yielded rhodamine B hydrazide with chemical formula, $C_{28}H_{32}N_4O_2$ as seen in **Scheme 4.1**. Colour change of reaction mixture from purple to light orange was observed after refluxing. Subsequent addition of HCl to the solution causes it to change from orange to clear red and finally peach coloured solution. Upon adding excess NaOH to the solution, precipitates were immediately observed. Recrystallization of the product with absolute ethanol yielded purple solid (yield: 85.0%) and its structure was confirmed by FTIR, ^{1}H NMR and ^{13}C NMR.

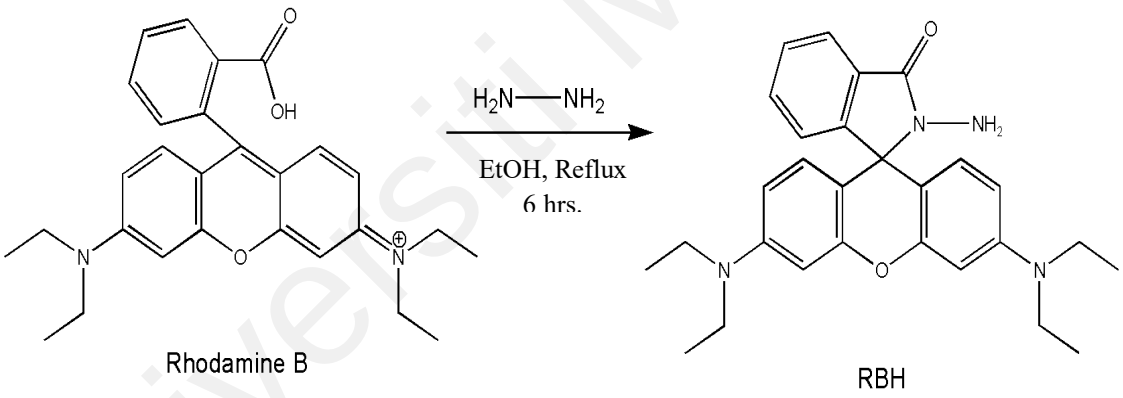

Scheme 4.1 Synthesis of Rhodamine B Hydrazide (RBH).

4.1.2 Synthesis of Rhodamine B 2-hydroxy-3-methoxybenzaldehyde, RBOV

The reaction of rhodamine B hydrazide, RBH with 2-hydroxy-3-methoxybenzaldehyde (ortho-vanillin) in ethanol yielded rhodamine B Schiff-base sensor, RBOV with chemical formula, $C_{36}H_{38}N_4O_4$ as seen in **Scheme 4.2**. Recrystallization of RBOV with DMF yielded red crystals (yield: 82.0%) and its structure was confirmed by FTIR, ^{1}H NMR, ^{13}C NMR, and mass spectroscopy.

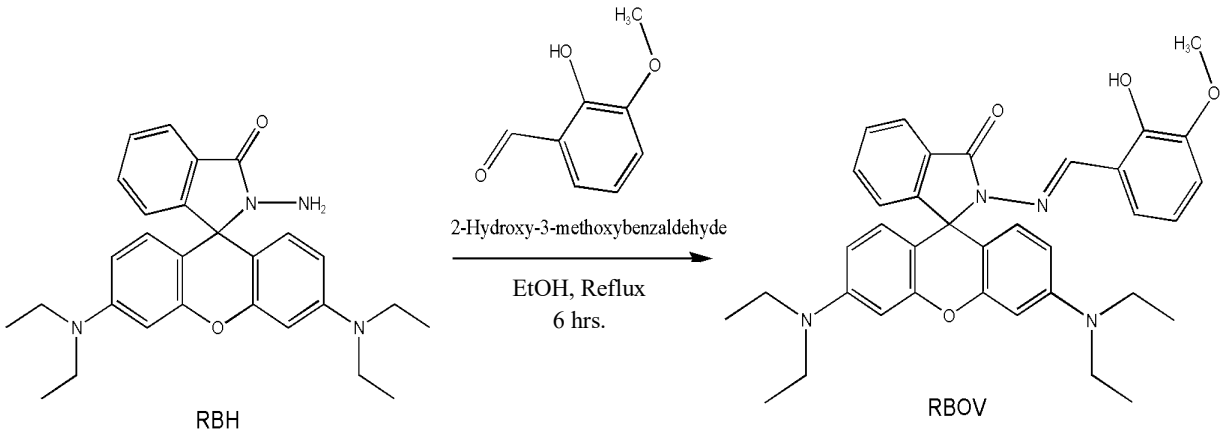

Scheme 4.2 Synthesis of Rhodamine B-2-Hydroxy-3-methoxybenzaldehyde (RBOV).

4.1.3 Synthesis of Rhodamine B fluorene-2-carboxaldehyde, RFC

The reaction of rhodamine B hydrazide, RBH with fluorene-2-carboxaldehyde in ethanol yielded rhodamine B Schiff-base sensor, RFC with chemical formula, $C_{42}H_{40}N_4O_2$ as seen in **Scheme 4.3**. Recrystallization of RFC with DMF yielded orange crystals (yield: 60.0%) and its structure was confirmed by FTIR, ^{1}H NMR, ^{13}C NMR, and x-ray crystallography.

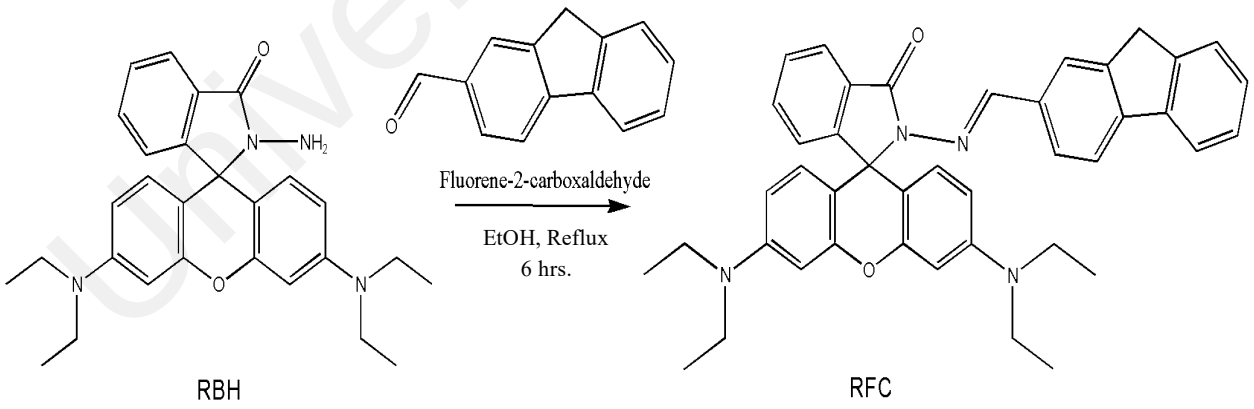

Scheme 4.3 Synthesis of Rhodamine B-Fluorene-2-carboxaldehyde (RFC).

4.1.4 Synthesis of Rhodamine B trans-4-(Diethylamino)cinnamaldehyde, RT4

The reaction of rhodamine B hydrazide, RBH with trans-4-(Diethylamino)cinnamaldehyde in ethanol yielded rhodamine B Schiff-base sensor, RT4 with chemical formula, $C_{41}H_{47}N_5O_2$ as seen in **Scheme 4.4**. Recrystallization of RT4 with DMF yielded orange crystals (yield: 70.0%) and its structure was confirmed by FTIR, ^{1}H NMR, ^{13}C NMR, and x-ray crystallography.

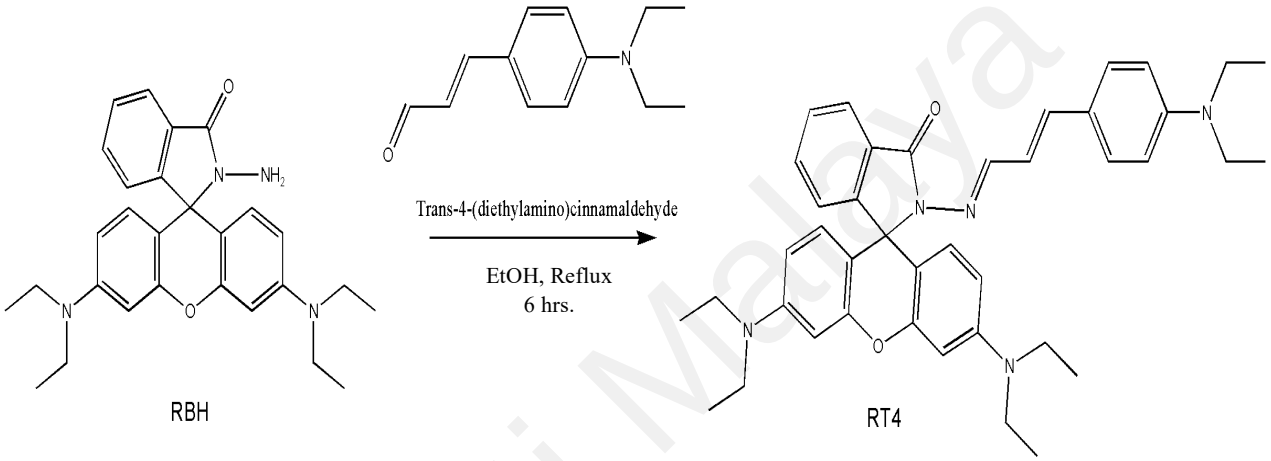

Scheme 4.4 Synthesis of Rhodamine B-Trans-4-(Diethylamino)cinnamaldehyde (RT4).

4.1.5 Synthesis of Rhodamine B 3,4,5-trimethoxybenzaldehyde, R3

The reaction of rhodamine B hydrazide, RBH with 3,4,5-trimethoxybenzaldehyde in ethanol yielded rhodamine B Schiff-base sensor, R3 with chemical formula, $C_{38}H_{42}N_4O_5$ as seen in **Scheme 4.5**. Recrystallization of R3 with DMF yielded white crystals (yield: 85.0%) and its structure was confirmed by FTIR, ^{1}H NMR, ^{13}C NMR, and x-ray crystallography.

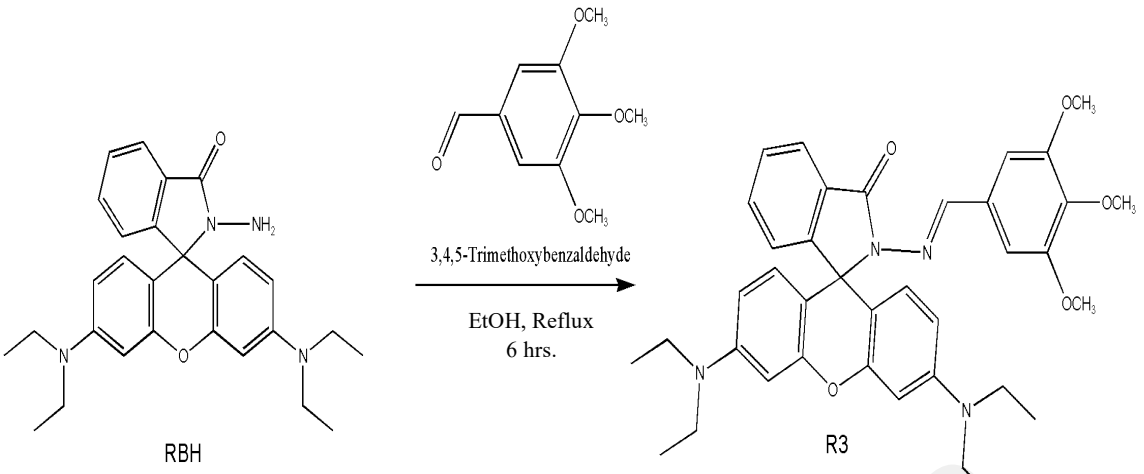

Scheme 4.5 Synthesis of Rhodamine B-3,4,5-Trimethoxybenzaldehyde (R3).

4.2 FT-IR Spectra

The main IR vibrational bands of RBH, RBOV, RFC, RT4 and R3, were found in their expected regions as shown in **Table 4.1** and their characteristic IR bands were listed in the experimental section. Formation of the Schiff-base sensors by condensation was indicated by the disappearance of the characteristic peak of amine group $\nu(NH_2)$ at 3327 cm^{-1} in RBH. The Schiff-base formation was further confirmed by the strong band attributed to imine linkage, ν(R2C=NR) observed at 1612 cm^{-1}, 1614 cm^{-1}, 1597 cm^{-1} and 1606 cm^{-1} for RBOV, RFC, RT4 and R3 respectively. In addition to that, a broad peak was also observed at 3388 cm^{-1} which corresponds to the ν(-OH), which is present in RBOV.

Table 4.1 Infrared Spectra of RBH, RBOV, RFC, RT4 and R3.

Compound	$\nu(-NH_2)$	ν(C=O)	ν(C=N)	ν(-OH)
RBH	3327 cm^{-1}	1716 cm^{-1}	-	-
RBOV	-	1687 cm^{-1}	1612 cm^{-1}	3388 cm^{-1}
RFC	-	1676 cm^{-1}	1614 cm-^{1}	-
RT4	-	1678 cm^{-1}	1597 cm^{-1}	-
R3	-	1686 cm^{-1}	1606 cm^{-1}	-

4.3 ^{1}H NMR and ^{13}C NMR Spectra

In order to confirm the structural information of the synthesized Schiff-base sensors, ^{1}H NMR and ^{13}C NMR spectra of the sensors and RBH was compared. Based on the ^{1}H NMR spectra, the chemical shift for the proton of terminal amine of RBH was observed at 3.60 ppm which is close to the reported literature value of 3.61 ppm (Dujols et al., 1997). On the contrary, this particular peak was not observed in all four sensors synthesized. Thus, this shows that an imine linkage was formed between the protons of terminal amine of RBH with carbonyl group of the respective carbonyl compound through condensation reaction. In addition, for both RBOV and R3, the distinctive peak of methoxy group, O-CH_3 could be observed at 3.67 ppm and 3.81 ppm respectively. On the other hand, from the ^{13}C NMR spectra, the methoxy group was observed for RBOV and R3 at 56.19 ppm and 56.15 ppm, 60.96 ppm respectively.

4.4 X-ray Crystallography

The crystal data and structure refinement parameters of RFC, RT4 and R3 are shown in **Table 4.2, 4.4** and **4.6** respectively. Whereas, the selected bond lengths and bond angles of RFC, RT4 and R3 are shown in **Table 4.3, 4.5** and **4.7** respectively. The crystal structures of RFC, RT4 and R3 are shown in **Figure 4.1, 4.3** and **4.5** respectively. While the unit cell packing of RFC, RT4 and R3 are shown in **Figure 4.2, 4.4** and **4.6** respectively.

RFC, RT4 and R3 were found to have crystallised into a monoclinic lattice with similar space groups of $P2_1/c$. The N–C bond length of the amino group attached to the xanthene core as observed in RFC, RT4 and R3 (1.505 (2) Å, 1.495 (2) Å, and 1.503 (2) Å). The N2=C1 bond length was seen at 1.276 (2) Å for RFC and RT4 and 1.271 (2) Å for R3, shorter than the N-C bond length, thereby suggesting the establishment of imine linkage. Whereas the N1–N2 bond lengths for RFC, RT4 and R3 were found to be at 1.374 (2) Å, 1.384 (2) Å, and 1.381 (2) Å respectively. These bond lengths are similar as those

observed in other rhodamine chemosensor reported upon formation of the Schiff base ligand (Suramitr et al., 2020).

In addition, the perpendicular orientation of the lactam moiety with the xanthene moiety of the rhodamine structure was observed for RFC, RT4 and R3 as illustrated in **Figure 4.1**, **4.3** and **4.5** respectively, where they also exhibit the E configuration. **Figure 4.2** shows RFC forming a linear chain that runs along the a-axis of the monoclinic unit cell. On the other hand, **Figure 4.4** exhibits the herringbone packing from the interaction of RT4 complexes along the b-axis. Finally, the interaction of R3 complexes has shown to form a distorted zig-zag chain from Van der Waals interaction along the a-axis as shown in **Figure 4.6**.

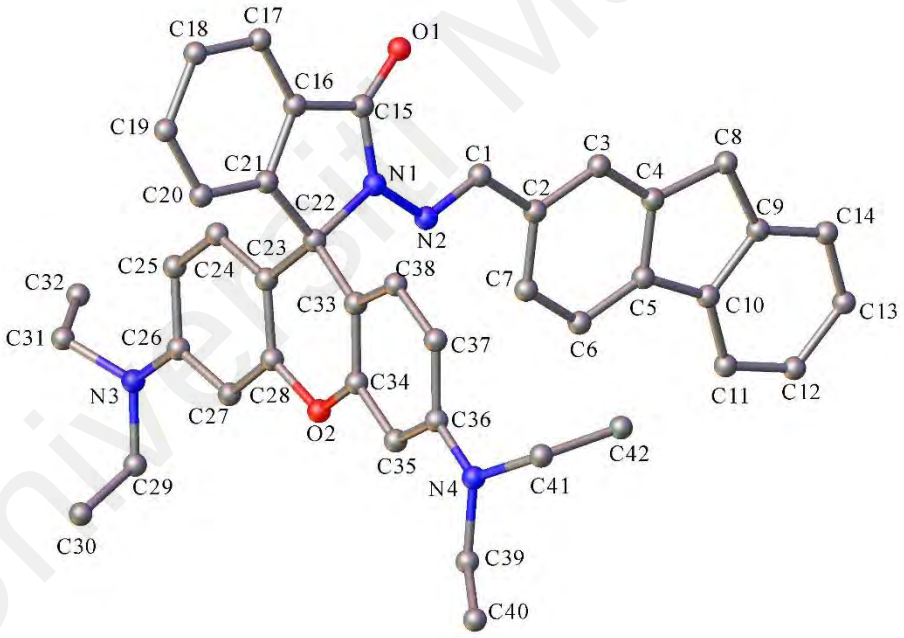

Figure 4.1 Ellipsoid plot of RFC drawn at 50 % probability level. Hydrogen atoms are omitted for clarity.

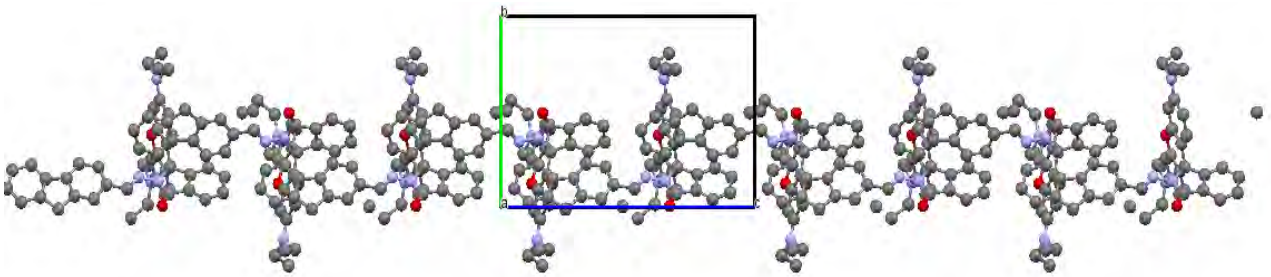

Figure 4.2 Linear chain formed from Van der Waals Interactions of RFC along the a-axis. Hydrogen atoms are omitted for clarity.

Table 4.2 Crystallographic data summary for RFC.

Compound	RFC
Empirical Formula	$C_{42}H_{39}N_4O_2$
Formula Weight	631.77
Crystal System	Monoclinic
Space Group	$P2_1/c$
Unit Cell Dimension	
a (Å)	16.3246 (10)
b (Å)	11.8464 (7)
c (Å)	19.0019 (12)
β (◦)	112.651 (7)
V (Å^3)	3391.3 (4)
Z	4
F (000)	1340
D_{calc} (mg m^{-3})	1.237
Absorption coefficient, μ (mm^{-1})	0.60
T (K)	293
Reflections collected	14468
Independent reflections (R_{int})	6709 (0.027)
Data/Restraints/Parameters	6709/0/437
R[$F^2 > 2\sigma(F^2)$]	0.065
wR(F^2)	0.194
S	1.05
Largest difference peak and hole (e Å^{-3})	0.48 and -0.39

Table 4.3 Selected bond lengths (Å) and bond angles (°) for RFC.

Bond lengths (Å)		Bond angles (°)	
O1—C15	1.226 (2)	C34—O2—C28	118.51 (4)
O2—C28	1.381 (2)	C15—N1—N2	129.87 (16)
O2—C34	1.376 (2)	C15—N1—C22	114.38 (15)
N1—N2	1.374 (2)	N2—N1—C22	115.10 (14)
N1—C15	1.368 (2)	C1—N2—N1	119.73 (16)
N1—C22	1.505 (2)		
N2—C1	1.276 (2)		

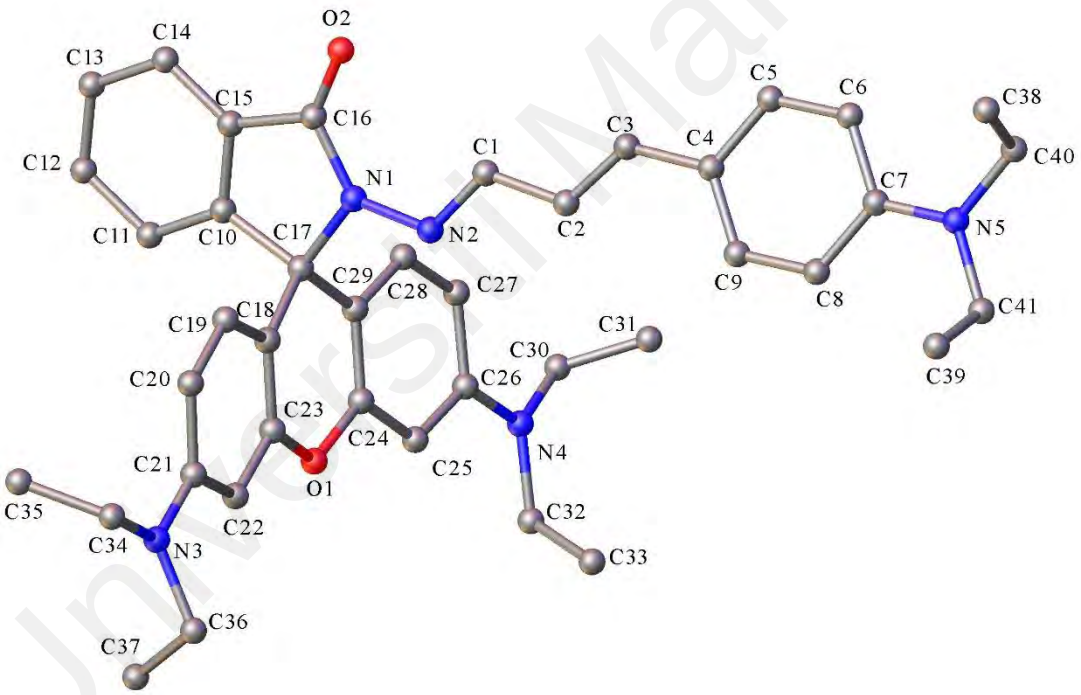

Figure 4.3 Ellipsoid plot of RT4 drawn at 50 % probability level. Hydrogen atoms are omitted for clarity.

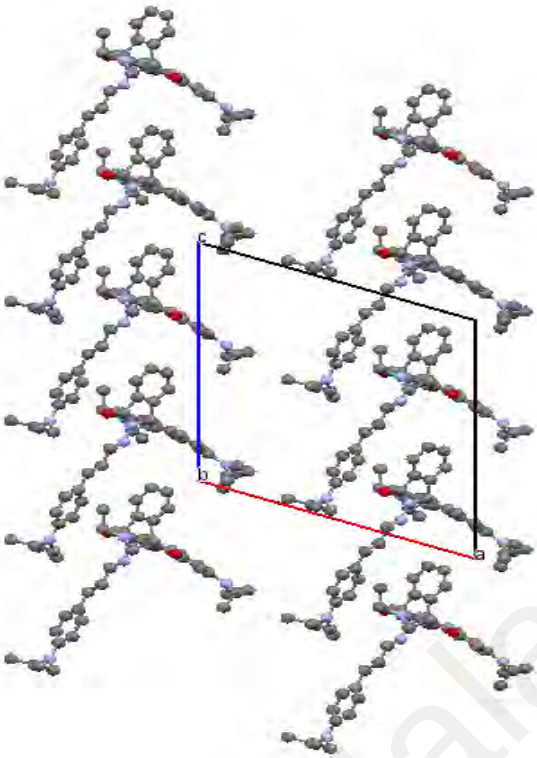

Figure 4.4 Herringbone packing formed from Van der Waals Interactions of RT4 along the b-axis. Hydrogen atoms are omitted for clarity.

Table 4.4 Crystallographic data summary for RT4.

Compound	RT4
Empirical Formula	$C_{41}H_{47}N_5O_2$
Formula Weight	641.67
Crystal System	Monoclinic
Space Group	$P2_1/c$
Unit Cell Dimension	
a (Å)	17.4896 (5)
b (Å)	11.9441 (2)
c (Å)	18.5213 (5)
β (◦)	110.354 (3)
V (Å^3)	3627.48 (17)
Z	4
F (000)	1375
D_{calc} (mg m^{-3})	1.175
Absorption coefficient, μ (mm^{-1})	0.57
T (K)	298
Crystal Size (mm)	0.2 x 0.2 x 0.1
Reflections collected	11964
Independent reflections (R_{int})	7054 (0.028)

Table 4.4 continued.

Compound	RT4
Data/Restraints/Parameters	7054/441/486
$R[F^2 > 2\sigma(F^2)]$	0.058
$wR(F^2)$	0.190
S	1.02
Largest difference peak and hole (e $Å^{-3}$)	0.23 and -0.21

Table 4.5 Selected bond lengths (Å) and bond angles (°) for RT4.

Bond lengths (Å)		Bond angles (°)	
O1—C23	1.380 (2)	C23—O1—C24	118.13 (16)
O1—C24	1.272 (2)	C16—N1—N2	129.87 (16)
O2—C16	1.226 (2)	C16—N1—C17	114.53 (16)
N1—N2	1.384 (2)	N2—N1—C17	115.16 (15)
N1—C17	1.495 (2)	C1—N2—N1	118.69 (19)
N1—C16	1.364 (3)	C7—N5—C40	122.00 (2)
N2—C1	1.276 (3)		
N5—C40	1.376 (3)		

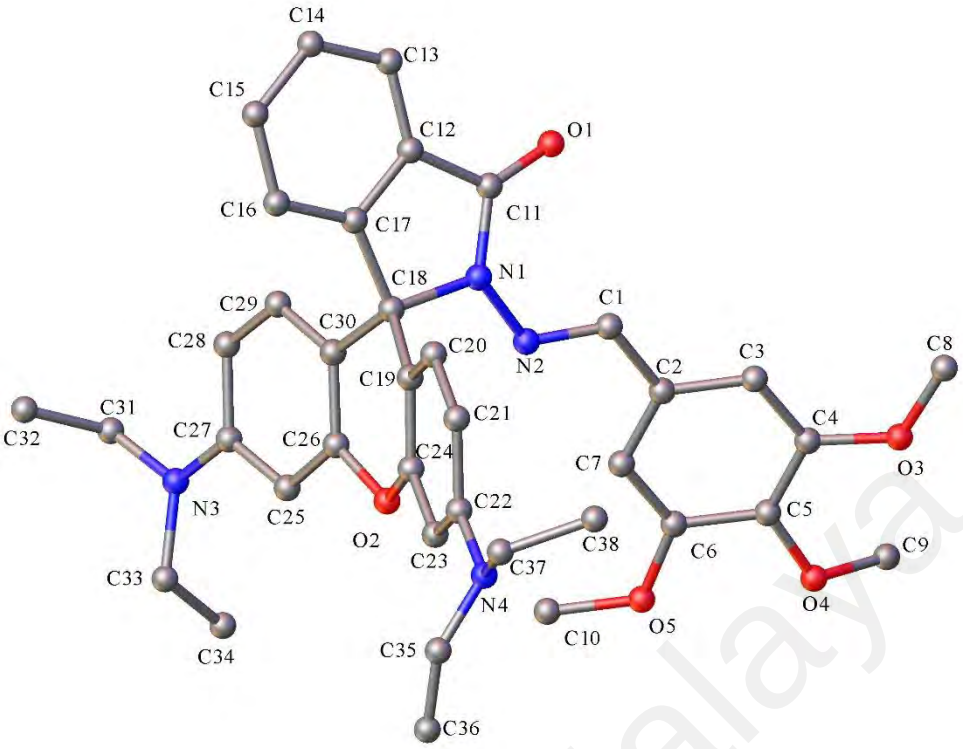

Figure 4.5 Ellipsoid plot of R3 drawn at 50 % probability level. Hydrogen atoms are omitted for clarity.

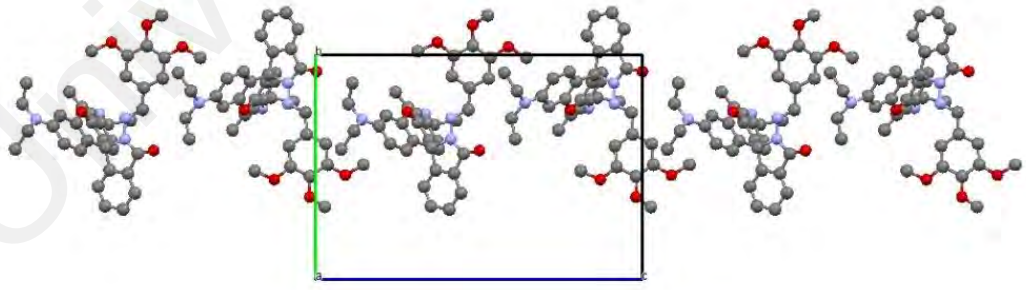

Figure 4.6 Distorted zig-zag chain formed from Van der Waals Interactions of R3 along the a-axis. Hydrogen atoms are omitted for clarity.

Table 4.6 Crystallographic data summary for R3.

Compound	R3
Empirical Formula	$C_{38}H_{42}N_4O_5$
Formula Weight	634.75
Crystal System	Monoclinic
Space Group	$P2_1/c$
Unit Cell Dimension	
a (Å)	11.1226 (6)
b (Å)	14.6628 (7)
c (Å)	21.4184 (4)
β (◦)	97.1650 (2)
V (Å^3)	3465.8 (3)
Z	4
F (000)	1352
D_{calc} (mg m^{-3})	1.216
Absorption coefficient, μ (mm^{-1})	0.65
T (K)	293
Reflections collected	12088
Independent reflections (R_{int})	6793 (0.021)
Data/Restraints/Parameters	6793/10/436
R[$F^2 > 2\sigma(F^2)$]	0.053
wR(F^2)	0.163
S	1.05
Largest difference peak and hole (e Å^{-3})	0.42 and -0.32

Table 4.7 Selected bond lengths (Å) and bond angles (°) for R3.

Bond lengths (Å)		Bond angles (°)	
O1—C11	1.222 (2)	C25—O2—C24	116.90 (13)
O2—C24	1.382 (2)	C4—O3—C8	118.82 (18)
O2—C25	1.377 (2)	C5—O4—C9	120.91 (18)
O3—C8	1.382 (3)	C6—O5—C10	117.57 (18)
O3—C4	1.364 (2)	C11—N1—N2	128.58 (14)
O4—C5	1.363 (2)	C11—N1—C18	114.50 (13)
O4—C9	1.388 (3)	N2—N1—C18	115.33 (12)
O5—C6	1.373 (2)	C1—N2—N1	114.50 (13)
O5—C10	1.412 (3)		
N1—N2	1.381 (19)		
N1—C18	1.503 (2)		
N1—C11	1.364 (2)		
N2—C1	1.271 (2)		

4.5 Selectivity Studies

The absorbance and fluorescence response of RBOV, RFC, RT4 and R3 were carried out with the respected nitrates and chlorides salts of metal ions which includes Ag^{+}, Al^{3+}, Ca^{2+}, Cd^{2+}, Co^{2+}, Cu^{2+}, Fe^{3+}, La^{3+}, Mn^{2+}, Na^{+}, Ni^{2+}, Pb^{2+}, Sn^{2+} and Zn^{2+}. For each sensor, the study was carried out in different solutions which provided the optimum desired outcome.

Previous work done on RBOV has shown that this sensor was able to detect single metal ion (Cu^{2+}) in CH_3CN/H_2O (1:1, v/v) buffered with PBS, giving rise to its colorimetric and fluorometric behavior (Lv et al., 2018). However, in this work we demonstrated a simple and cost-effective strategy in bestowing a known sensor with multiple cations recognition behavior through careful optimization of a different solvent system, in $DMSO/H_2O$ (2:1, v/v, pH 7.5) buffered with TN.

As seen in **Figure 4.7**, after addition of various metal ions (25 μM), colorimetric changes were observed upon binding with Cu^{2+}, Ni^{2+} and Co^{2+}. Since the color changes of RBOV (50 μM) towards these metal ions are within the visible region, purple (Cu^{2+}) and yellow (Ni^{2+} and Co^{2+}), absorption bands around 400-600 nm are expected in the UV-vis spectra. As demonstrated in **Figure 4.8,** a strong absorption peak for Cu^{2+} was observed around 560 nm and around 425 nm for Ni^{2+} and Co^{2+}.

In differentiating the detection of Ni^{2+} and Co^{2+} by RBOV, oxidizing agent was added into the solutions containing RBOV-Ni^{2+} and RBOV-Co^{2+} complexes. Upon addition of hydrogen peroxide, it could be seen that only RBOV-Co^{2+} complex changes from yellow to pink, whereas RBOV-Ni^{2+} complex remains unchanged, this correlates to the properties of the metal ion itself, as Ni^{2+} is known for its resistant towards oxidation. The change in colour (**Figure 4.9**) for RBOV-Co^{2+} complex suggests that Co^{2+} has been oxidized to Co^{3+}.

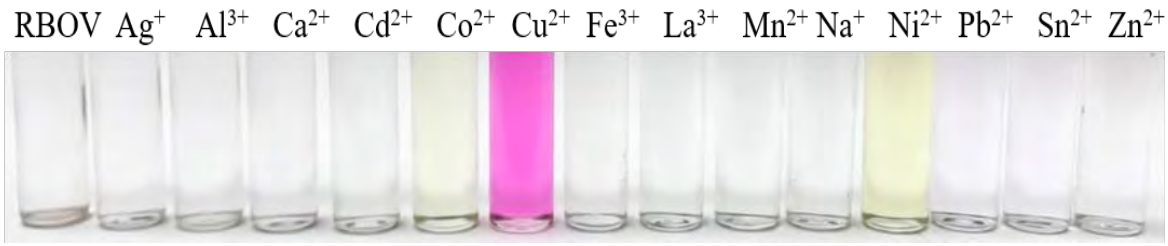

Figure 4.7 Colorimetric changes of RBOV (50 µM) upon addition of various metal ions (25 µm) in DMSO/TN (2:1, v/v, pH 7.5).

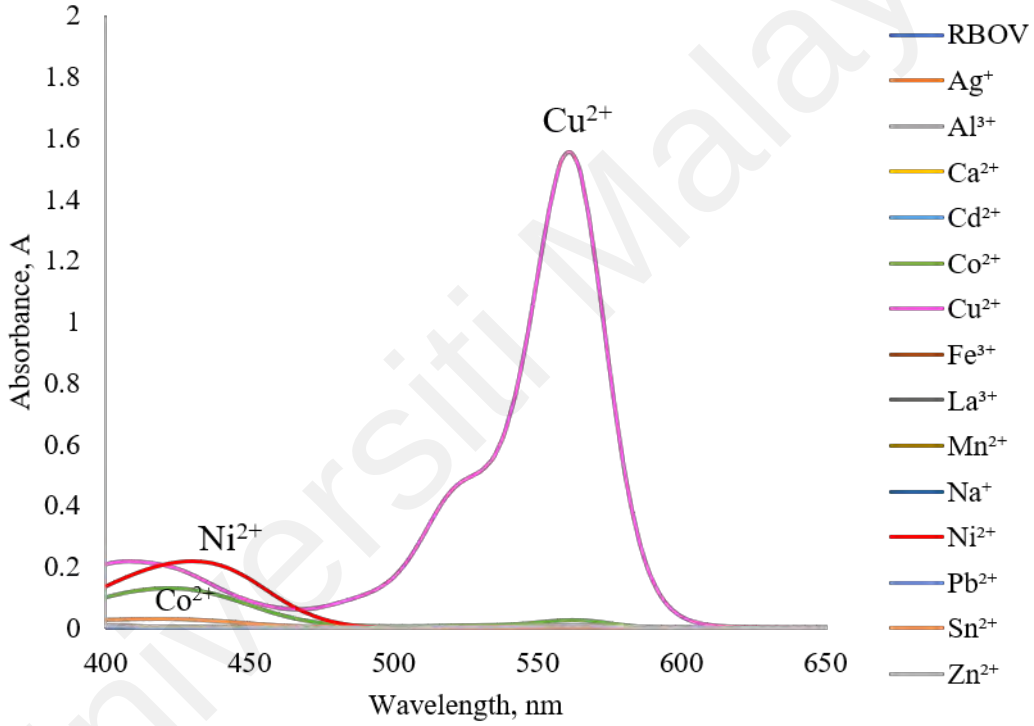

Figure 4.8 Absorption changes of RBOV (50 µM) upon addition of various metal ions (25 µM) in DMSO/TN solution (2:1, v/v, pH 7.5).

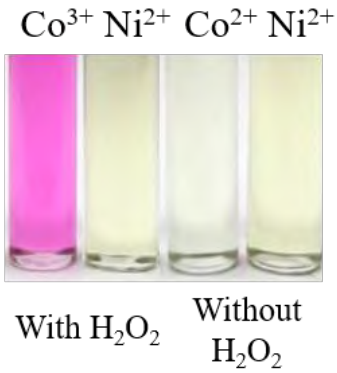

Figure 4.9 Colorimetric changes upon addition of hydrogen peroxide towards RBOV-Ni^{2+} and RBOV-Co^{2+} complexes.

Since there are numerous reports showing greater detection limit with fluorene based chemosensors (Belfield et al., 2010; Dhara et al., 2013; dos Santos Carlos et al., 2017), RFC was synthesized and the selectivity of this sensor (50 µM) was investigated by using the UV-vis and fluorescence spectroscopy in CH_3CN/H_2O (9:1, v/v, pH 7.5, Tris-HCl buffer, 0.1 mM) solution. Upon addition of 1 equivalent of Al^{3+}, Cu^{2+} and Fe^{3+}, an obvious colour change from colourless to purple was observed (**Figure 4.10 a**), giving rise to the potential of RFC as naked-eye detector for these metal ions. As shown in **Figure 4.11**, upon the coordination of RFC towards these ions, a peak is observed at 560 nm from the UV-vis spectra, and no peak was observed for the other cations.

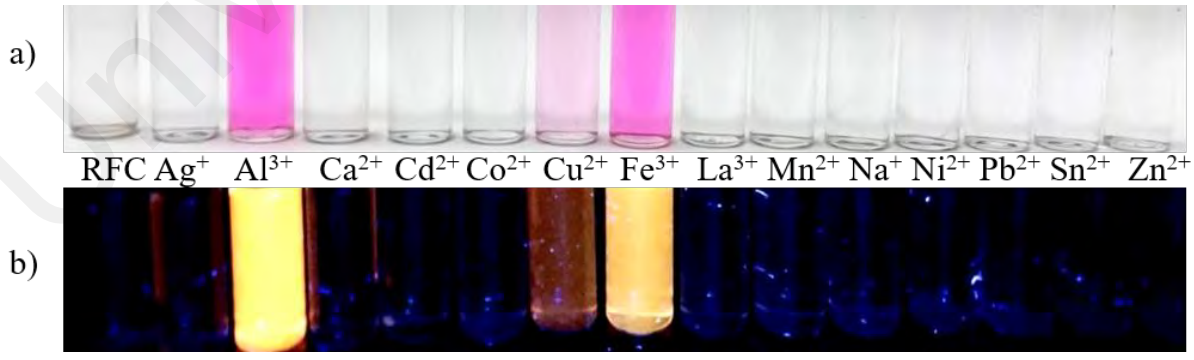

Figure 4.10 a) Colorimetric changes and b) Fluorescence emission (under UV light) of RFC upon addition of various metal ions.

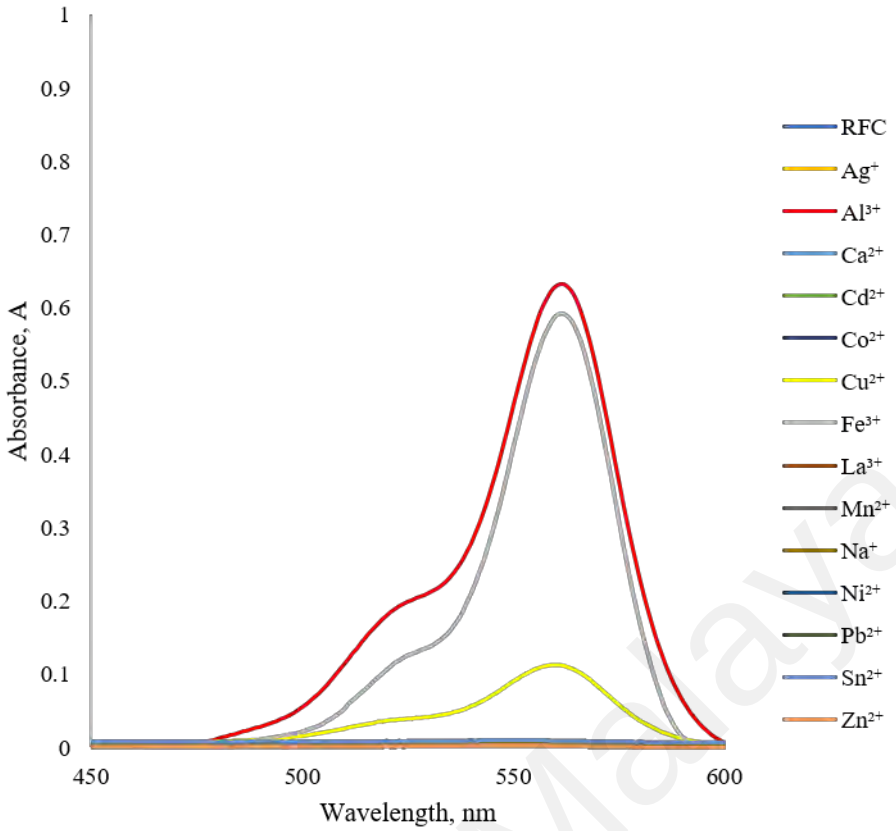

Figure 4.11 Absorption changes of RFC (50 µM) upon addition of various metal ions (50 µM) in CH_3CN/H_2O (9:1, v/v, pH 7.5, Tris-HCl buffer, 0.1mM) at λ = 560 nm.

The fluorogenic behavior of RFC towards the various metal ions was also studied via the same reaction condition. In the absence of metal ions, a weak band at 588 nm was observed, attributing to the closed spirolactam ring (Kim et al., 2008) of RFC. When metal ions are added, a strong peak was observed at λ = 588 nm for Al^{3+}, followed by Fe^{3+} and a significantly low peak was observed for Cu^{2+} as depicted in **Figure 4.12**, which is attributed to the opening of the spirolactam ring.

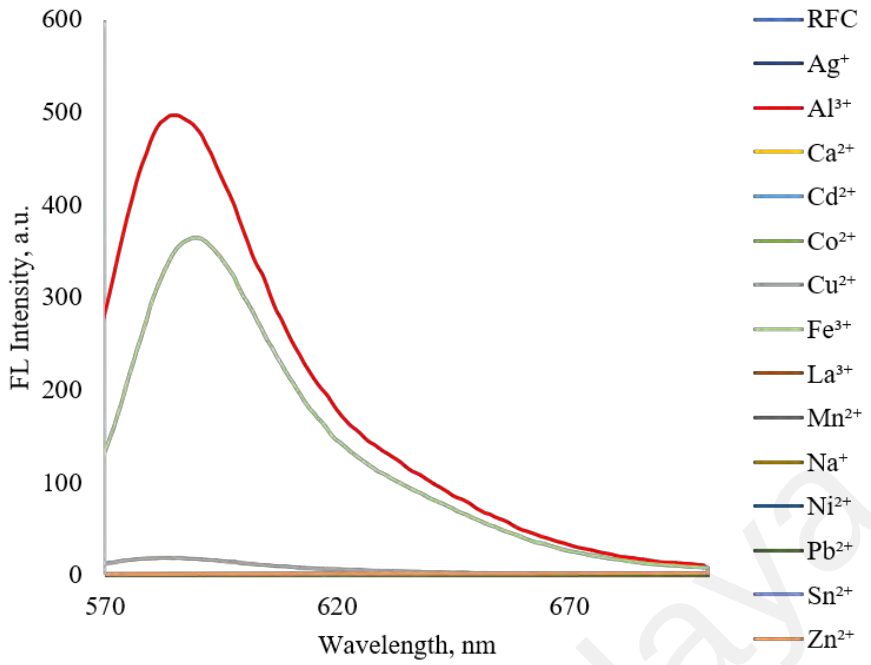

Figure 4.12 Emission changes of RFC (50 µM) upon addition of various metal ions (50 µM) in CH_3CN/H_2O (9:1, v/v, pH 7.5, Tris-HCl buffer, 0.1mM) at λ = 588 nm.

For the third sensor, the absorbance and fluorescence response of RT4 (50 µM) upon binding with metal ions were carried out in CH_3CN/H_2O (1:1. v/v, pH 7.5, Tris-HCl buffer, 1 mM) solution. From the UV-vis spectra, the free RT4 shows an absorbance peak at 406 nm which is attributed to the yellow colour of the solution as seen in **Figure 4.13**. In the presence of 1 equivalent of Cu^{2+} and Fe^{3+}, new absorbance peaks were observed at λ = 588 nm and 562nm respectively (**Figure 4.14**). The colour of the solution changes from yellow to red and orange upon complexation with Cu^{2+} and Fe^{3+} respectively. Although several rhodamine-based chemosensors (Lan et al., 2016; Tang et al., 2017; Wang et al., 2017; Yang et al., 2016), for the detection of Fe^{3+} and Cu^{2+} have been reported, only RT4 shows a unique colorimetric change from yellow to orange and red upon recognition of these metal ions respectively. Upon excitation at 562 nm, only Fe^{3+} and Cu^{2+} showed emission peak at 585 nm as seen in **Figure 4.15**. While the free RT4 along with other metal ions showed a slight emission peak at 561 nm.

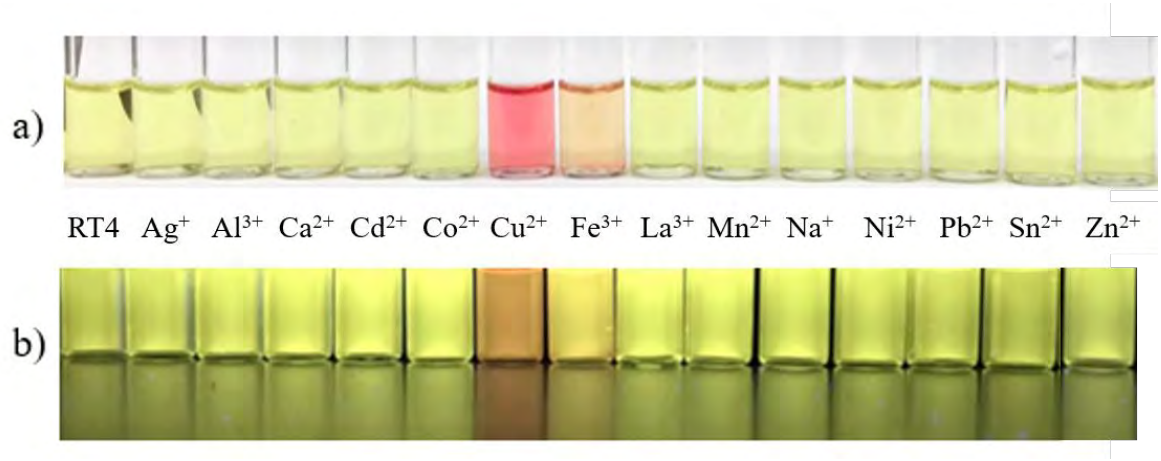

Figure 4.13 a) Colorimetric changes and b) Fluorescence emission (under UV light) of RT4 upon addition of various metal ions.

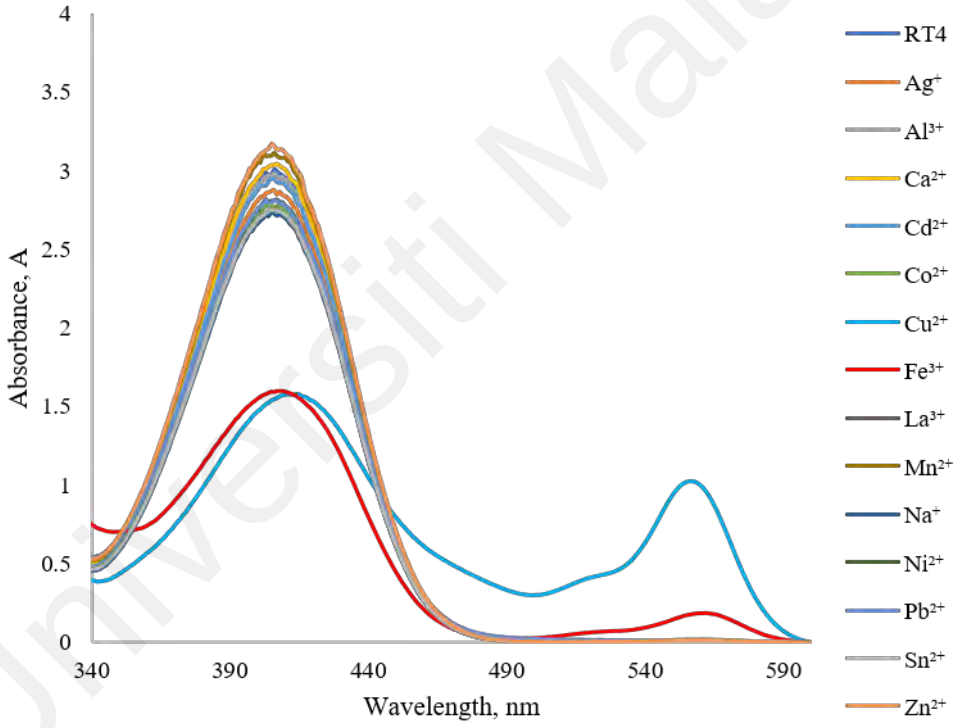

Figure 4.14 Absorption changes of RT4 (50 µM) in the presence of metal ions (50 µM) in MeCN/H_2O (1:1. v/v, pH 7.5 , Tris-HCl buffer, 1 mM) solution.

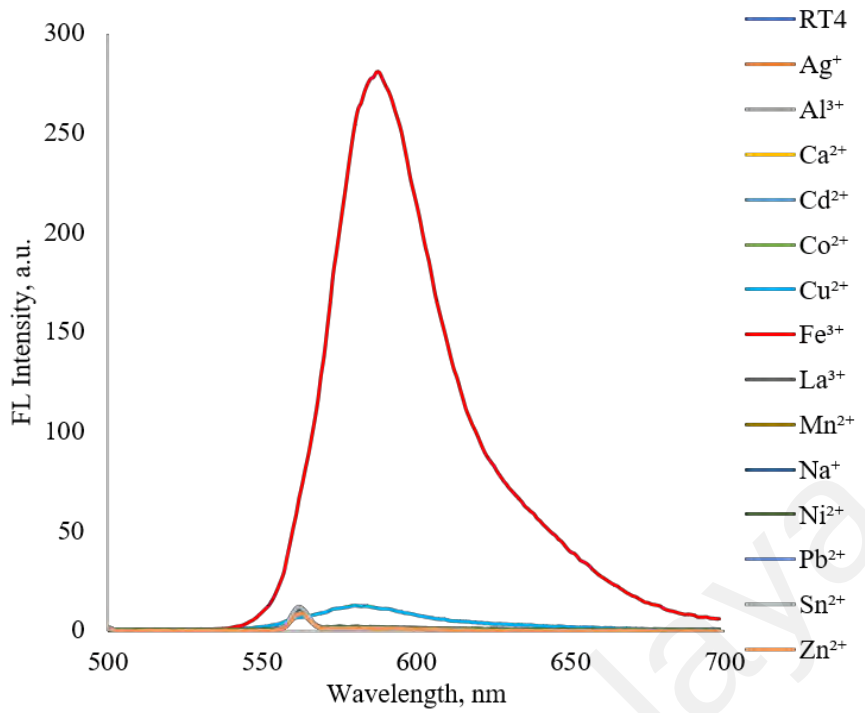

Figure 4.15 Emission changes of RT4 (50 µM) in the presence of metal ions (50 µM) in MeCN/H_2O (1:1. v/v, pH 7.5, Tris-HCl buffer, 1 mM) solution at λ = 585 nm.

In 2016, a "turn-on" fluorescent probe for Pb^{2+} has been reported by (Sunnapu et al., 2017). This fluorescent chemosensor RDP-1, was synthesized by reacting rhodamine 6G with 3,4,5-trimethoxybenzaldehyde. In this work, R3 sensor was synthesized by reacting rhodamine b hydrazide with 3,4,5-trimethoxybenzaldehyde, which showed high selectivity and sensitivity towards recognition of Fe^{3+} in EtOH/H_2O (7:3. v/v, pH 7.5, Tris-HCl buffer, 1 mM) solution.

As seen in **Figure 4.16**, only upon addition of Fe^{3+} colorimetric changes occur from colourless to purple. R3 sensor also showed a "turn-on" fluorescent behavior as a bright orange emission is seen in the presence of Fe^{3+}. The absorbance and emission changes of R3 (50 µM) in the presence of various metal ions (50 µM) could be observed in **Figure 4.17** and **Figure 4.18** respectively. The absorbance peak of R3 in the presence of Fe^{3+} was observed at λ = 560 nm and emission peak at λ = 585 nm.

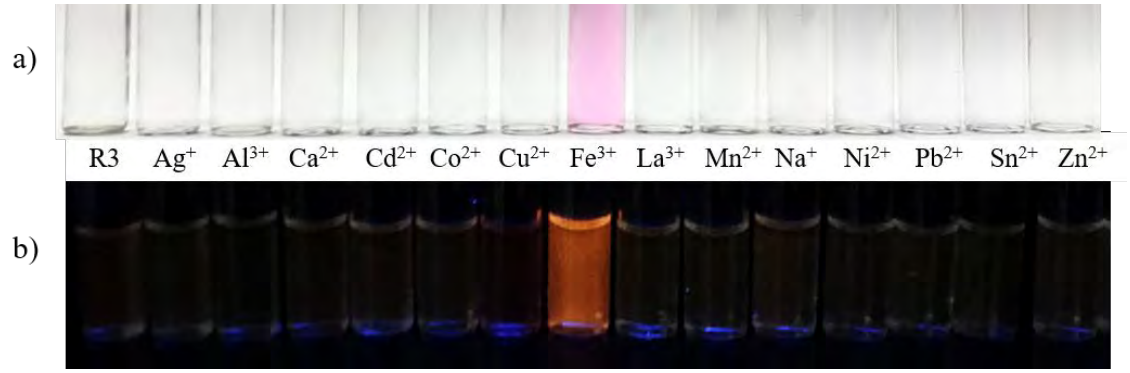

Figure 4.16 a) Colorimetric changes and b) Fluorescence enhancement (under UV light) of R3 upon addition of metal ions.

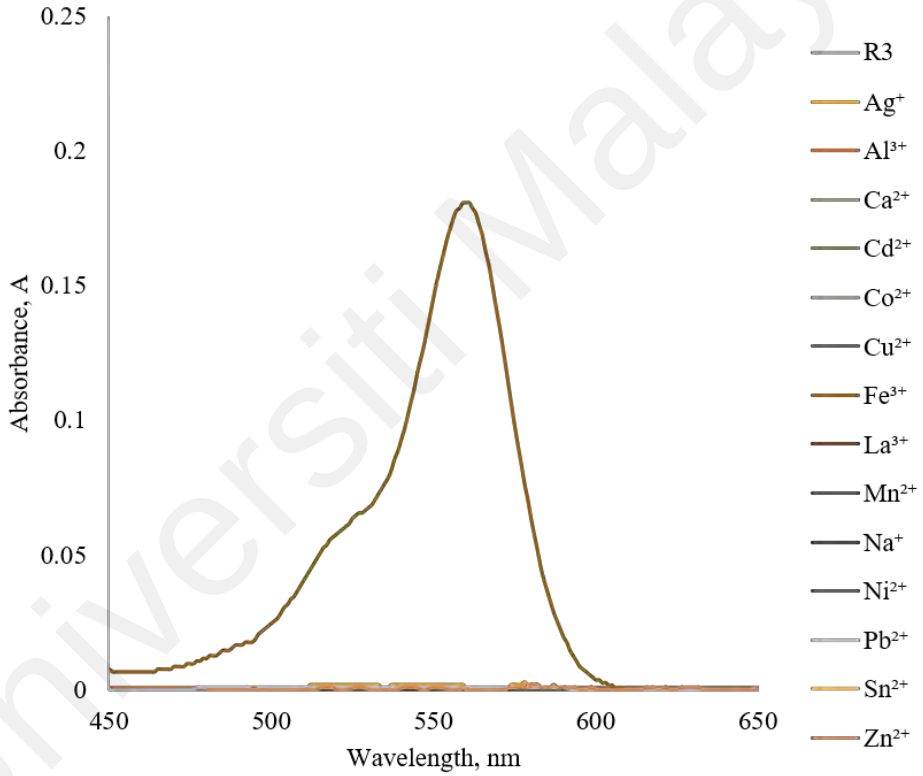

Figure 4.17 Absorption changes of R3 (50 µM) upon addition of metal ions (50 µM) in EtOH/H_2O (7:3. v/v, pH 7.5, Tris-HCl buffer, 1 mM) solution.

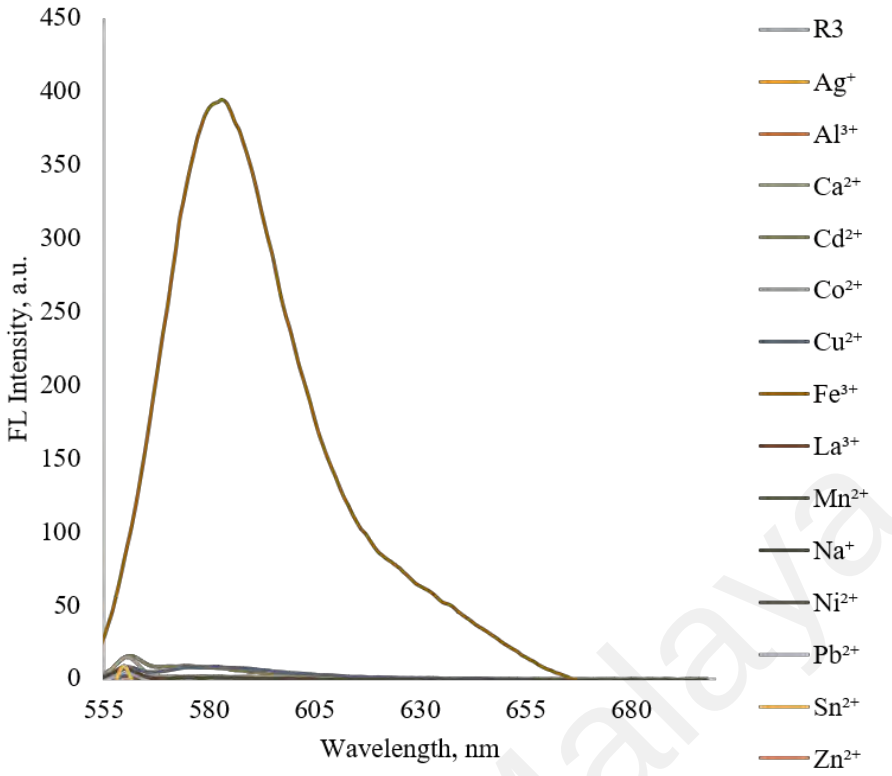

Figure 4.18 Emission changes of R3 (50 µM) upon addition of metal ions (50 µM) in EtOH/H_2O (7:3. v/v, pH 7.5, Tris-HCl buffer, 1 mM) solution.

4.6 Effects of pH

To determine the optimum stability of sensor metal complex (Sensor-M^{n+}), the effects of pH (2-12) was conducted. In acidic condition, the colourless and non-fluorescent rhodamine chemosensor may be protonated, resulting an obvious color change and fluorescence emission (Beija et al., 2009).

For RBOV sensor, the effect of pH was taken at two different wavelengths, at λ = 560 nm for RBOV-Cu^{2+} and at λ = 425 nm for RBOV-Ni^{2+}/Co^{2+} in DMSO/H_2O (2:1, v/v) solution. As evident from **Figure 4.19a**, the absorbance peak of RBOV-Cu^{2+} increases gradually from pH 2-7.5 and decreases from pH 8-12. On the other hand, no absorbance peak was observed for RBOV-Ni^{2+}/Co^{2+} in the acidic condition, a change in absorption was only observed from pH 7.5-12 (**Figure 4.19b**).

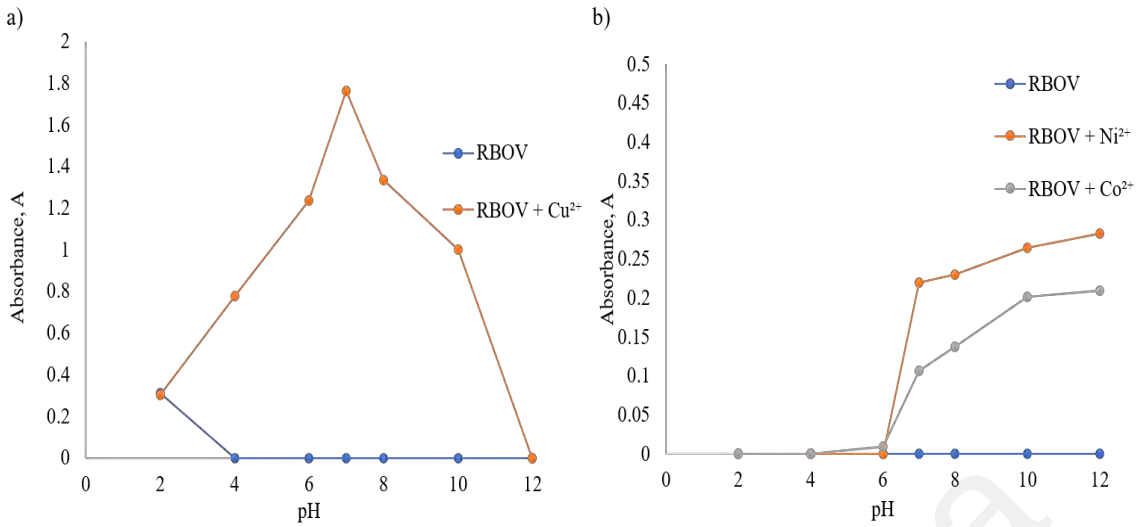

Figure 4.19 Absorption changes of RBOV with a) RBOV + Cu^{2+} (λ = 560 nm) and b) RBOV + Ni^{2+}, RBOV + Co^{2+} (λ = 425 nm) over a range of pH (2-12) in DMSO/H_2O (2:1, v/v) solution.

Similar result was observed in studying the effect of pH for the RFC sensor in CH_3CN/H_2O (9:1, v/v) solution. From pH 2-7.5, the absorbance and emission gradually increase in the presence of Cu^{2+} and Al^{3+}. However, in the case of RFC-Fe^{3+} (**Figure 4.20**), the emission peak was only observed at pH 7.5. The difference in presence of emission peak in terms of pH in detecting Al^{3+} and Fe^{3+}, is beneficial for practical application which will be discussed later.

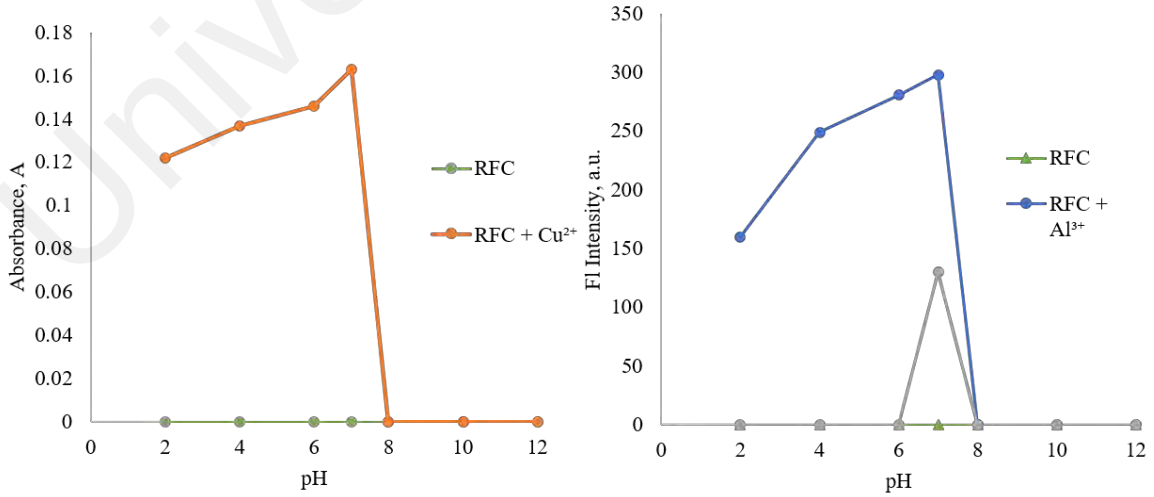

Figure 4.20 a) Absorption changes of RFC (50 µM) in the presence of Cu^{2+} (50 µM) at λ = 560 nm and b) emission changes of RFC in the presence of Al^{3+} and Fe^{3+} (50 µM) at λ = 588 nm, over a range of pH (2-12) in CH_3CN/H_2O (9:1, v/v) solution.

For RT4 and R3 sensors, the effect of acidic medium as mentioned earlier could be observed in **Figure 4.21 and Figure 4.22**, where an intense absorbance and emission peak was recorded for free RT4 in MeCN/H_2O (1:1, v/v) solution and free R3 in EtOH/H_2O (7:3, v/v) solution. As demonstrated from **Figure 4.21a** and **Figure 4.21b**, both RT4-Cu^{2+} and RT4-Fe^{3+} shows significant efficiency at pH 7.5. In the case of R3, a steady absorbance and emission changes was observed from pH 6-7 in the presence of Fe^{3+} (**Figure 4.22**). Since all the sensors showed great efficiency at neutral pH, all of the spectroscopic studies were conducted at pH 7.5, which further suggests its applicability in physiological conditions.

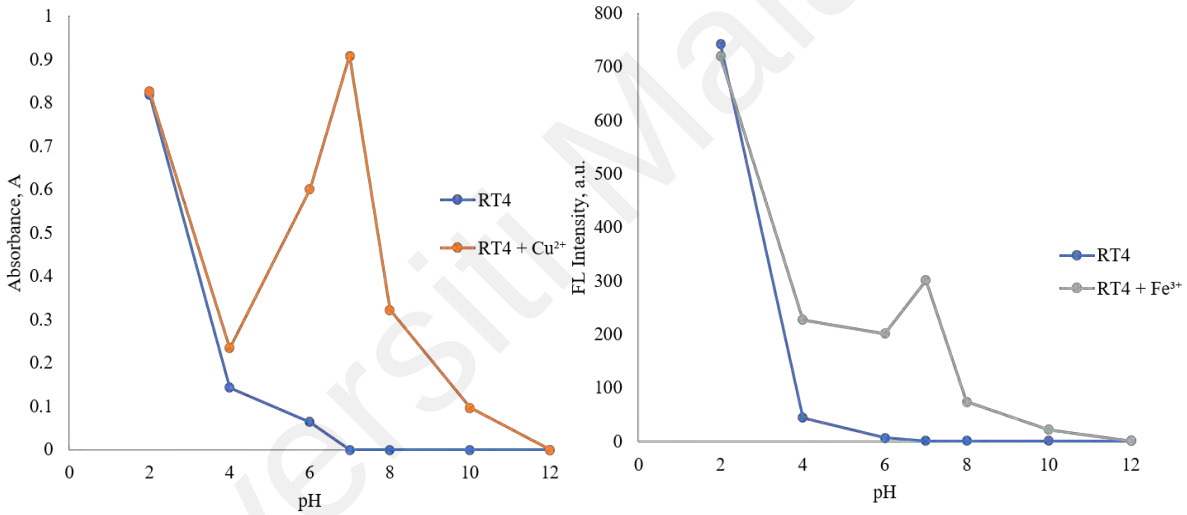

Figure 4.21 a) Absorption changes of RT4 (50 µM) in the presence of Cu^{2+} (50 µM) at λ = 560 nm and b) emission changes of RT4 in the presence of Fe^{3+} (50 µM) at λ = 585 nm, over a range of pH (2-12) in CH_3CN/H_2O (1:1, v/v) solution.

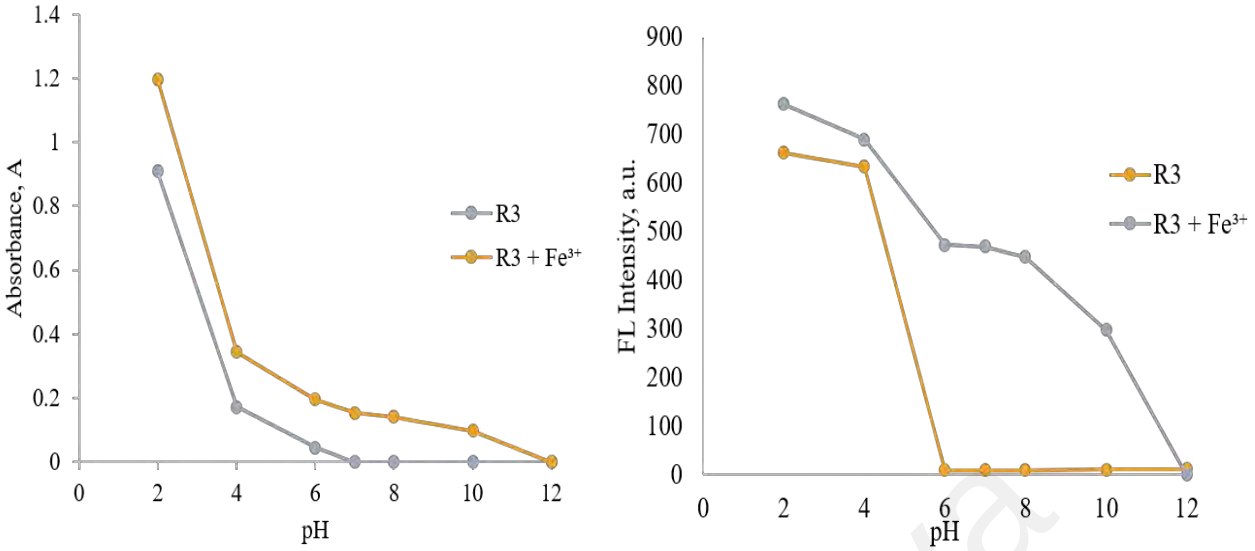

Figure 4.22 a) Absorption and b) emission changes of R3 (50 µM) in the presence of Fe^{3+} (50 µM) over a range of pH (2-12) in EtOH/H_2O (7:3, v/v) solution.

4.7 Titration Experiments

In determining the sensitivity of the chemosensors, absorption and fluorescence titration experiments were conducted to calculate the limit of detection (LOD) and association constant, K_a. In this study, the concentration of sensor is fixed while the concentration of metal ions was gradually increased and monitored using UV-vis and fluorescence spectroscopy.

From the titration experiments conducted, plot of absorbance against wavelength for each sensor showed gradual increase in absorbance and fluoresecence, as the concentration of metal ions increases. This is evident in **Figure 4.23**, **Figure 4.24**, **Figure 4.25,** and **Figure 4.26** for RBOV, RFC, RT4 and R3, respectively.

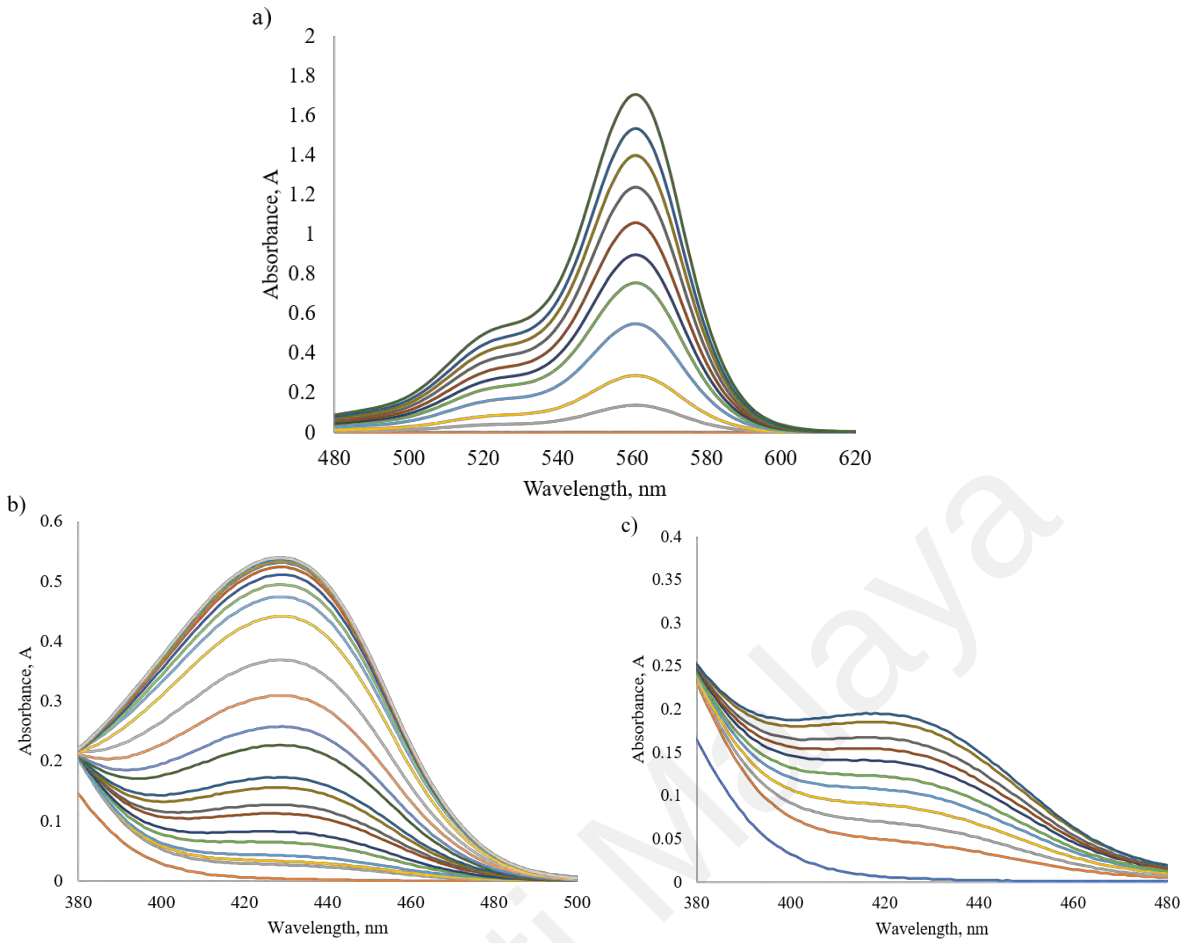

Figure 4.23 Absorbance spectrum of RBOV with increasing concentration at λ = 560 nm for a) Cu^{2+}, at λ = 425 nm for b) Ni^{2+} and c) Co^{2+}, with RBOV (50 µM) in DMSO/TN (2:1, v/v, pH 7.5) solution.

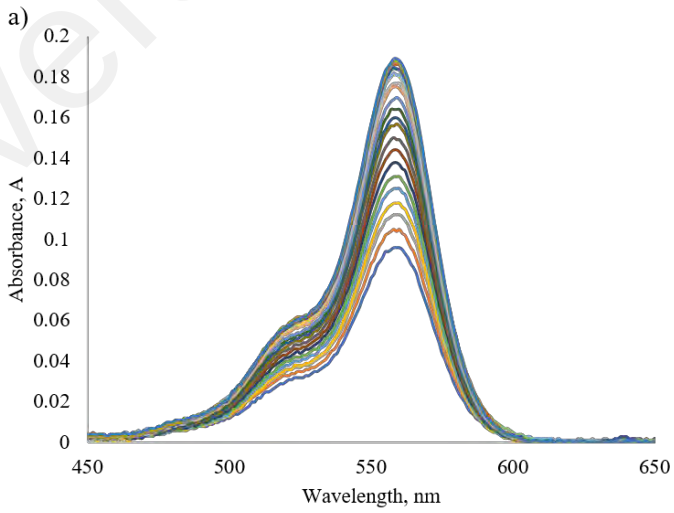

Figure 4.24 a) Absorbance spectrum of Cu^{2+} at λ=560 nm and Fluorescence spectrum of b) Al^{3+} and c) Fe^{3+} at λ=588 nm, with RFC in CH_3CN/H_2O (9:1, v/v, pH 7.5, Tris-HCl buffer, 0.1mM) solution.

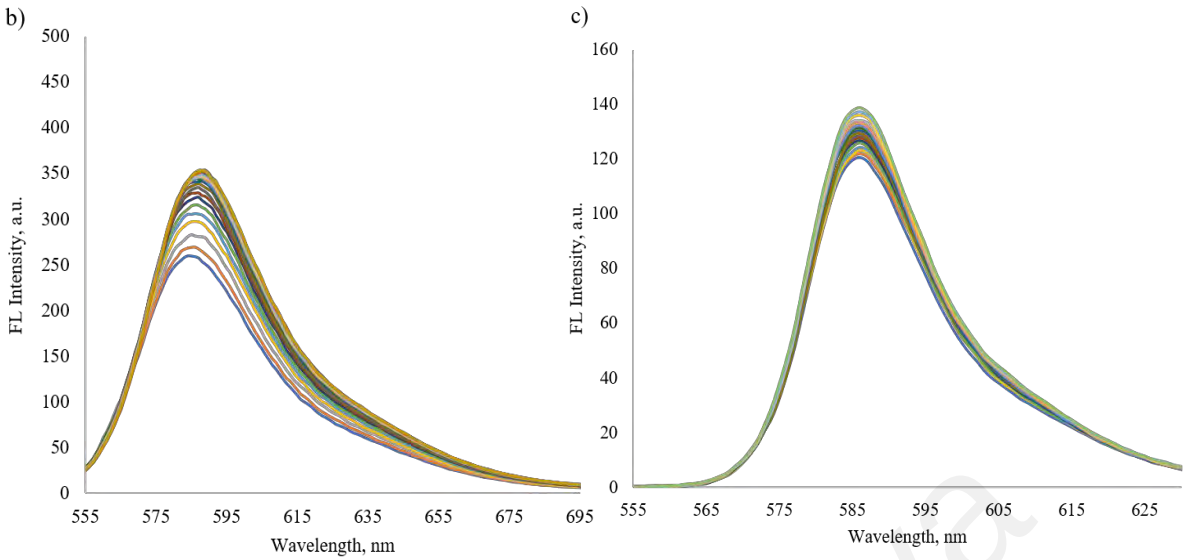

Figure 4.24 continued.

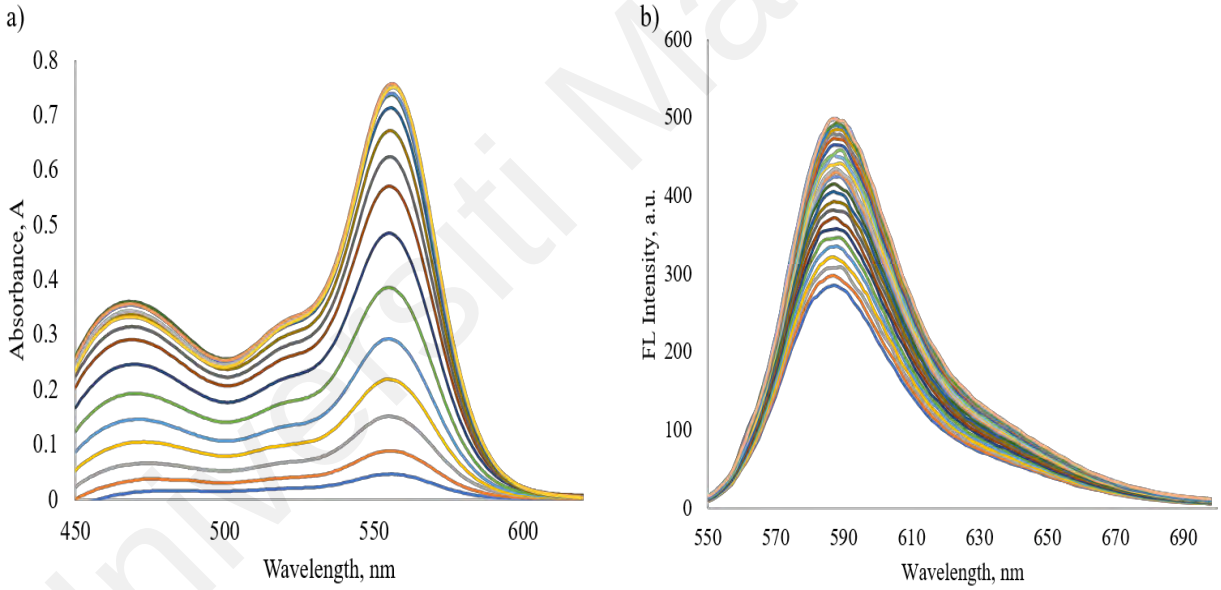

Figure 4.25 a) Absorbance spectrum of Cu^{2+} at λ=588 nm and b) Fluorescence spectrum of Fe^{3+} at λ=585 nm with RT4 in CH_3CN/H_2O (1:1. v/v, pH 7.5, Tris-HCl buffer, 1 mM) solution.

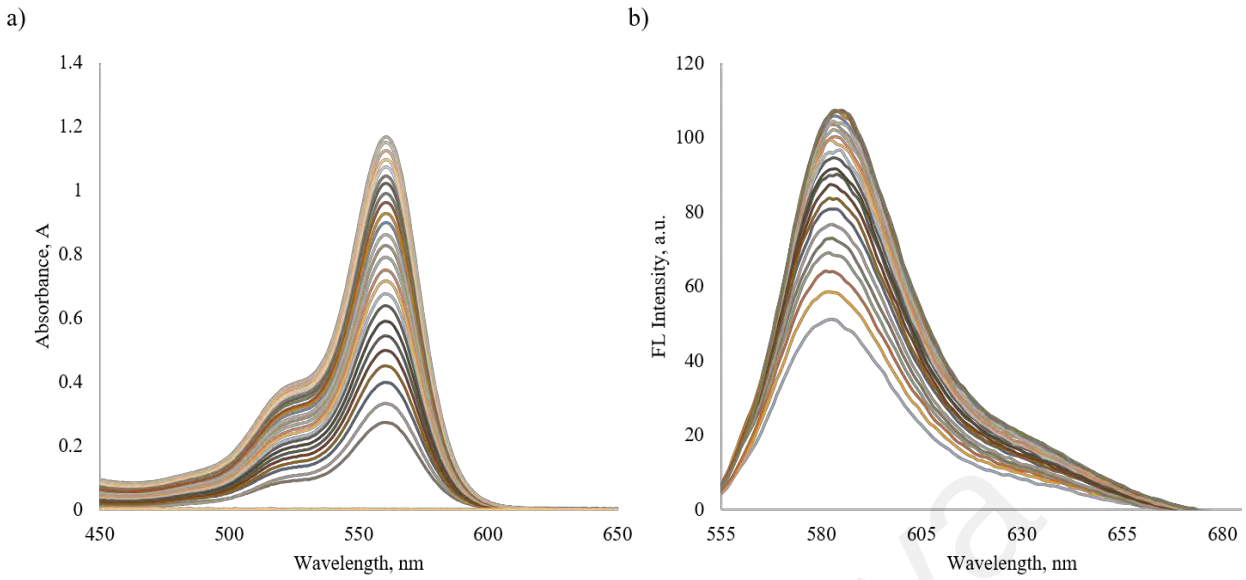

Figure 4.26 a) Absorbance and b) Fluorescence spectrum of R3 with Fe^{3+} at λ=560 nm and λ=585 nm respectively in EtOH/H_2O (7:3. v/v, pH 7.5, Tris-HCl buffer, 1 mM) solution.

4.7.1 Limit of Detection, LOD

In determining the limit of detection (LOD) of the sensors, a plot of absorbance/fluorescence against concentration of metal ions were plotted for RBOV (**Figure 4.27**), RFC (**Figure 4.28**), RT4 (**Figure 4.29**) and RFC (**Figure 4.30**) respectively. The detection limit of each sensor was then calculated from the slope of linear fittings with the standard deviation of 10 replicate blank measurements by using equation 3.1, mentioned in the previous chapter.

Based on the slope of linear fittings for each metal ions, the LOD of RBOV for Cu^{2+}, Ni^{2+} and Co^{2+} are, 0.04 µM, 0.32 µM and 0.48 µM respectively. The LOD of RFC for Al^{3+}, Cu^{2+} and Fe^{3+} was calculated as 0.12 µM, 1.14 µM and 0.36 µM respectively. The LOD of RT4 towards Cu^{2+} and Fe^{3+} were calculated to be 0.20 µM and 0.18 µM respectively. Finally, the LOD of R3 from the absorbance and fluorescence titration towards Fe^{3+} were calculated as 0.47 µM and 0.35 µM respectively. The LOD values of these sensors were found to be much lower than the recommended water quality standard for Al^{3+} (3.71 µM), Co^{2+} (37.0 µM), Cu^{2+} (20.5 µM), Fe^{3+} (5.4 µM), and Ni^{2+} (12.0 µM)

in drinking water by WHO and EPA (Colter & Mahler, 2006; Edition, 2008; Kim et al., 2006; WHO, 2003).

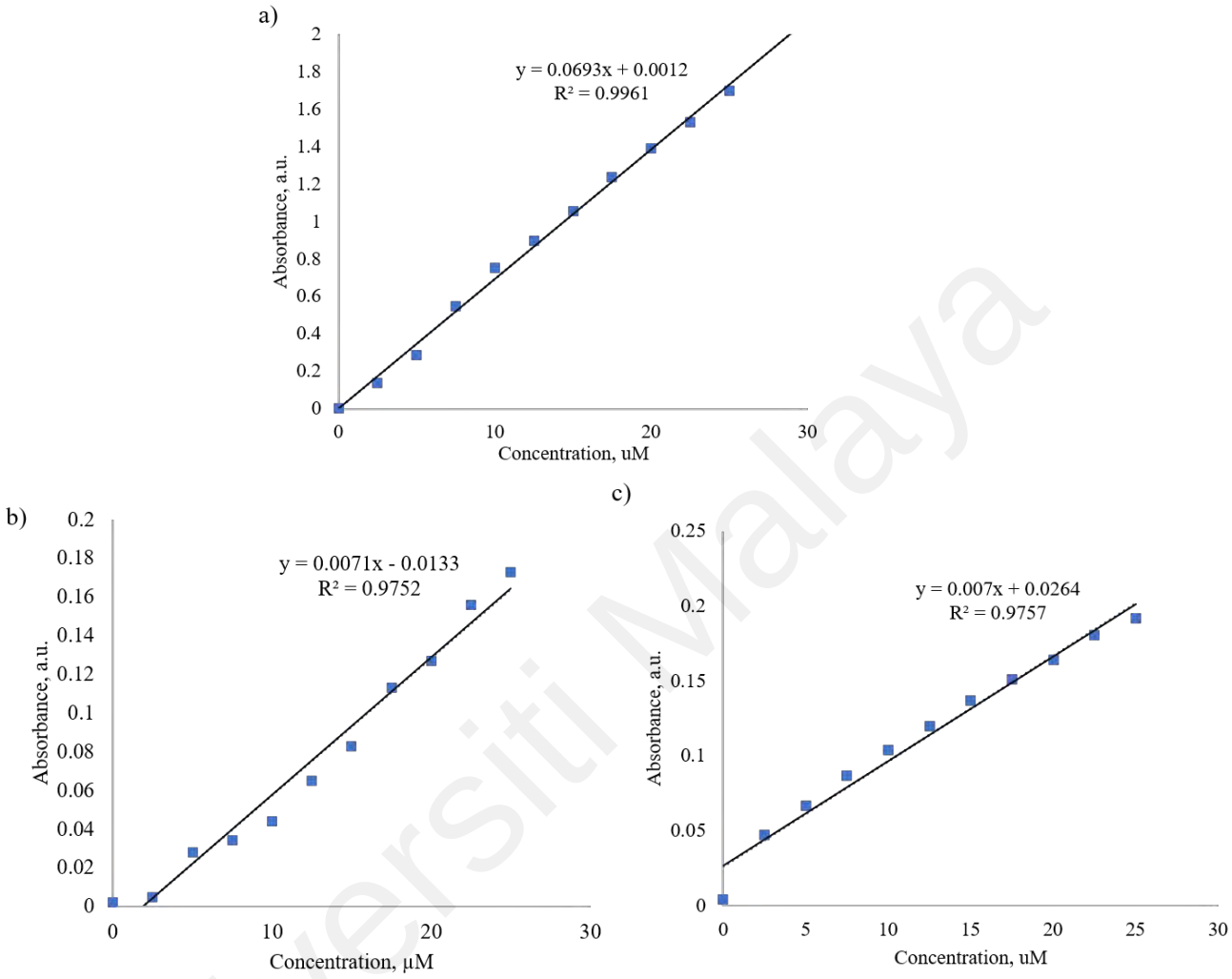

Figure 4.27 Plot of absorbance against concentration of a) Cu^2 b) Ni^{2+} and c) Co^{2+}, with RBOV (50 µM) in DMSO/TN solution (2:1, v/v, pH 7.5).

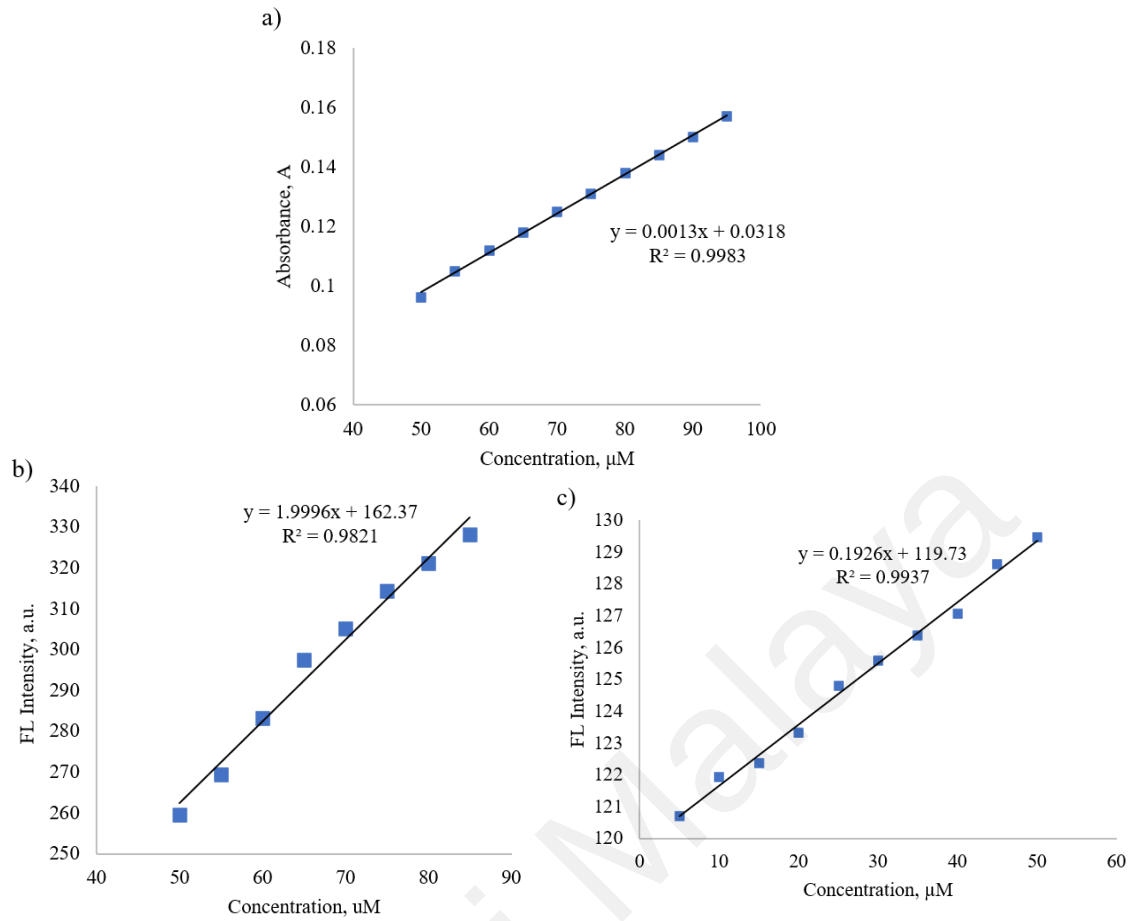

Figure 4.28 Plot of absorbance/fluorescence against concentration of a)Cu^{2+} at λ=560 nm and b) Al^{3+} and c) Fe^{3+} at λ=588 nm, in CH_3CN/H_2O (9:1, v/v, pH 7.5, Tris-HCl buffer, 0.1mM) solution.

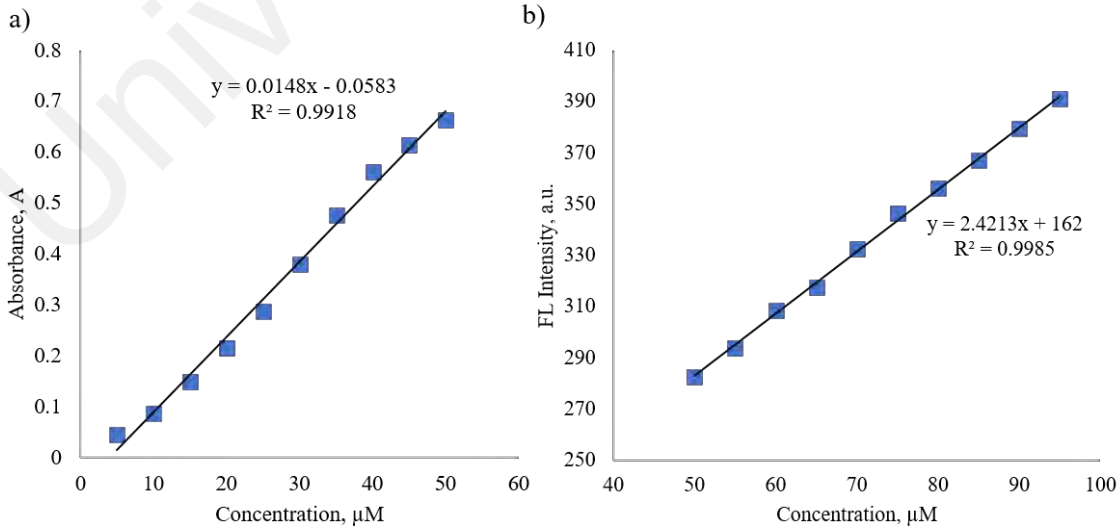

Figure 4.29 Plot of absorbance and fluorescence against concentration of a)Cu^{2+} at λ=588 nm and b) Fe^{3+} λ=585 nm in CH_3CN/H_2O (1:1. v/v, pH 7.5, Tris-HCl buffer, 1 mM) solution.

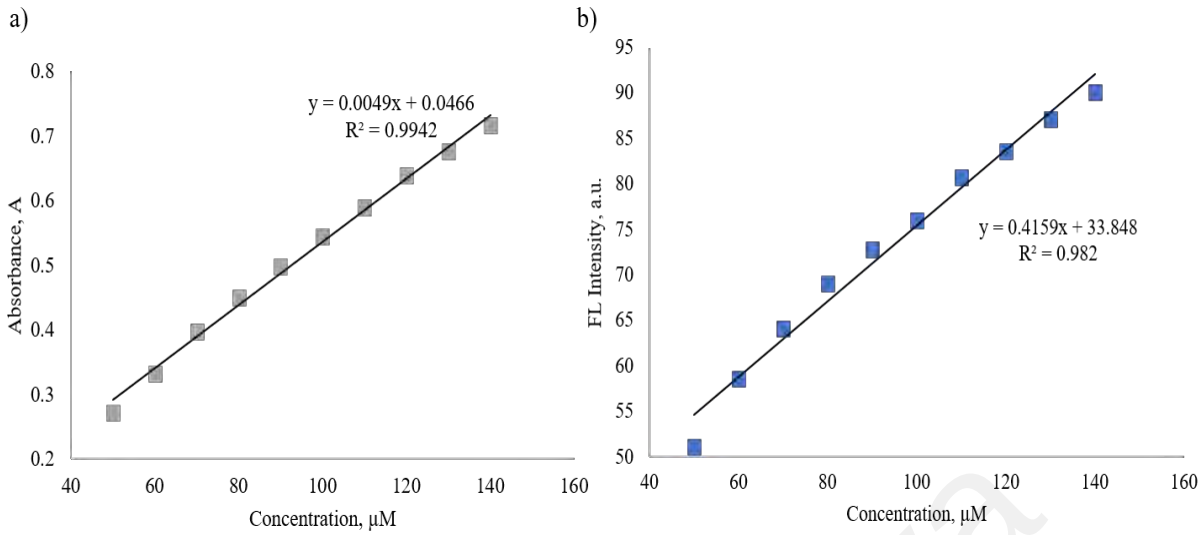

Figure 4.30 Plot of a) absorbance and b) fluorescence against concentration of Fe^{3+} at λ=585 nm in EtOH/H_2O (7:3. v/v, pH 7.5, Tris-HCl buffer, 1 mM) solution.

Furthermore, LOD comparison of all four sensors with other reported probes was also done as shown in **Table 4.8**. For RBOV sensor, it showed a great detection limit for Cu^{2+} despite detecting two other metal ions as compared to RH1 and RBO. On the other hand, the LOD comparison of RFC with 1 and F3, shows its great potency in detection of multiple analytes with the lowest detection limit for Al^{3+}. RT4 sensor also exhibits a great LOD value in detecting Cu^{2+} and Fe^{3+}. As compared to sensor L, RT4 showed a unique colorimetric change which could easily discern the detection of the two metal ions. Sensor R3, 2, and RDP-1 that was synthesized from a rhodamine moiety and trimethoxybenzaldehyde has shown to be a great single metal ion detector. Sensor R3 and 2 exhibit fluorometric and colorimetric properties of the metal ion detected with great detection limit.

Table 4.8 Comparison among reported chemosensors with RBOV, RFC, RT4 and R3 in respect to LOD of target metal ions.

Sensor	Detection Method	Chemosensor based	Solvent system	Metal (s) detected	LOD (μM)	Ref.
RBOV	Colorimetric	Rhodamine and 2-hydroxy-3-methoxy benzaldehyde	DMSO/H_2O (TN buffer)	Cu^{2+}, Co^{2+}, and Ni^{2+}	0.04 (Cu^{2+}) 0.32 (Co^{2+}) 0.48 (Ni^{2+})	This work
RH1	Fluorescence (Al^{3+} only) and colorimetric	Rhodamine and 3-allyl-2-hydroxybenzaldehyde	MeCN/H_2O (HEPES buffer)	$Cu^{2+}$and Al^{3+}	0.32 (Cu^{2+}) 0.57 (Al^{3+})	(Rai et al., 2018)
RBO	Fluorescence and colorimetric	Rhodamine and 2-hydroxy-3-methoxy benzaldehyde	MeCN/H_2O (PBS buffer)	Cu^{2+}	0.03 (Cu^{2+})	(Lv et al., 2018)
RFC	Fluorescence (Al^{3+} and Fe^{3+}) and Colorimetric	Rhodamine and fluorene	MeCN/H_2O (Tris-HCl buffer)	Cu^{2+}, Al^{3+} and Fe^{3+}	1.14 (Cu^{2+}) 0.12 (Al^{3+}) 0.36 (Fe^{3+})	This work
1	Fluorescence (Al^{3+} only) and Colorimetric	Rhodamine and fluorene	MeOH/H_2O (HEPES buffer)	Cu^{2+}, Al^{3+} and Fe^{3+}	2.40 (Al^{3+}) - (Cu^{2+}) - (Fe^{3+})	(Dhara et al., 2013)
F3	Fluorescence	Fluorene	MeCN	Cr^{3+} and Al^{3+}	0.31 (Al^{3+})	(Tajbakhsh et al., 2018)
RT4	Fluorescence (Fe^{3+} only) and Colorimetric	Rhodamine and cinnamaldehyde	MeCN/H_2O (Tris-HCl buffer)	Fe^{3+} and Cu^{2+}	0.20 (Cu^{2+}) 0.18 (Fe^{3+})	This work
3	Fluorescence and Colorimetric	Rhodamine and cinnamalydehyde	THF	Fe^{3+}	0.06	(Kumar et al., 2011)
L	Fluorescence (Fe^{3+} only) and Colorimetric	Rhodamine and trifluoromethylbenzaldehyde	EtOH	Fe^{3+} and Cu^{2+}	0.53 (Cu^{2+}) 0.01 (Fe^{3+})	(Wang et al., 2017)
R3	Fluorescence and Colorimetric	Rhodamine and trimethoxybenzaldehyde	EtOH/H_2O (Tris-HCl buffer)	Fe^{3+}	0.35	This work
2	Fluorescence	Rhodamine and trimethoxybenzaldehyde	Water Samples	Hg^{2+}	1.42	(Zhao et al., 2020)
RDP-1	Fluorescence and Colorimetric	Rhodamine and trimethoxybenzaldehyde	HEPES buffer	Pb^{2+}	0.015	(Sunnapu et al., 2016)

4.7.2 Association Constant, K_a

The association constant, K_a of RBOV with Cu^{2+}, Ni^{2+} and Co^{2+} was calculated by using the Benesi-Hildebrand plots (**Figure 4.31**). Based on the absorbance titration curves, good linear regression equations were obtained as $y = 2x10^{-5}x - 0.3336$, $y = 5x10^{-4}x - 24.003$ and $y = 5x10^{-5}x + 4.2184$ for Cu^{2+} Ni^{2+} and Co^{2+} respectively. By using the Benesi-Hildebrand equation (3.2), the K_a of RBOV with Cu^{2+}, Ni^{2+} and Co^{2+} was calculated to be 1.8 x 10^4 M^{-1}, 4.4 x 10^4 M^{-1}, and 8.6 x 10^4 M^{-1} respectively.

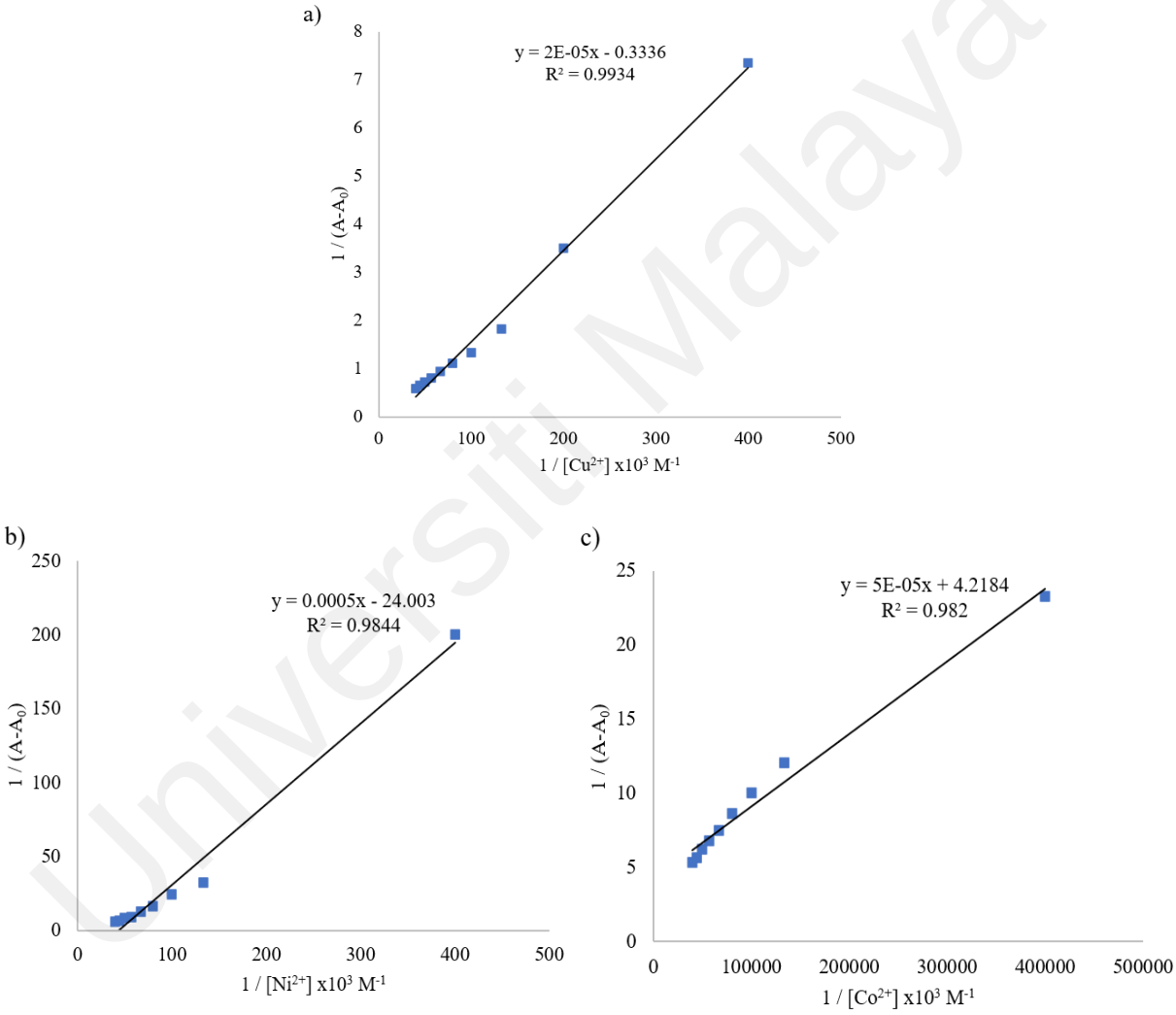

Figure 4.31 Benesi-Hildebrand plots of $1/(A-A_0)$ versus a) $1/[Cu^{2+}]$ at λ = 550 nm, b) $1/[Ni^{2+}]$ and c) $1/[Co^{2+}]$ at λ_{em} = 425 nm in DMSO/TN (2:1, v/v, pH 7.5) solution.

The K_a of RFC towards Al^{3+}, Cu^{2+} and Fe^{3+} were determined using the Benesi-Hildebrand equation 3.3 and equation 3.2 respectively. From the equation, by plotting a graph of $1/(F-F_0)$ or $1/(A-A_0)$ versus $1/[M^+]$ (**Figure 4.32**), a linear regression equation was obtained. Through the slope and intercept, the values of K_a of RFC for Al^{3+}, Cu^{2+} and Fe^{3+} were calculated as 1.83 x 10^4 M^{-1}, 4.56 x 10^3 M^{-1} and 8.25 x 10^5 M^{-1} respectively.

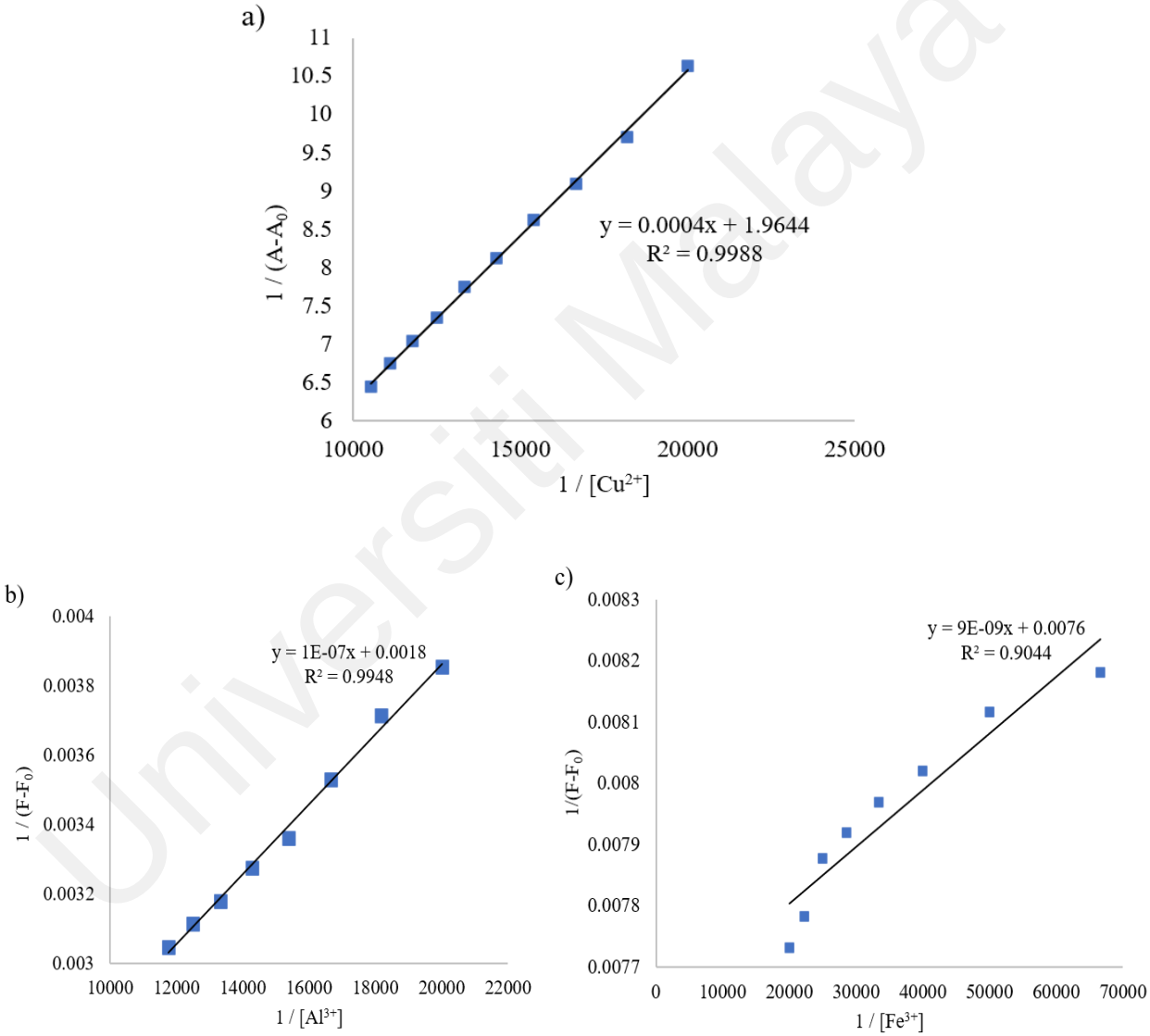

Figure 4.32 Benesi-Hildebrand plots of a) $1/(A-A_0)$ versus $1/[Cu^{2+}]$ at $\lambda = 588$ nm b) $1/(F-F_0)$ versus b) $1/[Al^{3+}]$ and c) $1/[Fe^{3+}]$ at $\lambda = 588$ nm in CH_3CN/H_2O (9:1, v/v, pH 7.5, Tris-HCl buffer, 0.1mM) solution.

For RT4 sensor, as evident in **Figure 4.33**, good linear regression equations were obtained as $y = 1x10^{-4}x - 1.0267$ and $y = 9x10^{6}x - 13922$ for Cu^{2+} and Fe^{3+} respectively. By using the Benesi-Hildebrand equations, the K_a of RT4 with Cu^{2+} and Fe^{3+} was calculated to be $8.28x10^{3}$ M^{-1} and $1.41x10^{4}$ M^{-1} respectively.

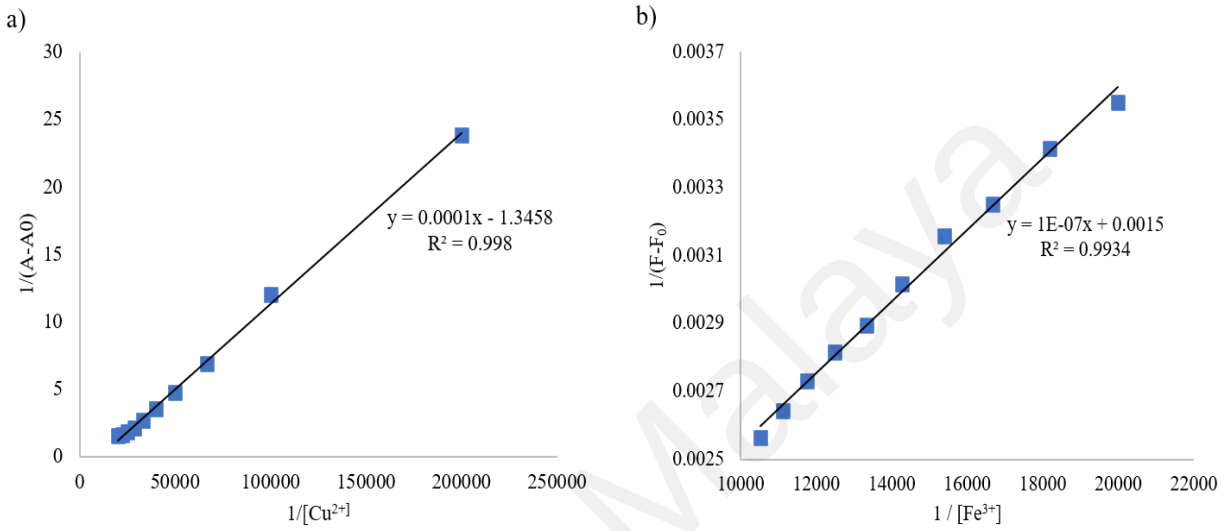

Figure 4.33 Benesi-Hildebrand plots of a) $1/(A-A_0)$ versus $1/[Cu^{2+}]$ at λ = 588 nm and b) $1/(F-F_0)$ versus $1/[Fe^{3+}]$ at λ= 585 nm in in CH_3CN/H_2O (1:1. v/v, pH 7.5, Tris-HCl buffer, 1 mM) solution.

Similar graph was plotted for R3 sensor (**Figure 4.34**) where both absorbance and fluorescence linear regression equations for Fe^{3+} were obtained as $y = 2x10^{-4}x + 0.0922$ and $y = 6x10^{-7}x + 0.0066$ respectively. The K_a of R3 for Fe^{3+} were calculated as 5.25 x 10^{2} M^{-1} and $1.02x10^{4}M^{-1}$ based on the absorbance and fluorescence Benesi-Hildebrand plot.

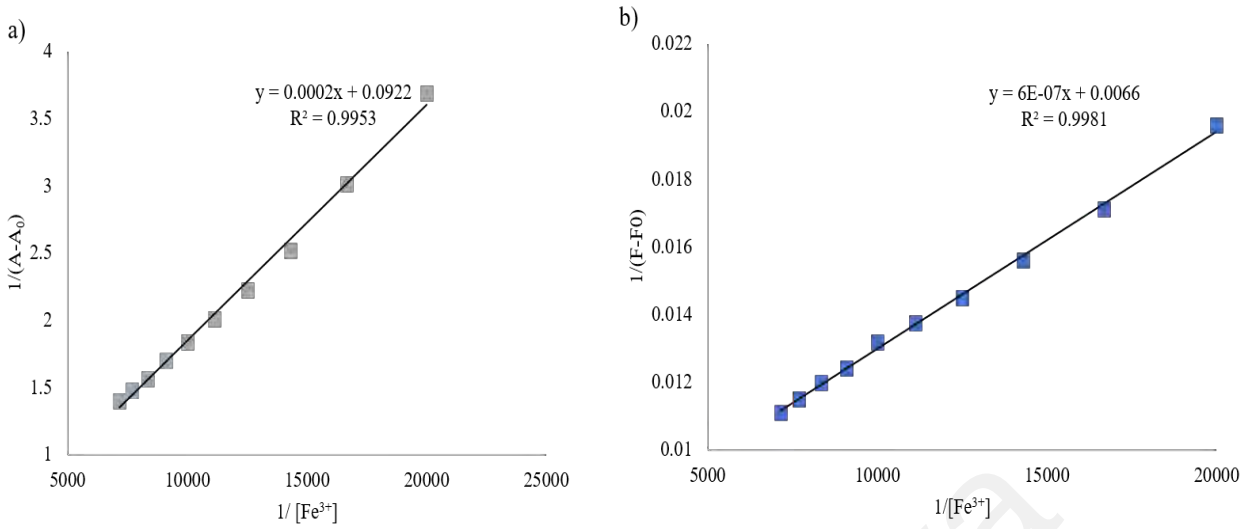

Figure 4.34 Benesi-Hildebrand plots of a) $1/(A-A_0)$ versus $1/[Fe^{3+}]$ at λ = 588 nm and b) $1/(F-F_0)$ versus $1/[Fe^{3+}]$ in EtOH/H_2O (7:3. v/v, pH 7.5, Tris-HCl buffer, 1 mM) solution.

4.8 Competitive Studies

To investigate the anti-interference property of the sensors, competitive study was conducted. In this study, equivalent concentration of sensor and metal ions were used in their respective solution.

The competitive study of RBOV with Cu^{2+} Ni^{2+} and Co^{2+} could be seen in **Figure 4.35**. From the figure, there's only slight interference on the absorbance of Cu^{2+}, Ni^{2+} and Co^{2+}, in the presence of other metal ions. For the detection of Co^{2+}, an increment in absorbance was observed upon presence of Ni^{2+}. This result was expected as RBOV detects Ni^{2+} at a higher absorbance than Co^{2+} at similar wavelength.

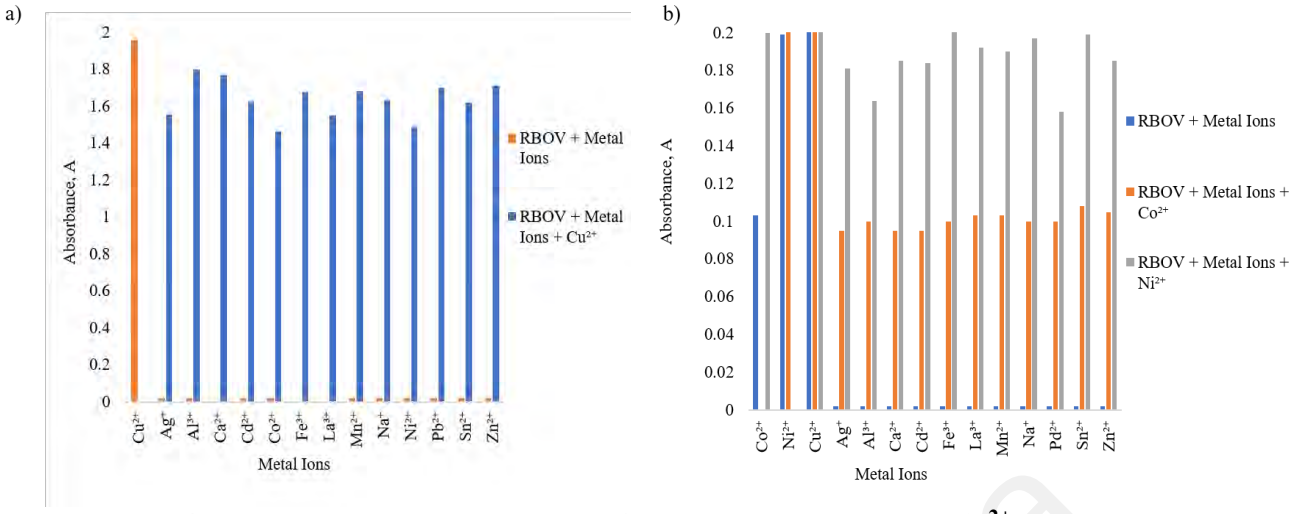

Figure 4.35 Relative absorbance of RBOV (50 µM) towards a) Cu^{2+} at λ = 560 nm, b) Ni^{2+} and Co^{2+} at λ = 425 nm in the presence of other metal ions (50 µM) in DMSO/TN (2:1, v/v, pH 7.5) solution.

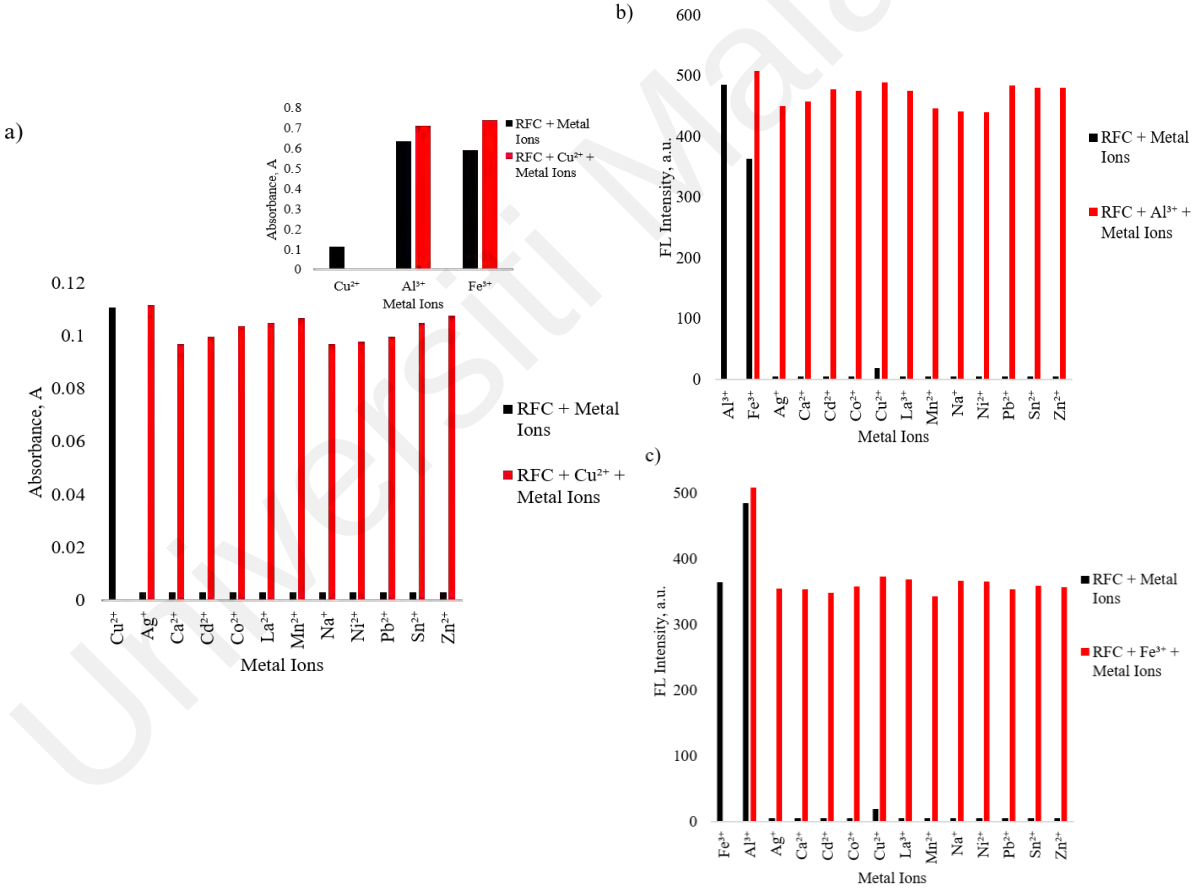

Figure 4.36 The competitive selectivity of RFC (50 µM) based on changes in absorbance intensity for a) Cu^{2+} at 560 nm, and fluorescence intensity for b) Al^{3+} and c) Fe^{3+} at 588 nm in the presence of various cations (50 µM) in CH_3CN/H_2O (9:1, v/v, pH 7.5, Tris-HCl buffer, 0.1mM) solution. Inset: Absorbance changes for Cu^{2+} in the presence of Al^{3+}.

From **Figure 4.36b**, the recognition of Al^{3+} and Fe^{3+} by RFC is not significantly influenced by other coexisting metal ions. For recognition of Cu^{2+}, the presence of other metal ions does not interfere much except in the presence of Al^{3+} and Fe^{3+}, where there is an increase in fluorescence and absorbance intensity as seen in inset of **Figure 4.36**, which is expected as the recognition of Al^{3+} and Fe^{3+} by RFC shows a higher absorbance compared to Cu^{2+}.

Next, the absorbance spectra in **Figure 4.37a** showed no significant changes were observed in the recognition of Cu^{2+} by RT4 in the presence of other cations. Similar observation of the emission peaks was observed in the recognition of Fe^{3+} by RT4 (**Figure 4.37b**). These results suggest that RT4 has a great selectivity for both Cu^{2+} and Fe^{3+} over other cations present.

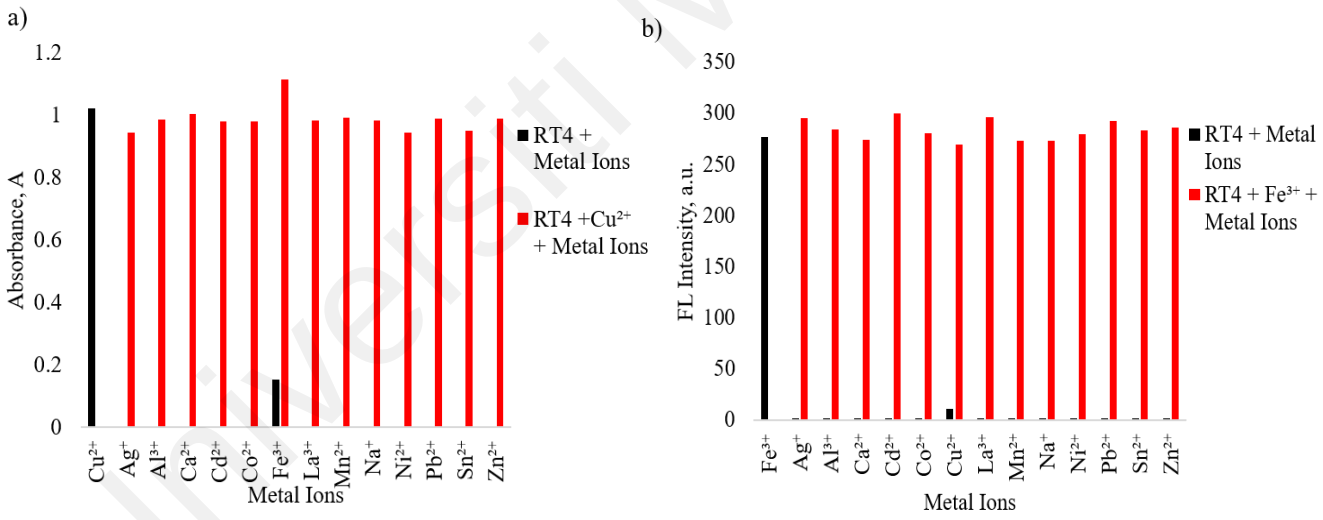

Figure 4.37 The competitive selectivity of RT4 (50 µM) based on change in absorbance intensity for a) Cu^{2+} at 588 nm, and fluorescence intensity for b) Fe^{3+} at 585 nm in the presence of various cations (50 µM) in CH_3CN/H_2O (1:1. v/v, pH 7.5, Tris-HCl buffer, 1 mM) solution.

Recognition of Fe^{3+} by R3 in the presence of other metal ions was done by UV-vis and fluorescence spectroscopy. As evident from **Figure 4.38**, comparing R3 with only Fe^{3+} present, the absorbance and fluorescence intensities of R3 solution in the presence of other metal ions showed only slight variation. These observations indicate that R3 exhibit a high selectivity in binding with Fe^{3+} over other metal ions tested.

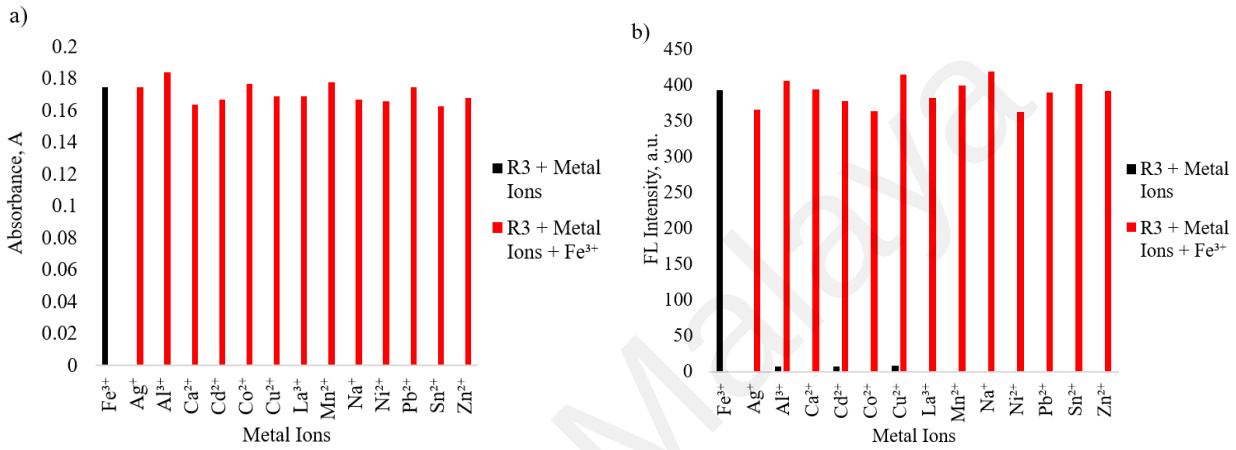

Figure 4.38 The competitive selectivity of R3 (50 µM) based on change in a) absorbance and b) fluorescence intensity for Fe^{3+} at λ = 560 and 585 nm respectively, in the presence of various cations (50 µM) in EtOH/H_2O (7:3. v/v, pH 7.5, Tris-HCl buffer, 1 mM) solution.

4.9 Plausible Binding Mechanism

4.9.1 Job's Plot

To further determine the recognition mode of sensors with metal ions, Job's plot was carried out by using UV-vis spectroscopy. In this study, the molar concentration of metal ions was varied from 0 to 1 with a fixed total concentration of sensor + M^{n+}. For the three sensors, RBOV, RFC and RT4, the maximum absorbance peak was achieved at molar fraction of 0.5, this shows that a 1:1 stoichiometry for the complexation of sensor-M^{n+} (**Figure 4.39**, **Figure 4.40** and **Figure 4.41** respectively). On the other hand, the maximum absorbance peak for R3 sensor was achieved at molar fraction of 0.6 (**Figure**

4.42), indicating a 1:2 stoichiometry for the complexation of R3-Fe^{3+}. The proposed binding mechanism of sensor-M^{n+} complexes could be found in **Table 4.8**.

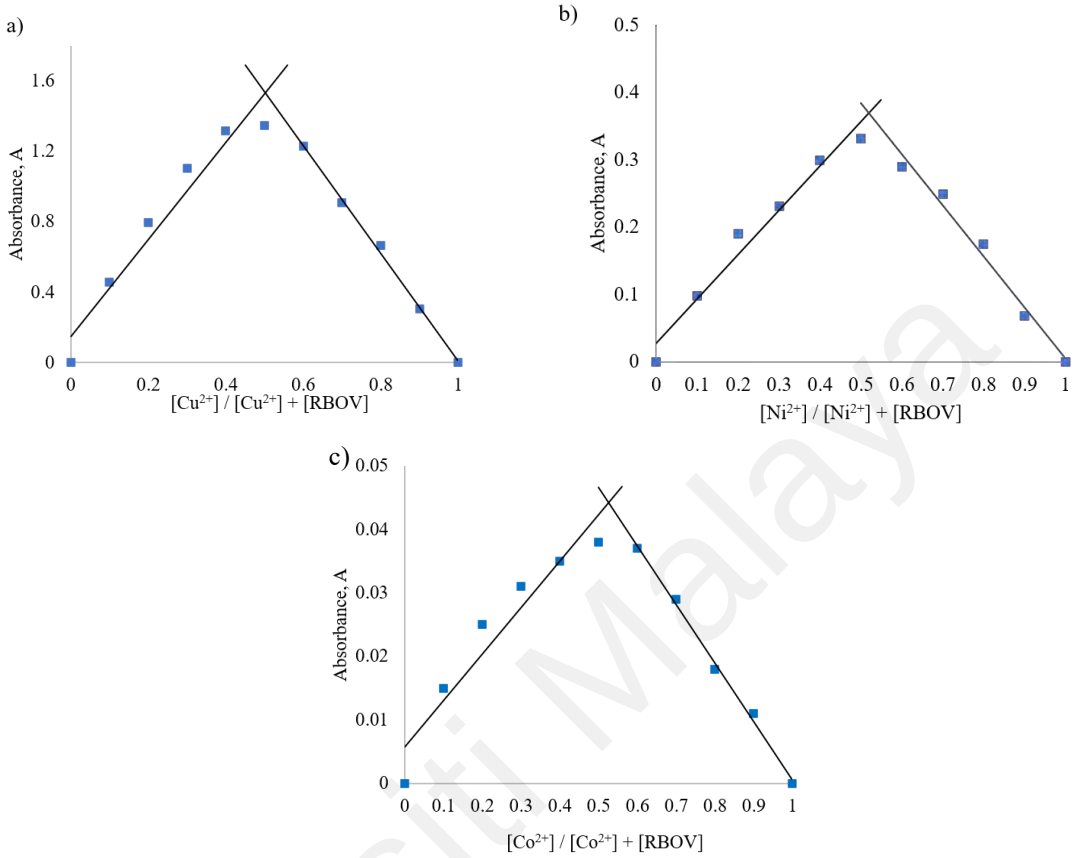

Figure 4.39 Job's plots of RBOV at λ =560 nm for a) Cu^{2+} and at λ = 425 nm for b) Ni^{2+} and c) Co^{2+} in DMSO/TN (2:1, v/v, pH 7.5) solution.

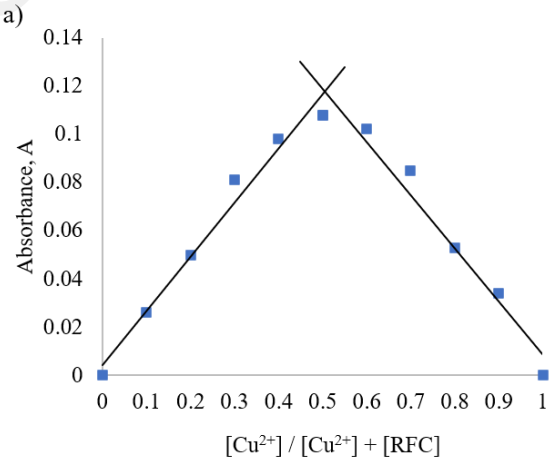

Figure 4.40 Job's plot of RFC with a) Cu^{2+} at λ=560 nm and b) Al^{3+} and b) Fe^{3+} at λ=585 nm in CH_3CN/H_2O (9:1, v/v, pH 7.5, Tris-HCl buffer, 0.1mM) solution.

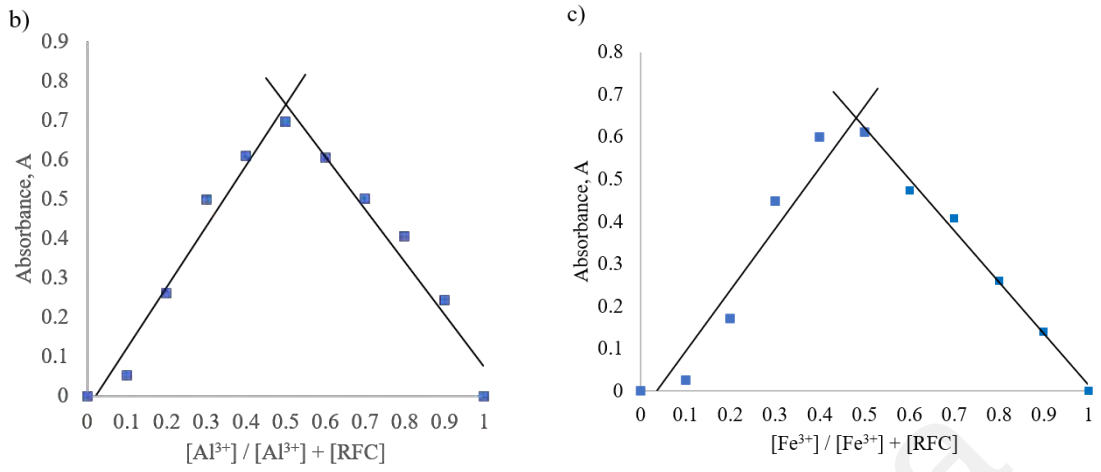

Figure 4.40 continued.

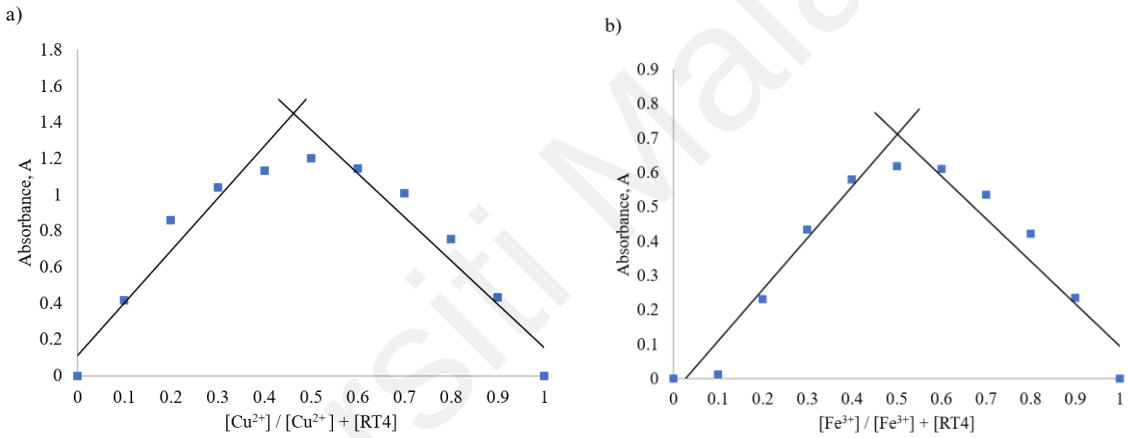

Figure 4.41 Job's plot of RT4 with a) Cu^{2+} at λ=588 nm and b) Fe^{3+} at λ=585 nm in CH_3CN/H_2O (1:1. v/v, pH 7.5, Tris-HCl buffer, 1 mM) solution.

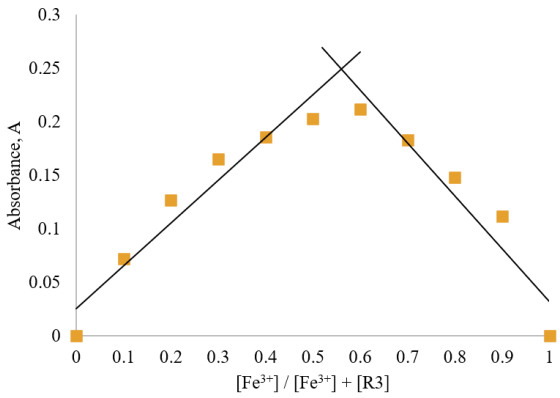

Figure 4.42 Job's plot of R3 with Fe^{3+} at λ=560 nm in $EtOH/H_2O$ (7:3. v/v, pH 7.5, Tris-HCl buffer, 1 mM) solution.

Table 4.9 Proposed binding mechanism of RBOV, RFC, RT4 and R3 sensors.

RBOV	RFC
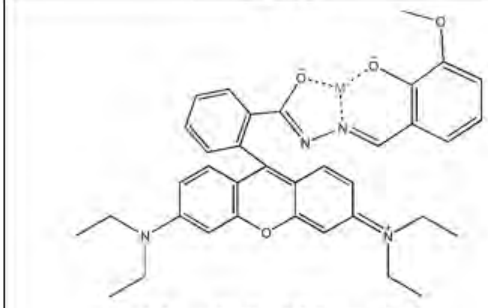 $M^{+} = Cu^{2+}$, Ni^{2+} or Co^{2+}	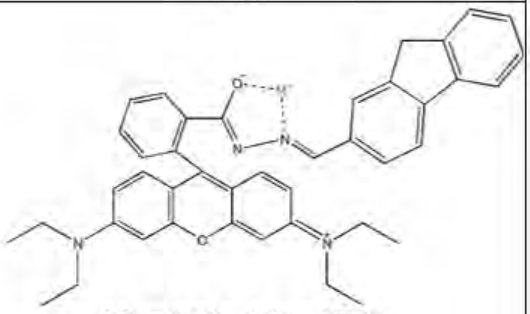 $M^{+} = Cu^{2+}$, Al^{3+} or Fe^{3+}
RT4	**R3**
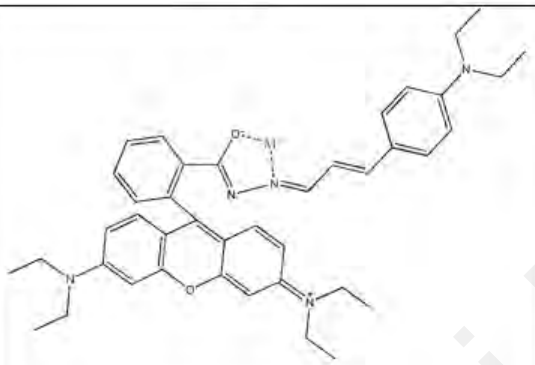 $M^{+} = Cu^{2+}$ or Fe^{3+}	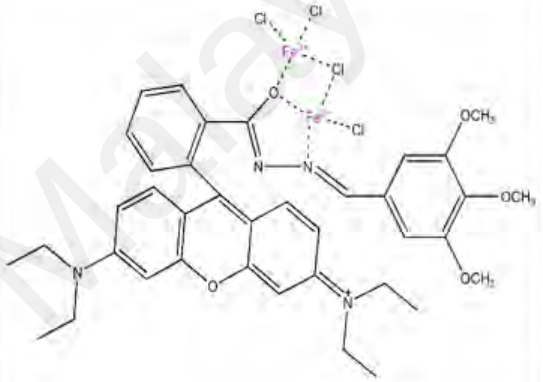

4.9.2 FT-IR Spectra of Sensor-Metal Complexes

In supporting the proposed binding mode of sensor-metal complexes as tabulated in **Table 4.9**, partial IR spectra of RBOV, RFC, RT4 and R3 with metal ions are shown in **Figure 4.43**, **Figure 4.44**, **Figure 4.45** and **Figure 4.46** respectively. The binding of sensors towards metal ions was done by observing the shifting of the characteristic amide carbonyl in the absence and presence of metal ions. The shifting of these peaks is summarized in **Table 4.10** below.

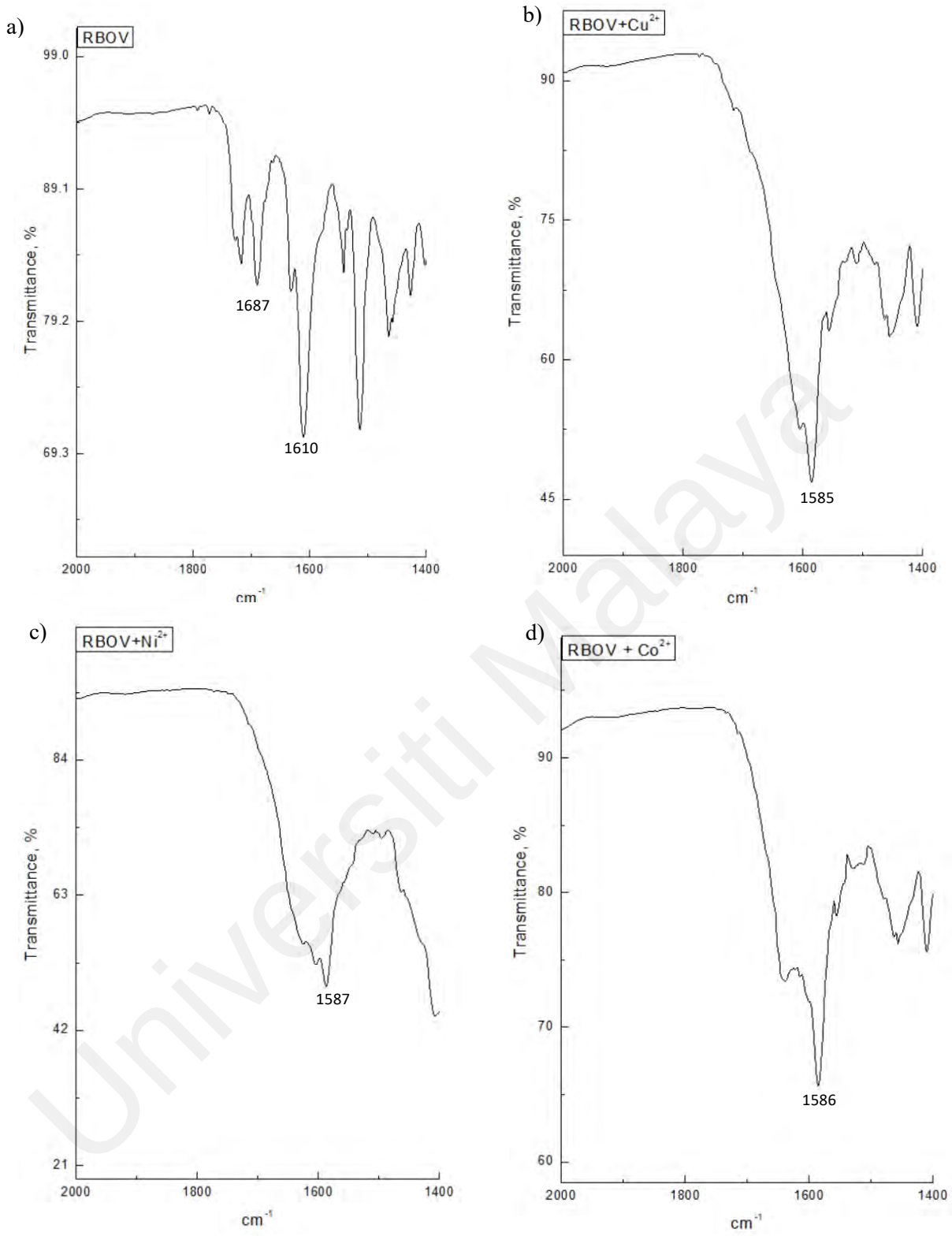

Figure 4.43 Partial IR spectra of a) RBOV b) RBOV-Cu^{2+} c) RBOV-Ni^{2+} and d) RBOV-Ni^{2+}.

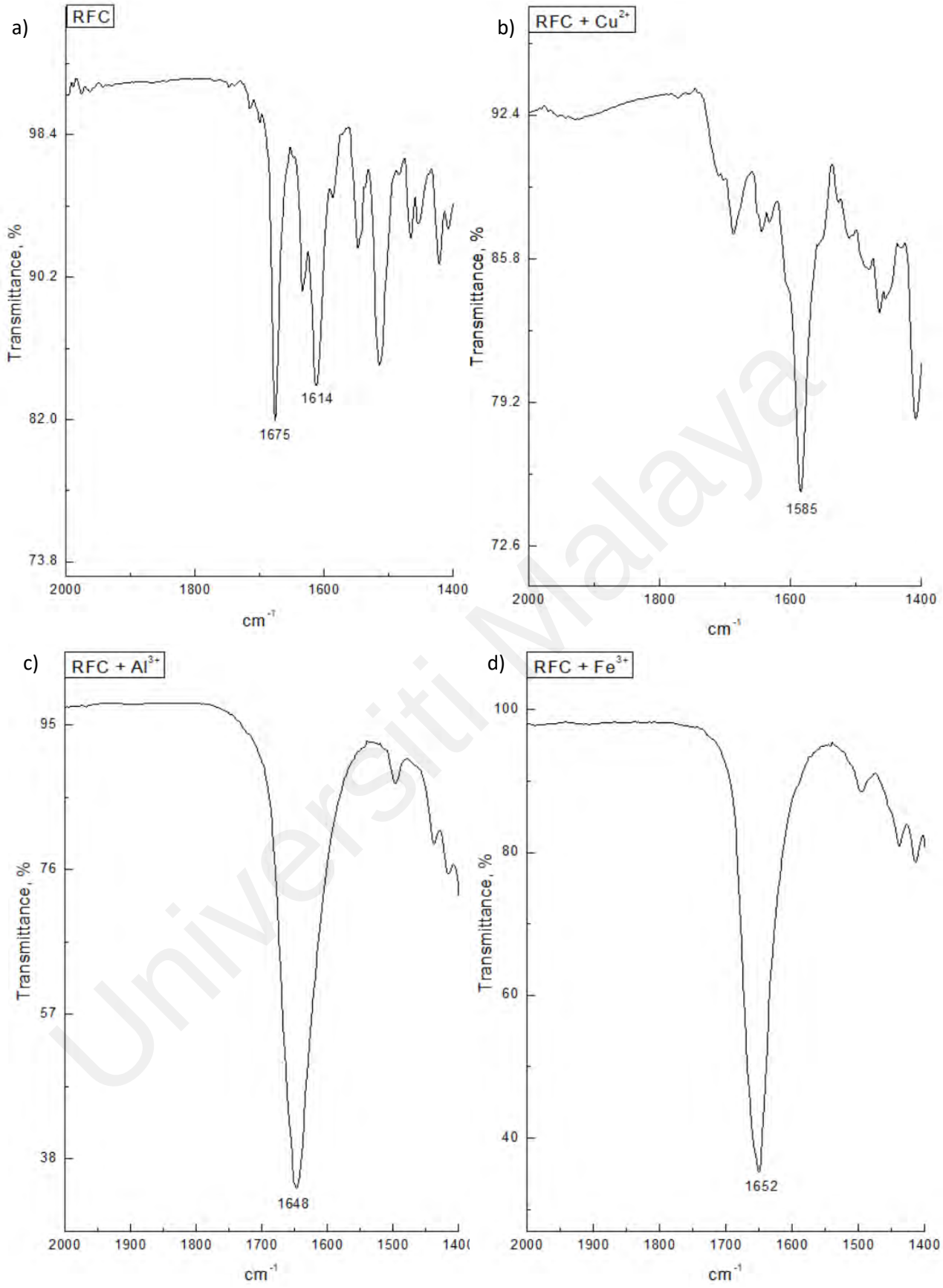

Figure 4.44 Partial IR spectra of a) RFC b) RFC-Cu^{2+} c) RFC-Al^{3+} and d) RFC-Fe^{3+}.

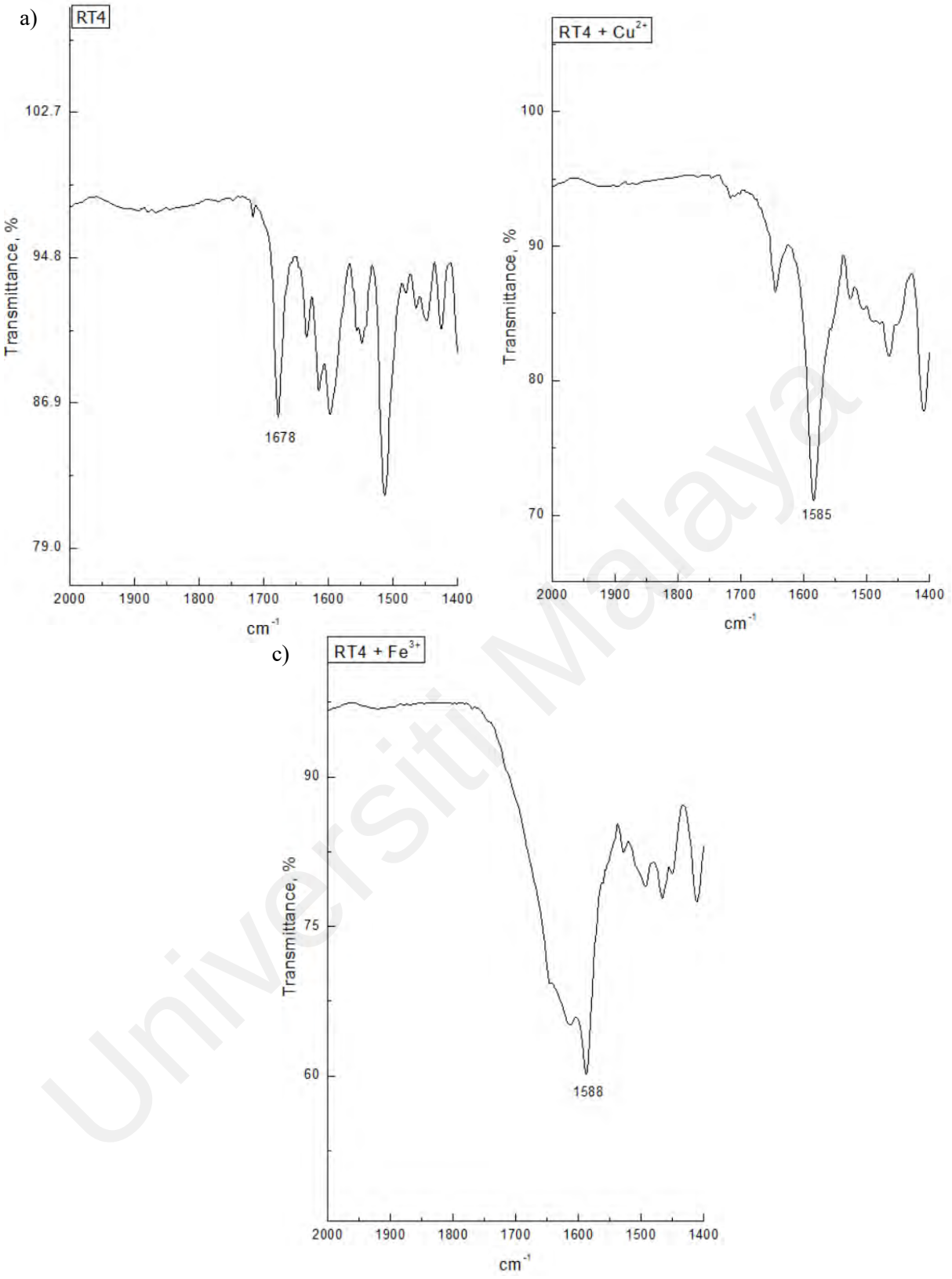

Figure 4.45 Partial IR spectra of a) RT4 b) RT4-Cu^{2+} and c) RT4-Fe^{3+}.

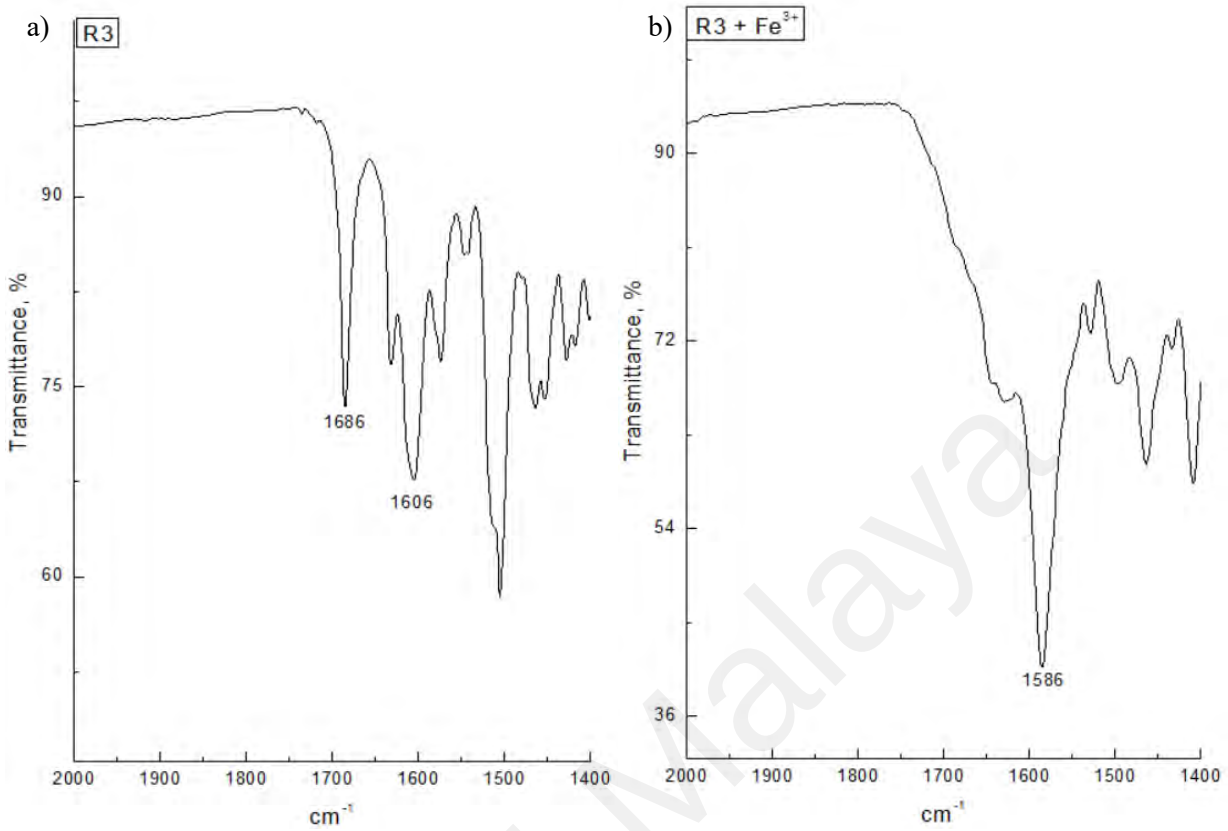

Figure 4.46 Partial IR spectra of a) R3 and b) R3-Fe^{3+}.

Table 4.10 Amide Carbonyl peaks in the absence and presence of metal ions for RBOV, RFC, RT4 and R3 sensors.

Sensor	*ν*(C=O) sensor	*ν*(C=O) sensor-metal complex
RBOV	1687 cm^{-1}	Cu^{2+} = 1585 cm^{-1} Ni^{2+} = 1587 cm^{-1} Co^{2+} = 1586 cm^{-1}
RFC	1675 cm^{-1}	Cu^{2+} = 1585 cm^{-1} Al^{3+} = 1648 cm^{-1} Fe^{3+} = 1652 cm^{-1}
RT4	1678 cm^{-1}	Cu^{2+} = 1585 cm^{-1} Fe^{3+} = 1588 cm^{-1}
R3	1686 cm^{-1}	Fe^{3+} = 1586 cm^{-1}

4.9.3 ^{1}H NMR Spectra of Sensor-Metal Complexes

The complexation was further supported by the ^{1}HNMR spectra of sensor-metal complexes of RFC, RT4 and R3 sensors. Due to the paramagnetism of Cu^{2+}, Ni^{2+} and Co^{2+}, nuclear magnetic titration of RBOV could not be done. In this study, the intensity, shifting and broadening of the characteristic proton of C=N and xanthene are recorded.

As seen in **Figure 4.47**, gradual addition of Al^{3+} and Fe^{3+} caused the proton of C=N at 8.58 ppm to become less intense, broadened and shifted, to 8.59 ppm (2 equivalent) and 8.73 ppm (4 equivalent) for Al^{3+} and from 8.55 to 8.55 ppm (2 equivalent) and 8.34 ppm (4 equivalent) for Fe^{3+} respectively. Besides that, decrease in intensity and broadening of peaks were also observed at 6.25 ppm, 6.27 ppm, 6.49 ppm, 6.55 ppm and 6.57 ppm (2 equivalent) and 6.41 ppm, 6.62 ppm, 6.64 ppm, and 6.70 ppm (4 equivalent) for Al^{3+}, and at 8.01 ppm, 7.80 ppm, 7.72 ppm, 7.65 ppm, 7.49 ppm, 7.29 ppm, 7.12 ppm, 6.50 ppm, and 6.25 ppm (2 equivalent) and 7.99 ppm, 7.67 ppm, 7.48 ppm, 7.30 ppm, 7.11 ppm, 6.49 ppm, and 6.24 ppm (4 equivalent) for Fe^{3+}, corresponding to the xanthene and aromatic protons of RFC. These results indicate that the shifting and broadening of peaks are due to the coordination of RFC with Al^{3+} and Fe^{3+} respectively.

Next, **Figure 4.48** shows the ^{1}HNMR spectrum of RT4 with Fe^{3+}. Upon gradual addition of Fe^{3+} (2-4 equivalent), the proton of C=N at 8.09 ppm becomes less intense and broadened. Similar occurrence could be observed at 6.25 ppm, 6.43 ppm, 6.55 ppm, 6.65 ppm, 7.03 ppm, 7.22 ppm, 7.41 ppm and 7.96 ppm, corresponding to the xanthene and aromatic protons. This behavior is attributed to the formation of the highly fluorescent ring-open form upon complexation of RT4 with Fe^{3+}.

The third ^{1}HNMR spectrum (**Figure 4.49**) shows the shifting and broadening peaks of R3 upon addition of Fe^{3+}. The characteristic proton of C=N at 8.71 ppm becomes less intense and broadened to 8.70 ppm and 8.56 ppm upon addition of 2 and 4 equivalent of Fe^{3+} respectively. Similar observation was recorded for xanthene and aromatic protons of R3 at 7.97 ppm, 7.50 ppm, 7.16 ppm, 6.79 ppm, 6.45 ppm and 6.23 ppm.

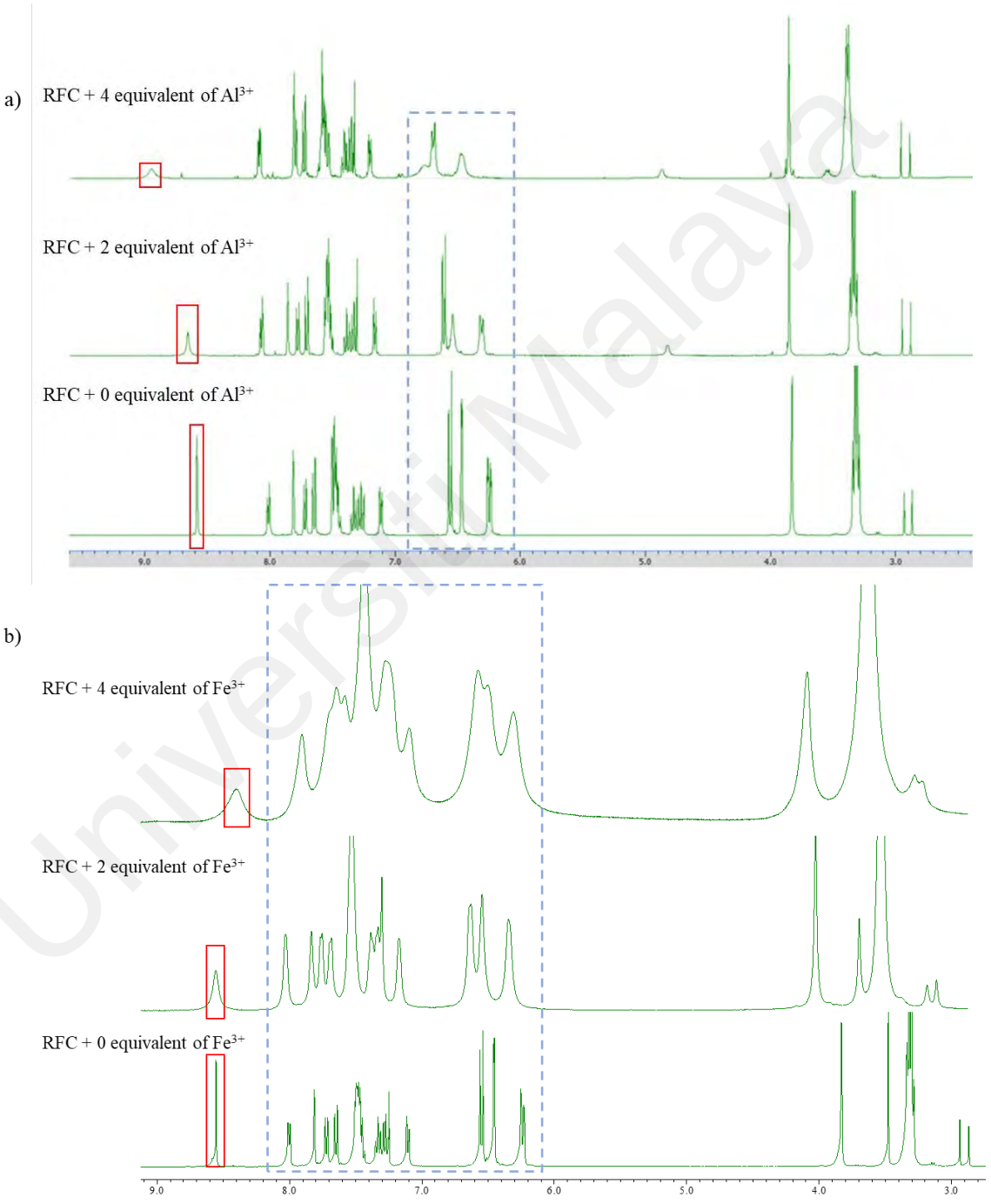

Figure 4.47 ^{1}HNMR spectral changes of RFC upon gradual addition of a) Al^{3+} and b) Fe^{3+} in $CHCl_3$-d.

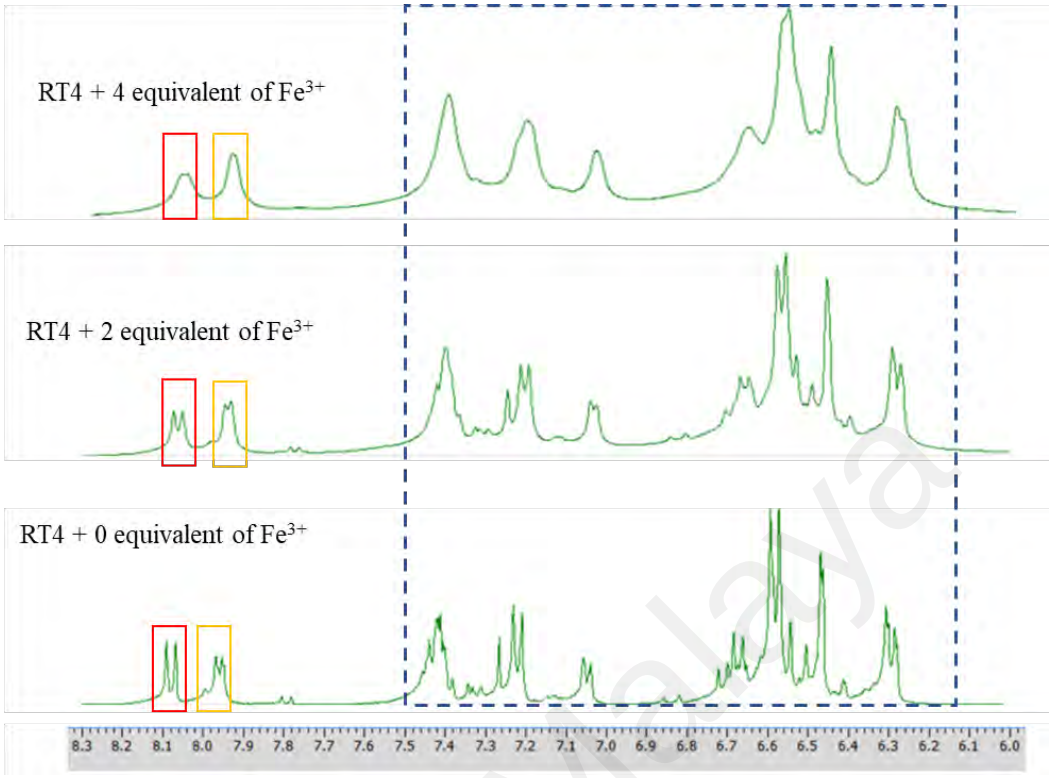

Figure 4.48 ^{1}HNMR spectral changes of RT4 upon gradual addition of Fe^{3+} in $CHCl_3$-d.

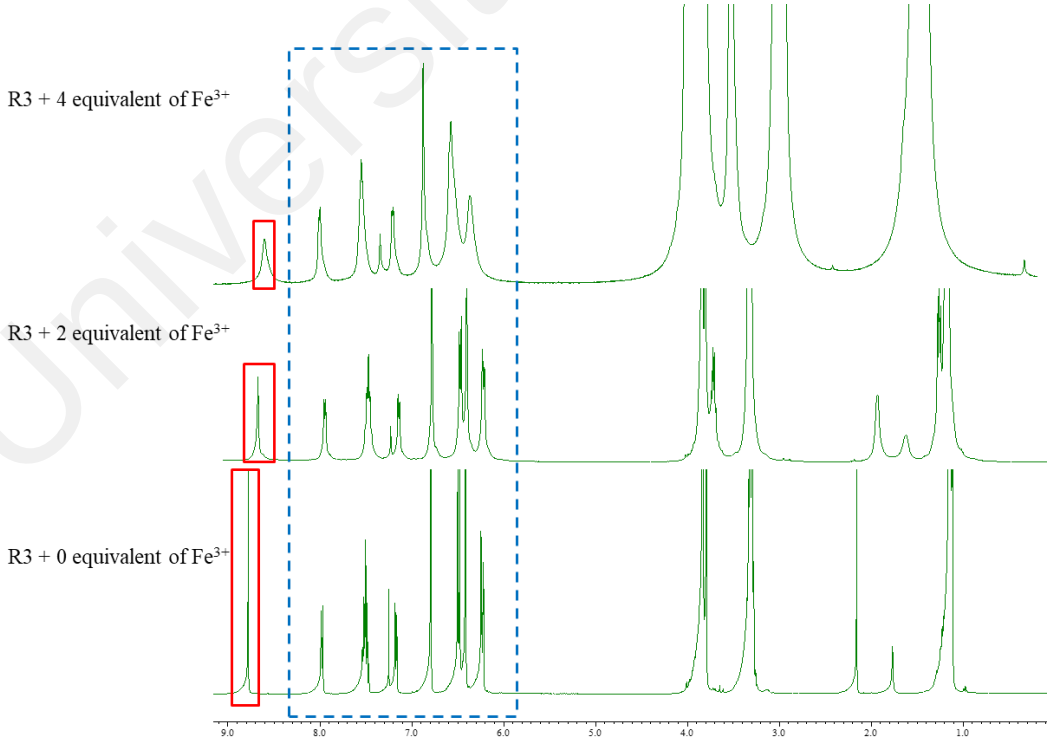

Figure 4.49 ^{1}HNMR spectral changes of R3 upon gradual addition of Fe^{3+} in $CHCl_3$-d.

4.10 Practical Application

4.10.1 Reversibility

The reversibility and regeneration of RBOV, RFC, RT4 and R3 sensors after binding with metal ions are one of the essential criteria for practical applications. The reversibility of these sensors could be seen in **Figure 4.50** for RBOV, **Figure 4.51** for RFC, **Figure 4.52** for RT4 and **Figure 4.53** for R3. As evident in all four figures, the addition of EDTA quenches the absorbance and fluorescence intensity of the sensors. Addition of metal ions into the system regenerate the original colour of the solution. The reversibility and regeneration of RBOV were up to 3 cycles for all metal ions, RFC were up to 5,9 and 4 cycles for Cu^{2+}, Al^{3+} and Fe^{3+} respectively, RT4 were up to 3 and 6 cycles for Cu^{2+} and Fe^{3+} respectively, and R3 were up to 5 (absorbance) and 6 (fluorescence) cycles for Fe^{3+}.

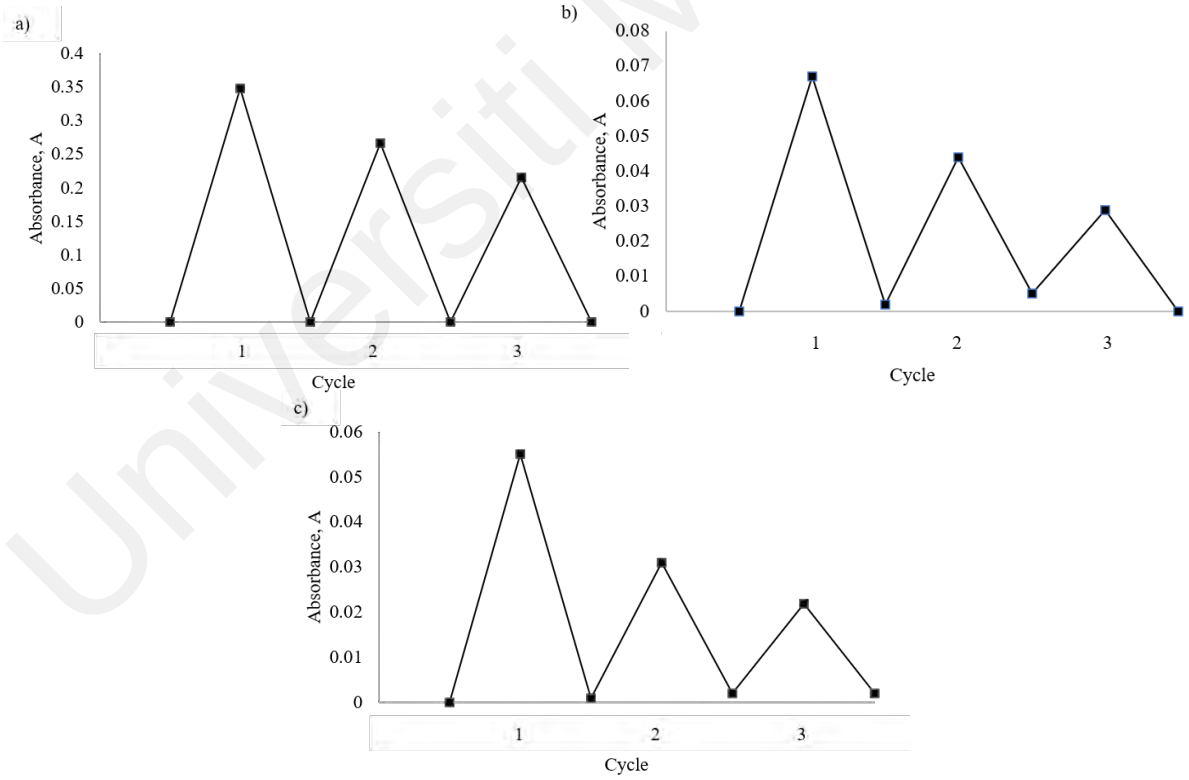

Figure 4.50 Reversibility of RBOV with addition of EDTA and re-addition of a) Cu^{2+}, b) Ni^{2+} and c) Co^{2+}.

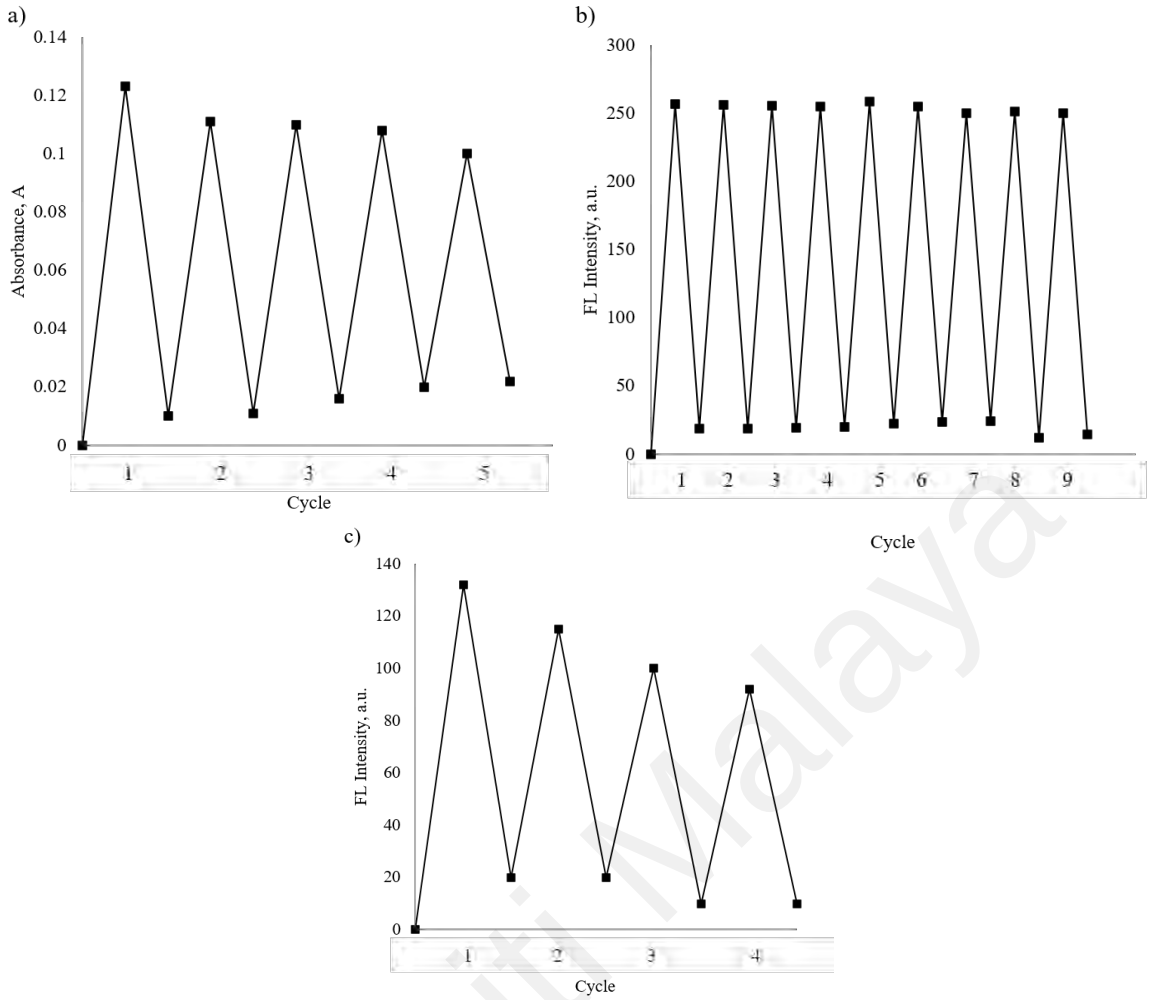

Figure 4.51 Reversibility of RFC with addition of EDTA and re-addition of a) Cu^{2+}, b) Al^{3+} and c) Fe^{3+}.

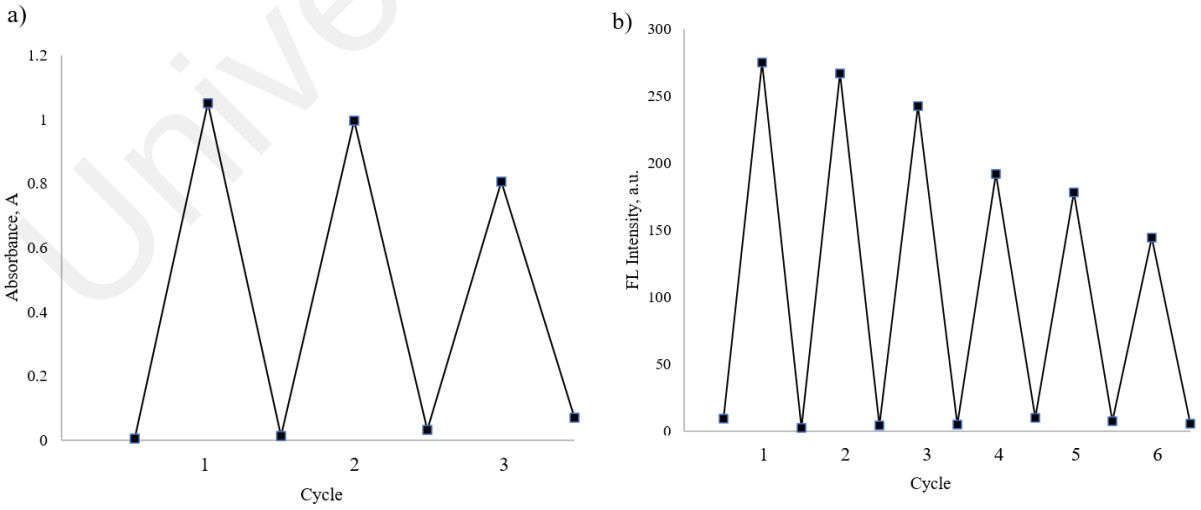

Figure 4.52 Reversibility of RT4 with addition of EDTA and re-addition of a) Cu^{2+} and b) Fe^{3+}.

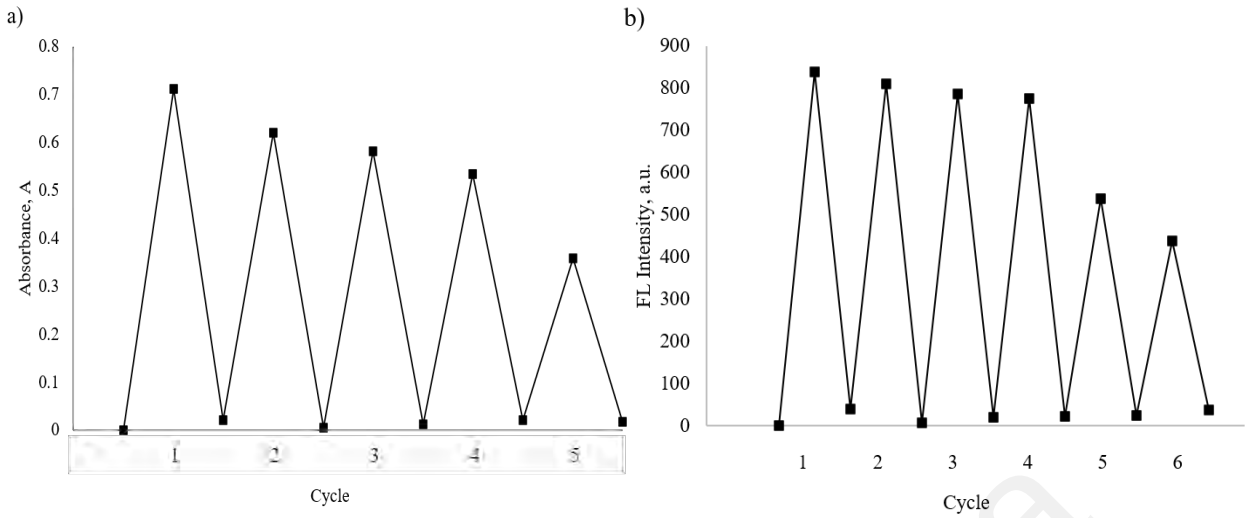

Figure 4.53 Reversibility of R3 with addition of EDTA and re-addition of Fe^{3+} based on change in a) absorbance and b) fluorescence intensity.

4.10.2 On-site Assay Kit

In order to test the potential of sensors developed for practical application, a paper based on-site visual detection of metal ions were prepared by using the common filter paper. The test strips were prepared by soaking the filter paper into solution of known concentration of sensors, in DMSO/TN (2:1, v/v, pH 7.5) solution for RBOV, in CH_3CN/H_2O (9:1, v/v, pH 7.5, Tris-HCl buffer, 0.1mM) solution for RFC, in CH_3CN/H_2O (1:1. v/v, pH 7.5, Tris-HCl buffer, 1 mM) solution for RT4 and in $EtOH/H_2O$ (7:3. v/v, pH 7.5, Tris-HCl buffer, 1 mM) solution for R3 respectively. Once it is dried in air, these test strips were immersed in different concentration of metal ions and the colorimetric changes were observed and recorded.

For RBOV sensor, the detection of the three metal ions were easily distinguishable by the difference in colour of the test strips, purple for Cu^{2+}, yellow for Ni^{2+} and orange for Co^{2+} (**Figure 4.54**). On the other hand, for all three ions, the test strips coated with RFC sensor changes to purple (**Figure 4.55**). In differentiating the recognition of RFC with Al^{3+} and Fe^{3+}, test strips coated with RFC solution (pH 6) were prepared. As evident in **Figure 4.55b**, only Cu^{2+} and Al^{3+} changes to purple. The test strips were further placed

under the uv light to differentiate between recognition of RFC towards Cu^{2+}, with Al^{3+} and Fe^{3+}.

For the third sensor, RT4 showed an interesting colorimetric change upon recognition with Cu^{2+} and Fe^{3+} with the test strips prepared. As evident in **Figure 4.56a**, the colour of the test strips change from yellow to orange, pink, red and purple as the concentration of Fe^{3+} increases. For Cu^{2+}, the test strips change from yellow to orange and finally red. Besides the obvious difference in the colour of the test strips, the two metal ions could also be distinguished under the UV-lamp as only Fe^{3+} gives off bright orange fluorescence (**Figure 4.56c**). Finally, test strips coated with R3 shows a gradual increase in the intensity of purple colour upon gradual increase in concentration of Fe^{3+} (**Figure 4.57**). These results show great applicability of the test strips for rapid on-site detection of metal ions.

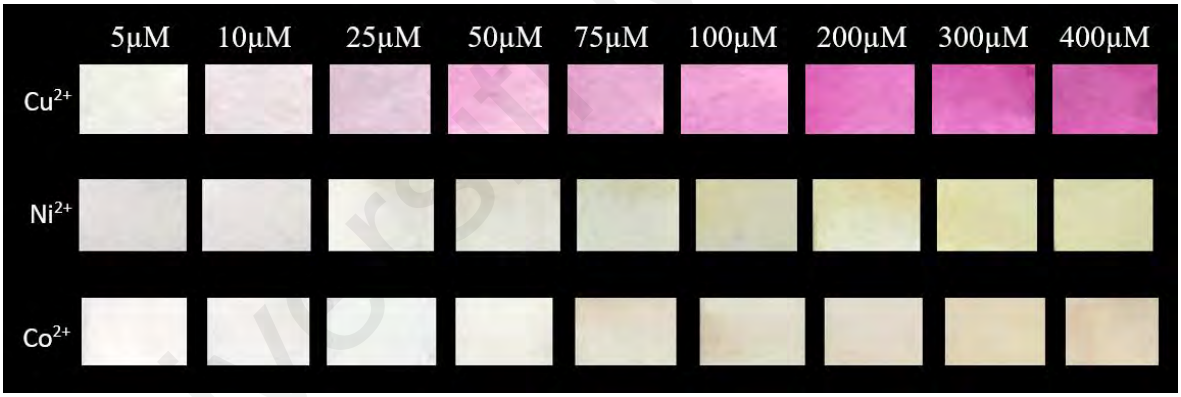

Figure 4.54 Colorimetric changes of test strips coated with RBOV (50 μM) with increasing concentrations of Cu^{2+} Ni^{2+}, and Co^{2+}.

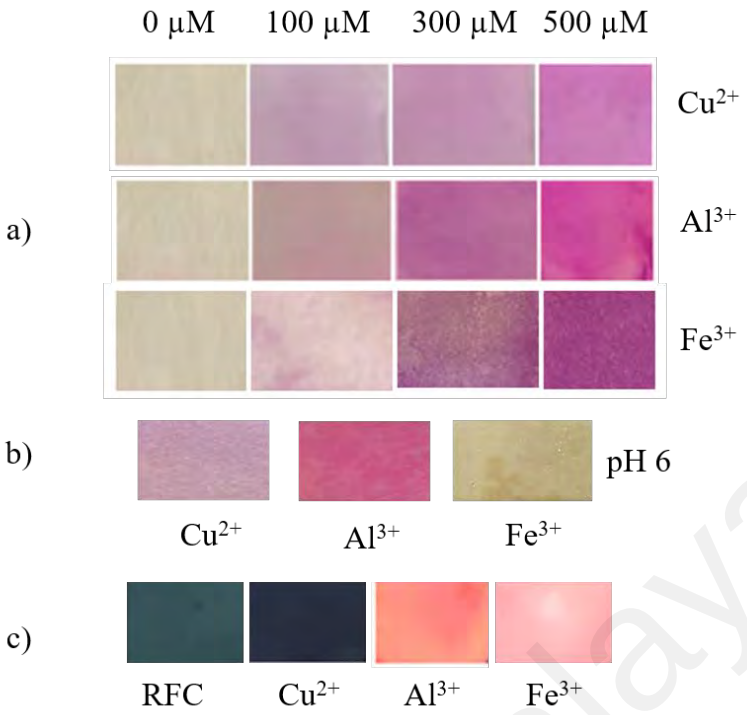

Figure 4.55 Colorimetric changes of test strips coated with RFC (25 mM) with increasing concentration of a) Cu^{2+}, Al^{3+}, and Fe^{3+} b) Test strips coated with RFC in pH 6, and c) Test strips under the UV light ($[M^{n+}]$ = 500 µM).

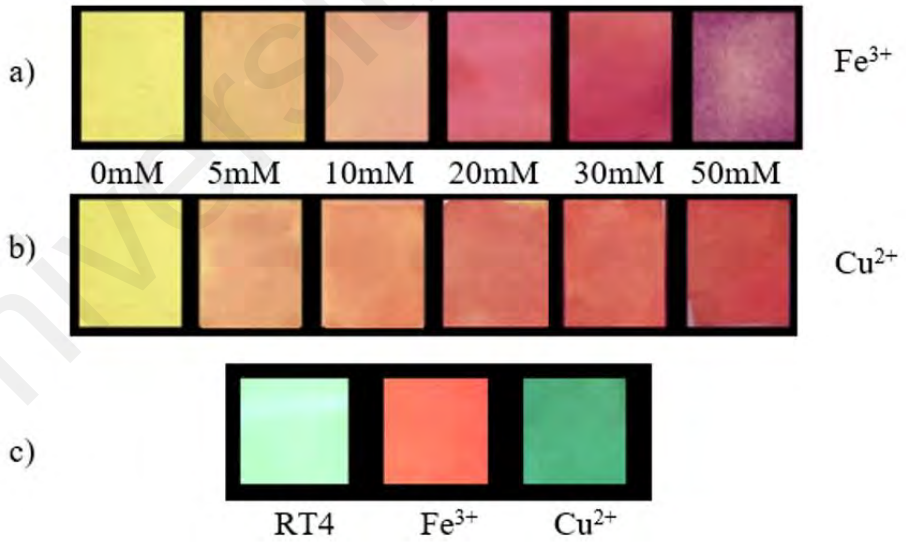

Figure 4.56 Colorimetric changes of test strips coated with RT4 (10 mM) with increasing concentration of a) Fe^{3+} b) Cu^{2+} and c) Test strips under the UV light.

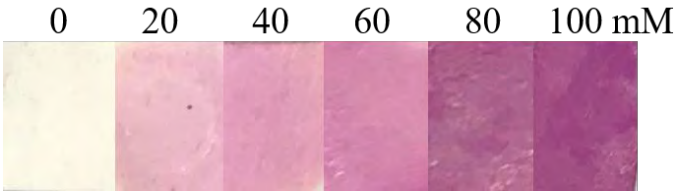

Figure 4.57 Colorimetric changes and of R3 (1 mM) with increasing concentration of Fe^{3+}.

4.10.3 MTT Assay

Finally, in order to determine the practicality of the sensors in biological assays, the cytotoxicity of the sensors was analyzed through MTT assay. The assay was done on the human colorectal adenocarcinoma (HT-29) and normal (CCD-18Co) cell lines with cisplatin as the positive control (**Table 4.11**, **Table 4.12**, **Table 4.13** and **Table 4.14** for RBOV, RFC, RT4 and R3 respectively).

Table 4.11 Cytotoxic activity of RBOV against HT-29 and CCD-18Co cell lines.

	Cell viability (%)											
	HT-29 (µg/mL)						**CCD-18Co (µg/mL)**					
	0.1	0.3	1.0	3.0	10.0	30.0	0.1	0.3	1.0	3.0	10.0	30.0
RBOV	62.59 ± 1.47*	66.72 ± 5.86*	83.31 ± 6.35*	86.86 ± 3.10*	82.52 ± 6.65*	59.59 ± 8.34*	80.40 ± 1.22*	84.04 ± 4.06*	76.02 ± 3.24*	94.18 ± 4.01	90.66 ± 6.10	85.78 ± 4.52*
Cisplatin	75.82 ± 5.92*	71.05 ± 0.57*	68.54 ± 1.79*	51.99 ± 6.93*	11.66 ± 0.74*	11.46 ± 0.71*	94.25 ± 8.42	108.61 ± 5.26	96.42 ± 7.44	96.30 ± 6.98	86.39 ± 3.98*	15.13 ± 0.56*

Data is expressed as mean ± SD (n = 3). Cisplatin was used as positive control. *$p < 0.05$ indicates significant different from untreated control.

Table 4.12 Cytotoxic activity of RFC against HT-29 and CCD-18Co cell lines.

	Cell viability (%)											
	HT-29 (µg/mL)						CCD-18Co (µg/mL)					
	0.1	0.3	1.0	3.0	10.0	30.0	0.1	0.3	1.0	3.0	10.0	30.0
RFC	53.75 ± 6.46*	57.21 ± 5.57*	76.24 ± 4.57*	68.16 ± 1.03*	63.99 ± 3.34*	47.47 ± 3.56*	58.47 ± 1.01*	70.93 ± 3.72*	79.62 ± 3.08*	78.39 ± 4.49*	76.86 ± 2.70*	66.00 ± 4.39*
Cisplatin	57.11 ± 1.75*	66.61 ± 4.44*	57.46 ± 3.43*	46.12 ± 2.12*	19.53 ± 1.36*	14.83 ± 1.48*	110.25 ± 7.80	98.93 ± 3.48	98.21 ± 2.87	90.34 ± 5.30	100.93 ± 2.980	16.90 ± 1.26*

Data is expressed as mean ± SD (n = 3). Cisplatin was used as positive control. *$p < 0.05$ indicates significant different from untreated control.

Table 4.13 Cytotoxic activity of RT4 against HT-29 and CCD-18Co cell lines.

	Cell viability (%)											
	HT-29 (µg/mL)						CCD-18Co (µg/mL)					
	0.1	0.3	1.0	3.0	10.0	30.0	0.1	0.3	1.0	3.0	10.0	30.0
RT4	117.70 ± 0.83*	113.48 ± 1.18*	110.85 ± 4.24*	114.80 ± 1.82*	113.03 ± 3.44*	116.74 ± 0.40*	101.08 ± 4.16*	107.13 ± 4.44*	112.13 ± 5.79*	119.60 ± 7.56*	116.14 ± 4.79*	112.18 ± 5.42*
Cisplatin	125.72 ± 6.65*	124.87 ± 5.38*	107.01 ± 2.98*	73.90 ± 2.88*	40.64 ± 0.97*	34.96 ± 0.76*	94.56 ± 0.75*	80.34 ± 0.47*	78.85 ± 1.52*	57.40 ± 2.02*	59.98 ± 2.92*	13.05 ± 0.47*

Data is expressed as mean ± SD (n = 3). Cisplatin was used as positive control. *$p < 0.05$ indicates significant different from untreated control.

Table 4.14 Cytotoxic activity of R3 against HT-29 and CCD-18Co cell lines.

	Cell viability (%)											
	HT-29 (µg/mL)						CCD-18Co (µg/mL)					
	0.1	0.3	1.0	3.0	10.0	30.0	0.1	0.3	1.0	3.0	10.0	30.0
R3	113.73 ± 4.47*	112.91 ± 0.06*	109.72 ± 1.95*	118.64 ± 1.10*	117.01 ± 0.13*	126.26 ± 0.83*	99.96 ± 5.51*	101.83 ± 13.13*	105.87 ± 5.69*	105.58 ± 5.66*	111.00 ± 4.93*	112.36 ± 3.85*
Cisplatin	125.72 ± 6.65*	124.87 ± 5.38*	107.01 ± 2.98*	73.90 ± 2.88*	40.64 ± 0.97*	34.96 ± 0.76*	94.56 ± 0.75*	80.34 ± 0.47*	78.85 ± 1.52*	57.40 ± 2.02*	59.98 ± 2.92*	13.05 ± 0.47*

Data is expressed as mean ± SD (n = 3). Cisplatin was used as positive control. *$p < 0.05$ indicates significant different from untreated control.

As depicted in **Figure 4.58**, at the highest concentration, at least 85% of the CCD-18Co cells and 59% of HT-29 cells remained alive after incubation with RBOV, whereas only 15% of the CCD-18Co cells and 11% of HT-29 cells remained alive after incubation with cisplatin for 72 hours. **Figure 4.69** showed that at least 58% of the CCD-18Co cells and 47% of HT-29 cells remained alive after incubation for 72 hours with RFC. On the other hand, at the highest concentration, the cell viability was less than 20% when both cells were treated with cisplatin.

RT4 and R3 sensor showed excellent cell viability whereby even after 72 hours of incubation with the sensors, at least 99% of both HT-29 and CCD-18Co cells remained alive even at the highest concentration of sensors at 30.0 µg/mL (**Figure 4.60** and **Figure 4.61**). However, the cells treated with cisplatin showed viability of 74% for HT-29 cells and 57% for CCD-18Co cells at 3.0 µg/mL. These results indicate that all four sensors do not exhibit substantial cytotoxicity towards both HT-29 and CCD-18Co cells and therefore could be used for further recognition of metal ions in biological samples.

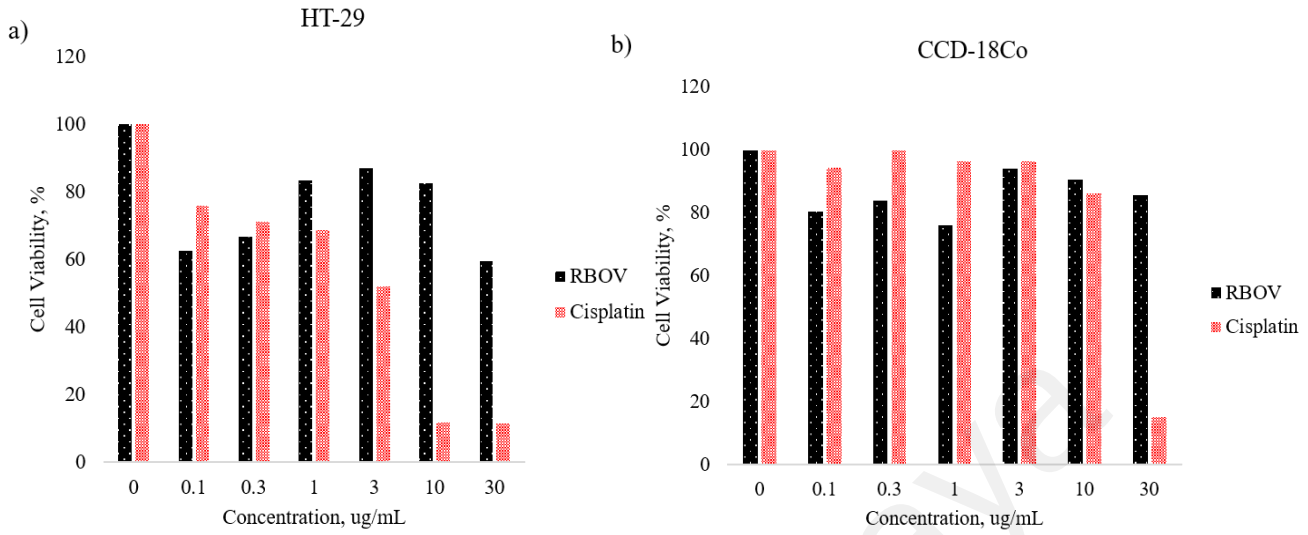

Figure 4.58 Cytotoxic activity of RBOV against a) HT-29 and b) CCD-18Co cell lines. Cisplatin was used as positive control. Data is expressed as mean ± SD (n = 3). *$p < 0.05$ indicates significant different from untreated control.

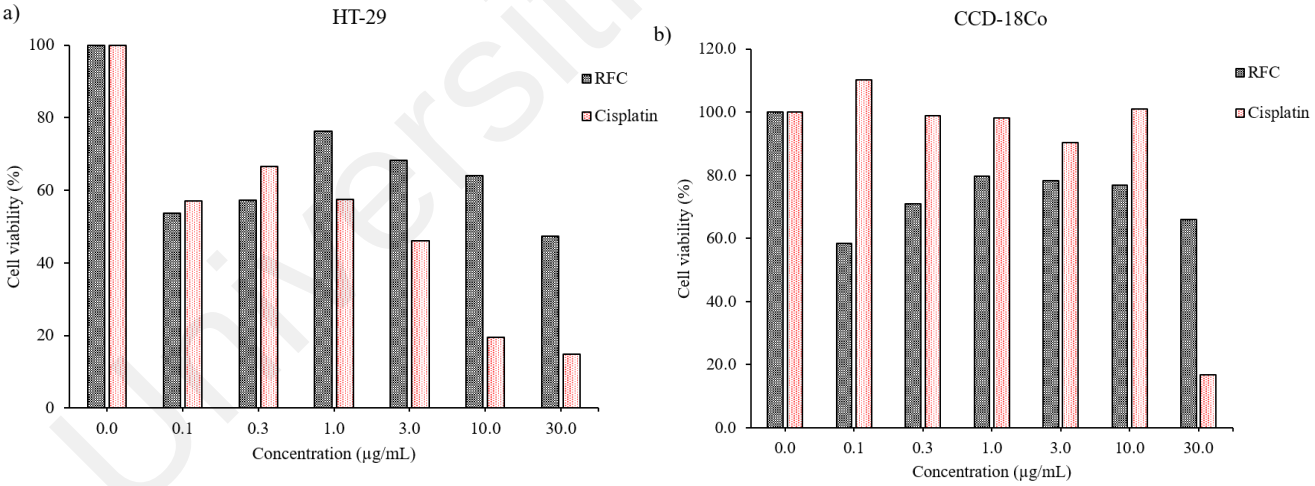

Figure 4.59 Cytotoxic activity of RFC against a) HT-29 and b) CCD-18Co cell lines. Cisplatin was used as positive control. Data is expressed as mean ± SD (n = 3). *$p < 0.05$ indicates significant different from untreated control.

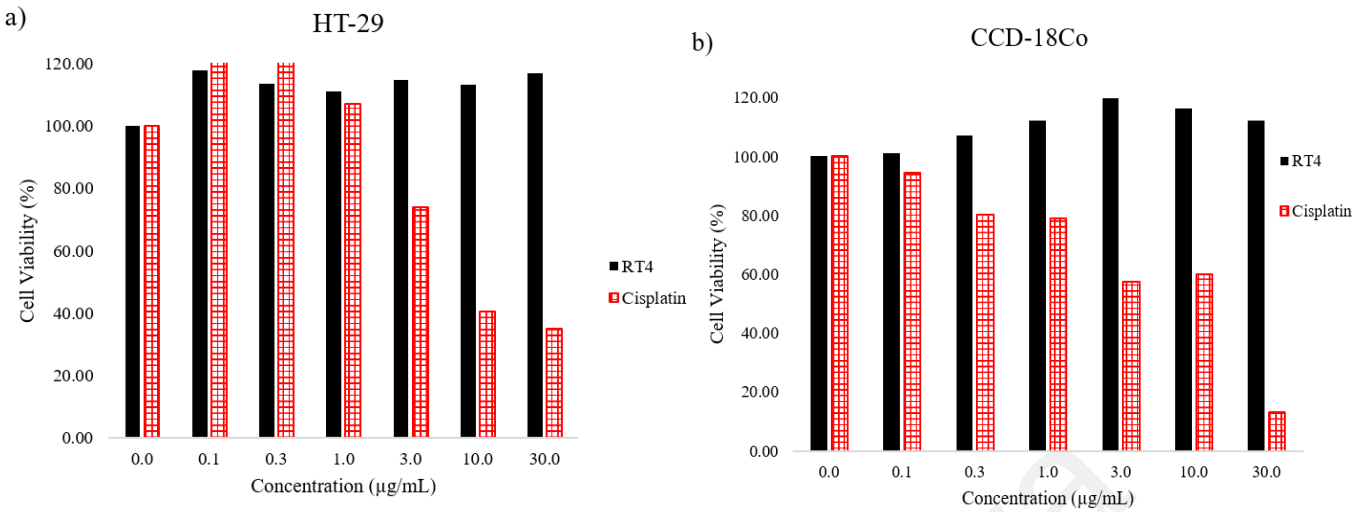

Figure 4.60 Cytotoxic activity of RT4 against a) HT-29 and b) CCD-18Co cell lines. Cisplatin was used as positive control. Data is expressed as mean ± SD (n = 3). *$p <$ 0.05 indicates significant different from untreated control.

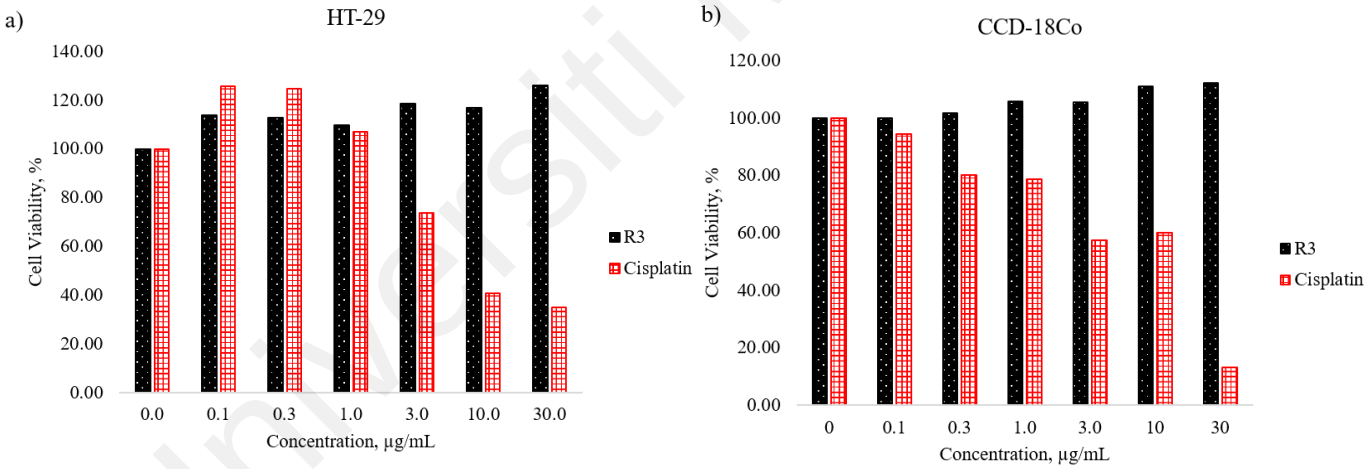

Figure 4.61 Cytotoxic activity of R3 against a) HT-29 and b) CCD-18Co cell lines. Cisplatin was used as positive control. Data is expressed as mean ± SD (n = 3). *$p <$ 0.05 indicates significant different from untreated control.

CHAPTER 5: CONCLUSION

Rhodamine B Schiff-base chemosensors have been successfully synthesized by reacting rhodamine B hydrazide with, 2-hydroxy-3-methoxybenzaldehyde, fluorene-2-carboxaldehyde, trans-4-(Diethylamino)cinnamaldehyde, and 3,4,5-trimethoxybenzaldehyde). These chemosensors have been successfully characterized by FTIR, ^{1}HNMR, ^{13}CNMR, mass spectroscopy and x-ray crystallography. In this work, it could be seen that the rhodamine B sensors have clearly shown their merits in the long excitation and emission wavelengths, which enable them to display the distinct colour and fluorescent changes due to the spirolactam ring-opening, and subsequently making these sensors more preferred for the detection of metal ions.

The rhodamine B-2-hydroxy-3-methoxybenzaldehyde (RBOV) sensor have exhibit unique colorimetric changes upon the detection of Cu^{2+}, Ni^{2+} and Co^{2+} in DMSO/TN (2:1, v/v, pH 7.5) solution. Although RBOV is not fluorescent, it still showed a very high sensitivity for detection of Cu^{2+}, with detection limit as low as 0.04 μM. On the other hand, rhodamine B-fluorene-2-carboxaldehyde (RFC) sensor was able to detect Al^{3+} and Fe^{3+} through fluorometric sensing, and colorimetric sensing for Cu^{2+}. As discussed earlier, pH and the solvent medium may affect the "switch-on" mechanism of a sensor, and this was observed when recognition of RFC towards these three metal ions was tested. As a result, the recognition of RFC towards Al^{3+} could be done in a range of pH 2-6, since Fe^{3+} could only be detected at pH 7.

Rhodamine B-trans-4-(Diethylamino)cinnamaldehyde (RT4), has shown a unique colorimetric and fluorometric changes upon detection of Cu^{2+} and Fe^{3+}. The free RT4 exhibits yellow colour in CH_3CN/H_2O (1:1. v/v, pH 7.5, 1 mM Tris-HCl buffer) solution, and yellow fluorescence enhancement under the UV light. Upon recognition of Cu^{2+} and Fe^{3+}, the solution changes to red and orange respectively. However, when it is placed under the UV light, RT4-Cu^{2+} shows a "switch-off" mechanism, while RT4-Fe^{3+} displays

orange fluorescence enhancement with a new maximum emission wavelength at 585 nm. Rhodmine B-3,4,5-trimethoxybenzaldehyde (R3) sensor, on the other hand showed a great selectivity and sensitivity upon recognition of Fe^{3+} through both colorimetric and fluorometric sensing. Furthermore, R3 sensor also exhibits great anti-interference property towards recognition of Fe^{3+} in the presence of other metal ions.

As discussed earlier, the development of new methods for detection of metal ions in sub molar concentration is imperative so that it could be done in real-time and real-space, since these analytes are important both environmentally and biologically. Thus, test strips coated with RBOV, RFC, RT4 and R3 has been successfully prepared for on-site assay application. These test strips show excellent colorimetric changes upon detection of metal ions, and also exhibit fluorescence enhancement under the UV light. Furthermore, the intensity of the colour on the test strips upon gradual increase in concentration of metal ions may enable the preliminary quantitative information during in-field application. These results suggest great potentiality in detecting metal ions by using the test strips for environmental contamination as it provides a rather simple, convenient, and effective method.

Besides, in determining the applicability of these sensor for biological assays, MTT assays were conducted. From the assay conducted, all of the sensors did not show significant toxicity towards HT-29 and CCD-18Co cells after 72 hours of incubation. Both RT4 and R3 shows excellent cell viability even at the highest concentration, as compared to cisplatin. The results indicate potential application in monitoring metal ions in normal and cancerous cells.

To sum it up, it is clear that structural modulation and ligand engineering of rhodamine B chemosensors plays a big role in its detection mode, dependency on

solvent and pH, and even colour changes. Since in some cases, the reason behind the ring-opening process, difference in colorimetric changes and other properties have yet to be fully understood, a wide horizon is open for further modifications to either enhance or inhibit certain properties to meet the needs and requirement of the desired sensor. In future, more focus and importance should be given to compounds similar to RT4 and RBOV in the development of chemosensors. This is because, both sensors had shown a unique and versatile colorimetric changes and detection of metal ions in different solvent system. In addition, future studies should also explore on the mechanism of action of the synthesized chemosensor towards living cell and its potentiality in the physiological field. As rhodamine derivatives are easily modified, the development of sensors based on biological or environmental purposes can be adjusted accordingly and this will certainly continue to be a field of interest of many researchers for many years to come.

REFERENCES

Abebe, F. A., & Sinn, E. (2011). Fluorescein-based fluorescent and colorimetric chemosensors for copper in aqueous media. *Tetrahedron Letters, 52*(41), 5234-5237.

Aharoni, R., Bronstheyn, M., Jabbour, A., Zaks, B., Srebnik, M., & Steinberg, D. (2008). Oxazaborolidine derivatives inducing autoinducer-2 signal transduction in Vibrio harveyi. *Bioorg Med Chem, 16*(4), 1596-1604.

Andersen, A., Berge, S. R., Engeland, A., & Norseth, T. (1996). Exposure to nickel compounds and smoking in relation to incidence of lung and nasal cancer among nickel refinery workers. *Occup Environ Med, 53*(10), 708.

Arcoumanis, C., McGuirk, J. J., & Palma, J. M. L. M. (1990). On the use of fluorescent dyes for concentration measurements in water flows. *Experiments in Fluids, 10*(2), 177-180.

Armstrong, B., Tremblay, C., Baris, D., & Thériault, G. (1994). Lung cancer mortality and polynuclear aromatic hydrocarbons: A case-cohort study of aluminum production workers in Arvida, Quebec, Canada. *American Journal of Epidemiology, 139*(3), 250-262.

Arredondo, M., & Núñez, M. T. (2005). Iron and copper metabolism. *Molecular Aspects of Medicine, 26*(4), 313-327.

Assi, M. A., Hezmee, M. N. M., Haron, A. W., Sabri, M. Y. M., & Rajion, M. A. (2016). The detrimental effects of lead on human and animal health. *Veterinary world, 9*(6), 660-671.

Atta, A. M., Shaker, N. O., & Maysour, N. E. (2006). Influence of the molecular structure on the chemical resistivity and thermal stability of cured Schiff base epoxy resins. *Progress in Organic Coatings, 56*(2), 100-110.

Badugu, R., Lakowicz, J. R., & Geddes, C. D. (2005). Cyanide-sensitive fluorescent probes. *Dyes and Pigments, 64*(1), 49-55.

Baeyer, A. V. (1871). Chem. Ber., *5*, 255.

Bangs, L. B. (1996). New developments in particle-based immunoassays: introduction. *Pure and Applied Chemistry, 68*(10), 1873-1879.

Barceloux, D. G., & Barceloux, D. (1999). Cobalt. *Journal of Toxicology: Clinical Toxicology, 37*(2), 201-216.

Barceloux, D. G., & Barceloux, D. (1999). Nickel. *Journal of Toxicology: Clinical Toxicology, 37*(2), 239-258.

Bargossi, C., Fiorini, M. C., Montalti, M., Prodi, L., & Zaccheroni, N. (2000). Recent developments in transition metal ion detection by luminescent chemosensors. *Coordination Chemistry Reviews, 208*(1), 17-32.

Becker, D. E., Smith, S. E., & Loosli, J. K. (1949). Vitamin B12 and cobalt deficiency in sheep. *Science, 110*(2846), 71-72.

Behera, K. C., & Bag, B. (2016). Switch in 'turn-on' signaling preferences from Fe(III) to Hg(II) as a function of solvent and structural variation in rhodamine based probes. *Dyes and Pigments, 135*, 143-153.

Beija, M., Afonso, C. A. M., & Martinho, J. M. G. (2009). Synthesis and applications of rhodamine derivatives as fluorescent probes. *Chemical Society Reviews, 38*(8), 2410-2433.

Belfield, K. D., Bondar, M. V., Frazer, A., Morales, A. R., Kachkovsky, O. D., Mikhailov, I. A., . . . Przhonska, O. V. (2010). Fluorene-based metal-ion sensing probe with high sensitivity to Zn2+ and efficient two-photon absorption. *The Journal of Physical Chemistry B, 114*(28), 9313-9321.

Benesi, H. A., & Hildebrand, J. H. (1949). A spectrophotometric investigation of the interaction of iodine with aromatic hydrocarbons. *Journal of the American Chemical Society, 71*(8), 2703-2707.

Berg, D., Gerlach, M., Youdim, M. B. H., Double, K. L., Zecca, L., Riederer, P., & Becker, G. (2001). Brain iron pathways and their relevance to Parkinson's disease. *Journal of Neurochemistry, 79*(2), 225-236.

Bicker, K. L., Wisku, S. L., & Lavign, J. J. (2011). Colorimetric sensor design. In *Chemosensors: Principles, Strategies, and Applications* (pp. 275-295).

Bishop, G. M., Robinson, S. R., Liu, Q., Perry, G., Atwood, C. S., & Smith, M. A. (2002). Iron: A pathological mediator of Alzheimer disease? *Developmental Neuroscience, 24*(2-3), 184-187.

Blake, D. A., & McLean, N. V. (1989). A colorimetric assay for the measurement of d-glucose consumption by cultured cells. *Analytical Biochemistry, 177*(1), 156-160.

Cempel, N., & Nikel, G. (2006). Nickel: A review of its sources and environmental toxicology. *Polish Journal of Environmental Studies, 15*(3), 375-382.

Chen, X., Pradhan, T., Wang, F., Kim, J. S., & Yoon, J. (2012). Fluorescent chemosensors based on spiroring-opening of xanthenes and related derivatives. *Chemical Reviews, 112*(3), 1910-1956.

Chen, Y., Chen, B., & Han, Y. (2016). A novel rhodamine-based fluorescent probe for the fluorogenic and chromogenic detection of Pd2+ ions and its application in live-cell imaging. *Sensors and Actuators B: Chemical, 237*, 1-7.

Ciardelli, G., & Ranieri, N. (2001). The treatment and reuse of wastewater in the textile industry by means of ozonation and electroflocculation. *Water Research, 35*(2), 567-572.

Clark, S. F. (2008). Iron deficiency anemia. *Nutrition in Clinical Practice, 23*(2), 128-141.

Colter, A., & Mahler, R. L. (2006). *Iron in drinking water*: University of Idaho Moscow.

Coogan, T. P., Latta, D. M., Snow, E. T., Costa, M., & Lawrence, A. (1989). Toxicity and carcinogenicity of nickel compounds. *CRC Critical Reviews in Toxicology, 19*(4), 341-384.

CrysAlis, P. (2009). Oxford Diffraction Ltd. *Yarnton England*.

Cuadrado, C., Kumpulainen, J., Carbajal, A., & Moreiras, O. (2000). Cereals contribution to the total dietary intake of heavy metals in Madrid, Spain. *Journal of Food Composition and Analysis, 13*(4), 495-503.

da Silva, C. M., da Silva, D. L., Modolo, L. V., Alves, R. B., de Resende, M. A., Martins, C. V. B., & de Fátima, Â. (2011). Schiff bases: A short review of their antimicrobial activities. *Journal of Advanced Research, 2*(1), 1-8.

Darbre, P. D. (2005). Aluminium, antiperspirants and breast cancer. *Journal of Inorganic Biochemistry, 99*(9), 1912-1919.

de Silva, A. P., Gunaratne, H. Q. N., Gunnlaugsson, T., Huxley, A. J. M., McCoy, C. P., Rademacher, J. T., & Rice, T. E. (1997). Signaling recognition events with fluorescent sensors and switches. *Chemical Reviews, 97*(5), 1515-1566.

Dhara, A., Jana, A., Konar, S., Ghatak, S. K., Ray, S., Das, K., . . . Kar, S. K. (2013). A novel rhodamine-based colorimetric chemodosimeter for the rapid detection of Al3+ in aqueous methanol: fluorescent 'OFF–ON' mechanism. *Tetrahedron Letters, 54*(28), 3630-3634.

DiCesare, N., & Lakowicz, J. R. (2002). New sensitive and selective fluorescent probes for fluoride using boronic acids. *Analytical Biochemistry, 301*(1), 111-116.

Dong, M., Ma, T. H., Zhang, A. J., Dong, Y. M., Wang, Y. W., & Peng, Y. (2010). A series of highly sensitive and selective fluorescent and colorimetric "off-on" chemosensors for Cu (II) based on rhodamine derivatives. *Dyes and Pigments, 87*(2), 164-172.

dos Santos Carlos, F., Nunes, M. C., De Boni, L., Machado, G. S., & Nunes, F. S. (2017). A novel fluorene-derivative Schiff-base fluorescent sensor for copper(II) in organic media. *Journal of Photochemistry and Photobiology A: Chemistry, 348*, 41-46.

Duan, Y., Liu, M., Sun, W., Wang, M., S, L., & Li, Q. X. (2009). Recent progress on synthesis of fluorescein probes. *Mini-Reviews in Organic Chemistry, 6(1)*, 35-43.

Dujols, V., Ford, F., & Czarnik, A. W. (1997). A long-wavelength fluorescent chemodosimeter selective for Cu(II) ion in water. *Journal of the American Chemical Society, 119*(31), 7386-7387.

Edition, T. (2008). Guidelines for drinking-water quality. *WHO chronicle, 1*(3), 334-415.

Erçağ, E., Üzer, A., & Apak, R. (2009). Selective spectrophotometric determination of TNT using a dicyclohexylamine-based colorimetric sensor. *Talanta, 78*(3), 772-780.

Fang, Y., Zhou, Y., Li, J. Y., Rui, Q. Q., & Yao, C. (2015). Naphthalimide–Rhodamine based chemosensors for colorimetric and fluorescent sensing Hg2+ through different signaling mechanisms in corresponding solvent systems. *Sensors and Actuators B: Chemical, 215*, 350-359.

Fergusson, J. E. (1990). *The heavy elements : chemistry, environmental impact and health effects*. Oxford [England]: Pergamon Press.

Gaetke, L. M., & Chow, C. K. (2003). Copper toxicity, oxidative stress, and antioxidant nutrients. *Toxicology, 189*(1), 147-163.

Gaggelli, E., Kozlowski, H., Valensin, D., & Valensin, G. (2006). Copper homeostasis and neurodegenerative disorders (Alzheimer's, Prion, and Parkinson's diseases and amyotrophic lateral sclerosis). *Chemical Reviews, 106*(6), 1995-2044.

Georgopoulos, P. G., Roy, A., Yonone-Lioy, M. J., Opiekun, E., & Lioy, P. J. (2001). Environmental copper: Its dynamic and human exposure issues. *Journal of Toxicology and Environmental Health, Part B, 4*(4), 341-394.

Ghorai, A., Mondal, J., Chowdhury, S., & Patra, G. K. (2016). Solvent-dependent fluorescent-colorimetric probe for dual monitoring of Al3+ and Cu2+ in aqueous solution: An application to bio-imaging. *Dalton Transactions, 45*(28), 11540-11553.

Giepmans, B. N. G., Adams, S. R., Ellisman, M. H., & Tsien, R. Y. (2006). The fluorescent toolbox for assessing protein location and function. *Science, 312*(5771), 217.

Godbold, D. L., Fritz, E., & Hüttermann, A. (1988). Aluminum toxicity and forest decline. *Proceedings of the National Academy of Sciences, 85*(11), 3888.

Gopalakrishnan, A., Krishnan, R., Thangavel, S., Venugopal, G., & Kim, S. J. (2015). Removal of heavy metal ions from pharma-effluents using graphene-oxide nanosorbents and study of their adsorption kinetics. *Journal of Industrial and Engineering Chemistry, 30*, 14-19.

Gupta, V. K., Mergu, N., & Kumawat, L. K. (2016). A new multifunctional rhodamine-derived probe for colorimetric sensing of Cu(II) and Al(III) and fluorometric sensing of Fe(III) in aqueous media. *Sensors and Actuators B: Chemical, 223*, 101-113.

Hama, Y., Urano, Y., Koyama, Y., Bernardo, M., Choyke, P. L., & Kobayashi, H. (2006). A comparison of the emission efficiency of four common green fluorescence dyes after internalization into cancer cells. *Bioconjug Chem, 17*(6), 1426-1431.

Heike, B. (2005). *Heavy Metals in the Environment: Origin, Interaction and Remediation*: Elsevier/Academic Press.

Heng, M. K., Tan, C. H., Saad, H. M., Sim, K. S., & Tan, K. W. (2020). Mitochondria-dependent apoptosis inducer: Testosterone-N4-ethylthiosemicarbazonate and its metal complexes with selective cytotoxicity towards human colorectal carcinoma cell line (HCT 116). *Inorganica Chimica Acta, 507*, 119581.

Hengstler, J. G., Bolm-Audorff, U., Faldum, A., Janssen, K., Reifenrath, M., Götte, W., . . . Oesch, F. (2003). Occupational exposure to heavy metals: DNA damage induction and DNA repair inhibition prove co-exposures to cadmium, cobalt and lead as more dangerous than hitherto expected. *Carcinogenesis, 24*(1), 63-73.

Kennedy, A., Dornan, J. D., & King, R. (1981). Fatal myocardial disease associated with industrial exposure to cobalt. *Lancet, 1*(8217), 412-414.

Kim, Lee, M. H., Kim, H. J., Kim, J. S., & Yoon, J. (2008). A new trend in rhodamine-based chemosensors: application of spirolactam ring-opening to sensing ions. *Chemical Society Reviews, 37*(8), 1465-1472.

Kim, H.-S., Angupillai, S., & Son, Y.-A. (2016). A dual chemosensor for both Cu2+ and Al3+: A potential Cu2+ and Al3+ switched YES logic function with an INHIBIT logic gate and a novel solid sensor for detection and extraction of Al3+ ions from aqueous solution. *Sensors and Actuators B: Chemical, 222*, 447-458.

Kim, J. H., Gibb, H. J., & Howe, P. (2006). Cobalt and inorganic cobalt compounds (No. 69). *World Health Organization,*

.

Kim., Choi, M. G., Noh, J. H., Ahn, S. D., & Chang, S. K. (2008). Rhodamine B hydrazide revisited: chemodosimetric Hg2+ - selective signaling behavior in aqueous environements. *Bulleting of the Korean Chemical Society, 29(3)*, 571-574.

Klevay, L. M. (2000). Cardiovascular disease from copper deficiency—A history. *The Journal of Nutrition, 130*(2), 489S-492S.

Knopf, B., & König, H. (2010). Biomethylation of heavy metals in soil and terrestrial invertebrates. In *Soil Heavy Metals* (pp. 315-328). Berlin, Heidelberg: Springer Berlin Heidelberg.

Körbahti, B. K., Artut, K., Geçgel, C., & Özer, A. (2011). Electrochemical decolorization of textile dyes and removal of metal ions from textile dye and metal ion binary mixtures. *Chemical Engineering Journal, 173*(3), 677-688.

Krewski, D., Yokel, R. A., Nieboer, E., Borchelt, D., Cohen, J., Harry, J., . . . Rondeau, V. (2007). Human health risk assessment for aluminium, aluminium oxide, and aluminium hydroxide. *Journal of Toxicology and Environmental Health, Part B, 10*(sup1), 1-269.

Kumar, M., Kumar, N., & Bhalla, V. (2011). FRET-induced nanomolar detection of Fe2+ based on cinnamaldehyde-rhodamine derivative. *Tetrahedron Letters, 52*(33), 4333-4336.

Kuvibidila, S. R., Kitchens, D., & Baliga, B. S. (1999). In vivo and in vitro iron deficiency reduces protein kinase C activity and translocation in murine splenic and purified T cells. *Journal of Cellular Biochemistry, 74*(3), 468-478.

Lan, T., Wang, F. H., Xi, X. J., Cheng, C. W., Lei, W., Xia, M. Z., & Wang, F. Y. (2016). A rhodamine-based dual chemosensor for the simultaneous detection of Fe3+ and Cu2+. *Analytical Sciences, 32*(11), 1223-1229.

Lansdown, A. B. G. (1995). Physiological and toxicological changes in the skin resulting from the action and interaction of metal ions. *Critical Reviews in Toxicology, 25*(5), 397-462.

Lenart-Boroń, A., & Boroń, P. (2014). Chapter 26 - The effect of industrial heavy metal pollution on microbial abundance and diversity in soils—a review. In *Environmental risk assessment of soil contamination* (pp. 754-783): InTech.

Lewis, S., Donkin, M. E., & Depledge, M. H. (2001). Hsp70 expression in Enteromorpha intestinalis (Chlorophyta) exposed to environmental stressors. *Aquatic Toxicology, 51*(3), 277-291.

Li, K., Xiang, Y., Wang, X., Li, J., Hu, R., Tong, A., & Tang, B. (2014). Reversible photochromic system based on rhodamine B salicylaldehyde hydrazone metal complex. *Journal of the American Chemical Society, 136*(4), 1643-1649.

Lutwak, L. (1974). Continuing need for dietary calcium throughout life. *Geriatrics, 29*(5), 171-174 passim.

Lv, T., Xu, Y., Li, H., Liu, F., & Sun, S. (2018). A Rhodamine B-based fluorescent probe for imaging Cu(2+) in maize roots. *Bioorg Med Chem, 26*(8), 1448-1452.

Maass, T., Hertel, R. F., & Muller, V. R. (1991). *Environmentral health criteria 108: Nickel*. Geneva, Switzerland: World Health Organization (WHO).

Macrae, C. F., Bruno, I. J., Chisholm, J. A., Edgington, P. R., McCabe, P., Pidcock, E., . . . Wood, P. A. (2008). Mercury CSD 2.0– new features for the visualization and investigation of crystal structures. *Journal of Applied Crystallography, 41*(2), 466-470.

Maity, D., & Govindaraju, T. (2011). Highly selective colorimetric chemosensor for Co2+. *Inorganic Chemistry, 50*(22), 11282-11284.

Marr, J. C. A., Lipton, J., Cacela, D., Hansen, J. A., Bergman, H. L., Meyer, J. S., & Hogstrand, C. (1996). Relationship between copper exposure duration, tissue copper concentration, and rainbow trout growth. *Aquatic Toxicology, 36*(1), 17-30.

Martínez-Máñez, R., & Sancenón, F. (2003). Fluorogenic and chromogenic chemosensors and reagents for anions. *Chemical Reviews, 103*(11), 4419-4476.

McConnell, J. R., & Edwards, R. (2008). Coal burning leaves toxic heavy metal legacy in the Arctic. *Proceedings of the National Academy of Sciences, 105*(34), 12140.

Mertz, E., & Zimmerman, S. C. (2003). Cross-linked dendrimer hosts containing reporter groups for amine guests. *Journal of the American Chemical Society, 125*(12), 3424-3425.

Milindanuth, P., & Pisitsak, P. (2018). A novel colorimetric sensor based on rhodamine-B derivative and bacterial cellulose for the detection of Cu(II) ions in water. *Materials Chemistry and Physics, 216*, 325-331.

Miller, W. S., Zhuang, L., Bottema, J., Wittebrood, A. J., De Smet, P., Haszler, A., & Vieregge, A. (2000). Recent development in aluminium alloys for the automotive industry. *Materials Science and Engineering: A, 280*(1), 37-49.

Mohammed, A. S., Kapri, A., & Goel, R. (2011). Heavy metal pollution: source, impact, and remedies. In *Biomanagement of metal-contaminated soils* (pp. 1-28): Springer.

Mohr, G. J. (2005). Covalent bond formation as an analytical tool to optically detect neutral and anionic analytes. *Sensors and Actuators B: Chemical, 107*(1), 2-13.

Mora, A. P. d., Ortega-Calvo, J. J., Cabrera, F., & Madejón, E. (2005). Changes in enzyme activities and microbial biomass after “in situ” remediation of a heavy metal-contaminated soil. *Applied Soil Ecology, 28*(2), 125-137.

Nagajyoti, P. C., Lee, K. D., & Sreekanth, T. V. M. (2010). Heavy metals, occurrence and toxicity for plants: a review. *Environmental Chemistry Letters, 8*(3), 199-216.

Niessen, W. M. A., & Tinke, A. P. (1995). Liquid chromatography-mass spectrometry general principles and instrumentation. *Journal of Chromatography A, 703*(1), 37-57.

Noelting, E., & Dziewoński, K. (1905). Zur Kenntniss der Rhodamine. *Berichte der deutschen chemischen Gesellschaft, 38*(3), 3516-3527.

Novey, H. S., Habib, M. P., & Wells, I. D. (1983). Asthma and IgE antibodies induced by chromium and nickel salts. *Journal of Allergy and Clinical Immunology, 72*(4), 407-412.

Peltonen, L. (1979). Nickel sensitivity in the general population. *Contact Dermatitis, 5*(1), 27-32.

Prodi, L., Bolletta, F., Montalti, M., & Zaccheroni, N. (2000). Luminescent chemosensors for transition metal ions. *Coordination Chemistry Reviews, 205*(1), 59-83.

Pryzbylski, P., Huczyński, A. W., Pyta, K. K., Brzezinski, B., & Bartl, F. (2009). Biological properties of schiff bases and azo derivatives of phenols. *Current Organic Chemistry, 13*, 124-148.

Quinlan, E., Matthews, S. E., & Gunnlaugsson, T. (2007). Colorimetric recognition of anions using preorganized tetra-amidourea derived calix[4]arene sensors. *The Journal of Organic Chemistry, 72*(20), 7497-7503.

Rai, A., Kumari, N., Nair, R., Singh, K., & Mishra, L. (2015). A new rhodamine derivative as a single optical probe for the recognition of Cu2+ and Zn2+ ions. *RSC Advances, 5*(19), 14382-14388.

Rai, A., Singh, A. K., Tripathi, K., Sonkar, A. K., Chauhan, B. S., Srikrishna, S., . . . Mishra, L. (2018). A quick and selective rhodamine based “smart probe” for “signal-on” optical detection of Cu2+ and Al3+ in water, cell imaging, computational studies and solid state analysis. *Sensors and Actuators B: Chemical, 266*, 95-105.

Rascio, N., & Navari-Izzo, F. (2011). Heavy metal hyperaccumulating plants: How and why do they do it? And what makes them so interesting? *Plant Science, 180*(2), 169-181.

Reck, B. K., Müller, D. B., Rostkowski, K., & Graedel, T. E. (2008). Anthropogenic nickel cycle: Insights into use, trade, and recycling. *Environmental Science & Technology, 42*(9), 3394-3400.

Reinke, C. M., Breitkreutz, J., & Leuenberger, H. (2003). Aluminium in over-the-counter drugs. *Drug Safety, 26*(14), 1011-1025.

Robinson, J. W. (1960). Atomic absorption spectroscopy. *Analytical Chemistry, 32*(8), 17A-29A.

Rurack, K. (2001). Flipping the light switch 'ON' – the design of sensor molecules that show cation-induced fluorescence enhancement with heavy and transition metal ions. *Spectrochimica Acta Part A: Molecular and Biomolecular Spectroscopy, 57*(11), 2161-2195.

Ryan, M. F. (1991). The role of magnesium in clinical biochemistry: An overview. *Annals of Clinical Biochemistry, 28*(1), 19-26.

Saiyed, S. M., & Yokel, R. A. (2005). Aluminium content of some foods and food products in the USA, with aluminium food additives. *Food Additives & Contaminants, 22*(3), 234-244.

Savir, S., Wei, Z. J., Liew, J. W. K., Vythilingam, I., Lim, Y. A. L., Saad, H. M., . . . Tan, K. W. (2020). Synthesis, cytotoxicity and antimalarial activities of thiosemicarbazones and their nickel (II) complexes. *Journal of Molecular Structure, 1211*, 128090.

Schiff, H. (1864). Mittheilungen aus dem Universitätslaboratorium in Pisa: Eine neue Reihe organischer Basen. *Justus Liebigs Annalen der Chemie, 131*(1), 118-119.

Shaw, B. P., Sahu, S. K., & Mishra, R. K. (2004). Heavy metal induced oxidative damage in terrestrial plants. In M. N. V. Prasad (Ed.), *Heavy Metal Stress in Plants: From Biomolecules to Ecosystems* (pp. 84-126). Berlin, Heidelberg: Springer Berlin Heidelberg.

Sheldrick, G. M. (2008). SHELXL and SHELXS. *Acta Crystallogr., Sect. A, 64*(1), 112.

Shen, H. M., & Zhang, Q. F. (1994). Risk assessment of nickel carcinogenicity and occupational lung cancer. *Environmental health perspectives, 102 Suppl 1*(Suppl 1), 275-282.

Singh, R., & Das, G. (2018). Fluorogenic detection of Hg2+ and Ag+ ions via two mechanistically discrete signal genres: A paradigm of differentially responsive metal ion sensing. *Sensors and Actuators B: Chemical, 258*, 478-483.

Sobha, K., Poornima, A., Harini, P., & Veeraiah, K. (2007). A study on biochemical changes in the fresh water fish, catla catla (hamilton) exposed to the heavy metal toxicant cadmium chloride. *Kathmandu University Journal of Science, Engineering and Technology, 1(4)*, 1-11.

Soliman, Z. I. (2006). A study of heavy metals pollution in some aquatic organisms in Suez Canal in Port-Said harbour. *Journal of Applied Sciences Research, 2(10)*, 657-663.

Speir, T. W., Kettles, H. A., Percival, H. J., & Parshotam, A. (1999). Is soil acidification the cause of biochemical responses when soils are amended with heavy metal salts? *Soil Biology and Biochemistry, 31*(14), 1953-1961.

Sun, T., Niu, Q., Li, Y., Li, T., & Liu, H. (2017). Novel oligothiophene-based dual-mode chemosensor: "Naked-Eye" colorimetric recognition of Hg2+ and sequential off-on fluorescence detection of Fe3+ and Hg2+ in aqueous media and its application in practical samples. *Sensors and Actuators B: Chemical, 248*, 24-34.

Sunnapu, O., Kotla, N. G., Maddiboyina, B., Asthana, G. S., Shanmugapriya, J., Sekar, K., . . . Sivaraman, G. (2017). Rhodamine based effective chemosensor for Chromium(III) and their application in live cell imaging. *Sensors and Actuators B: Chemical, 246*, 761-768.

Sunnapu, O., Kotla, N. G., Maddiboyina, B., Singaravadivel, S., & Sivaraman, G. (2016). A rhodamine based "turn-on" fluorescent probe for Pb(ii) and live cell imaging. *RSC Advances, 6*(1), 656-660.

Suramitr, S., Teanwarawat, J., Ithiapa, N., Wattanathana, W., & Suramitr, A. (2020). Crystal structure, Hirshfeld surface analysis and computational study of a rhodamine B-salicyl-aldehyde Schiff base derivative. *Acta crystallographica. Section E, Crystallographic communications, 76*(Pt 7), 1027-1032.

Tainer, J. A., Getzoff, E. D., Richardson, J. S., & Richardson, D. C. (1983). Structure and mechanism of copper, zinc superoxide dismutase. *Nature, 306*(5940), 284-287.

Tajbakhsh, M., Chalmardi, G. B., Bekhradnia, A., Hosseinzadeh, R., Hasani, N., & Amiri, M. A. (2018). A new fluorene-based Schiff-base as fluorescent chemosensor for selective detection of Cr3+ and Al3+. *Spectrochimica Acta Part A: Molecular and Biomolecular Spectroscopy, 189*, 22-31.

Tang, X., Han, J., Wang, Y., Ni, L., Bao, X., Wang, L., & Zhang, W. (2017). A multifunctional Schiff base as a fluorescence sensor for Fe3+ and Zn2+ ions, and a colorimetric sensor for Cu2+ and applications. *Spectrochimica Acta Part A: Molecular and Biomolecular Spectroscopy, 173*, 721-726.

Tayade, K. C., Kuwar, A. S., Fegade, U. A., Sharma, H., Singh, N., Patil, U. D., & Attarde, S. B. (2014). Design and synthesis of a pyridine based chemosensor: Highly selective fluorescent probe for Pb2+. *Journal of Fluorescence, 24*(1), 19-26.

Taylor, A., & Marks, V. (1978). Cobalt: A review. *Journal of Human Nutrition, 32(3)*, 165-177.

Vallero, D. (2014). Chapter 29 - Air pollutant emissions. In D. Vallero (Ed.), *Fundamentals of Air Pollution (Fifth Edition)* (pp. 787-827). Boston: Academic Press.

Verstraeten, S. V., Aimo, L., & Oteiza, P. I. (2008). Aluminium and lead: molecular mechanisms of brain toxicity. *Archives of Toxicology, 82*(11), 789-802.

Wang, B., & Anslyn, E. V. (2011). *Chemosensors: Principles, atrategis, and applications.* (Vol. 15): John Wiley & Sons.

Wang, L., Ye, D., Li, W., Liu, Y., Li, L., Zhang, W., & Ni, L. (2017). Fluorescent and colorimetric detection of Fe(III) and Cu(II) by a difunctional rhodamine-based probe. *Spectrochimica Acta Part A: Molecular and Biomolecular Spectroscopy, 183*, 291-297.

Wang, Q., Tan, Y., Wang, N., Lu, Z., & Wang, W. (2018). A multifunctional fluorescence sensor for Cd2+, PO43− and Cr3+ in different system and the practical application. *Spectrochimica Acta Part A: Molecular and Biomolecular Spectroscopy, 201*, 216-222.

Weinberg, E. D. (2008). Role of iron in osteoporosis. *Pediatric endocrinology reviews : PER, 6 Suppl 1*, 81-85.

Wessendorf, M. W., & Brelje, T. C. (1992). Which fluorophore is brightest? A comparison of the staining obtained using fluorescein, tetramethylrhodamine, lissamine rhodamine, texas red, and cyanine 3.18. *Histochemistry, 98*(2), 81-85.

Westrip, S. P. (2010). publCIF: software for editing, validating and formatting crystallographic information files. *Journal of Applied Crystallography, 43*(4), 920-925.

WHO. (2003). Aluminium in drinking-water: Background document for development of WHO guidelines for drinking-water quality. (No.WHO/SDE/WSH/03.04/53), World Health Organization.

Wong, M. H., & Tam, F. Y. (1977). Soil and vegetation contamination by iron-ore tailings. *Environmental Pollution (1970), 14*(4), 241-254.

Woo, S., Yum, S., Park, H. S., Lee, T. K., & Ryu, J. C. (2009). Effects of heavy metals on antioxidants and stress-responsive gene expression in Javanese medaka (Oryzias javanicus). *Comparative Biochemistry and Physiology Part C: Toxicology & Pharmacology, 149*(3), 289-299.

Xavier, A., & Srividhya, N. (2014). Synthesis and study of Schiff base ligands. *IOSR Journal of Applied Chemistry, 7(11)*, 6-15.

Xiang, Y., Tong, A., Jin, P., & Ju, Y. (2006). New fluorescent rhodamine hydrazone chemosensor for Cu(II) with high selectivity and sensitivity. *Organic Letters, 8*(13), 2863-2866.

Yang, Y., Gao, C. Y., Zhang, N., & Dong, D. (2016). Tetraphenylethene functionalized rhodamine chemosensor for Fe3+ and Cu2+ ions in aqueous media. *Sensors and Actuators B: Chemical, 222*, 741-746.

Yoon, J., & Czarnik, A. W. (1992). Fluorescent chemosensors of carbohydrates. A means of chemically communicating the binding of polyols in water based on chelation-enhanced quenching. *Journal of the American Chemical Society, 114*(14), 5874-5875.

Zhao, X., Liu, Y., Shu, B., Guo, Z., Song, C., Huang, X., & Jiao, Z. (2020). Portable smartphone-based device for on-site detection of Hg2+ in water samples. *International Journal of Environmental Analytical Chemistry*, 1-10.

Zheng, H., Zhan, X. Q., Bian, Q. N., & Zhang, X. J. (2013). Advances in modifying fluorescein and rhodamine fluorophores as fluorescent chemosensors. *Chemical Communications, 49*(5), 429-447.

Zhou, F., Wang, H., Liu, P., Hu, Q., Wang, Y., Liu, C., & Hu, J. (2018). A highly selective and sensitive turn-on probe for aluminum(III) based on quinoline Schiff's base and its cell imaging. *Spectrochimica Acta Part A: Molecular and Biomolecular Spectroscopy, 190*, 104-110.

Zhou, Y., Li, Z. X., Zang, S. Q., Zhu, Y. Y., Zhang, H. Y., Hou, H. W., & Mak, T. C. W. (2012). A novel sensitive turn-on fluorescent Zn2+ chemosensor based on an easy to prepare c3-symmetric Schiff-base derivative in 100% aqueous solution. *Organic Letters, 14*(5), 1214-1217.

Zitka, O., Krystofova, O., Hynek, D., Sobrova, P., Kaiser, J., Sochor, J., . . . Adam, V. (2013). Metal Transporters in Plants. In D. K. Gupta, F. J. Corpas, & J. M. Palma (Eds.), *Heavy Metal Stress in Plants* (pp. 19-41). Berlin, Heidelberg: Springer Berlin Heidelberg.